Institut für Feuerungs- und Kraftwerkstechnik

Universität Stuttgart

Direktor: Prof. Dr. techn. G. Scheffknecht
Pfaffenwaldring 23 • 70569 Stuttgart
Tel. +49 (0) 711-685 63487 • Fax +49 (0) 711-685 63491

Diploma Thesis Nr. 3266

cand. Mach. Ioannis Papandreou

ERASMUS Student

Experimental study of the Calcium Looping process under high CO_2 concentrations at a 10kWth Dual Fluidized Bed facility

Address: Allmandring 26B, 70569 Stuttgart

Date of issue: 15.07.2013

Date of submission: 15.01.2014

Supervisor: Dipl.-Ing. Glykeria Duelli (Varela)

Abstract

Energy production from fossil fuel power plants is contributing to the global emissions of CO_2, a major greenhouse gas. One of the technologies being researched and developed to limit those emissions is Calcium Looping, a post-combustion process which takes advantage of the reversible carbonation of CaO during which CO_2 contained in flue gasses is adsorbed by CaO forming $CaCO_3$ and then is released when the reverse step of the reaction named calcination takes place. In the scope of the present Thesis experiments were performed in IFK's $10kW_{th}$ Dual Fluidized Bed facility consisting of a Circulating Fluidized Bed (CFB) which was used as the carbonator operating at 630°C, coupled with a Bubbling Fluidized Bed (BFB) which was used as the regenerator operating at 900-930°C. In this experimental campaign the reactor and sorbent performance was studied for high values of CO_2 concentrations in the regenerator. This is because in a realistic scenario the heat required for the calcination reaction will be provided by oxy-combustion of coal, which, along with flue gas recirculation to control the temperature is expected to result in very high CO_2 concentrations in the reactor. The results showed that regenerator efficiencies dropped for high CO_2 concentrations, requiring higher space time. The effect on the regenerator performance also affected the CO_2 capture efficiency of the carbonator, requiring more Calcium Looping Ratio to reach higher values. As far as sorbent performance is concerned, its maximum carbonation conversion decayed to a residual activity matching the theoretical deactivation curve for a typical limestone, with a few deviations during the first cycles, possibly due to the pre-calcination of the material. Lastly, the material losses were not as significant as the ones recorded in previous experiments, presumably due to different fluidization regimes as well as the high concentrations of CO_2.

Contents

List of Figures

List of Tables

Notation

Symbol	Significance	Unit
A	Area	[m^2]
Ar	Archimedes Number	[-]
C_{CO2}	Molar CO_2 Concentration	[mol/m^3]
$C_{CO2,\ eq}$	Equilibrium Molar CO_2 Concentration	[mol/m^3]
d_p	Surface-volume mean diameter of particles	[m]
E_{ac}	Activation energy	[J]
E_{calc}	Calcination efficiency	[-]
E_{reg}	Regenerator efficiency	[-]
E_{CO2}	CO_2 capture efficiency	[-]
$E_{CO2,eq}$	Maximum CO_2 capture efficiency as dictated by the chemical equilibrium	[-]
F_0	Sorbent make-up flow	[mol/h]
f_a	Fraction of active particles in the reactor	[-]
F_{Ca}	Molar Calcium flow	[mol/h]
F_{CO2in}	Molar CO_2 inlet flow	[mol/h]
F_{CO2out}	Molar CO_2 outlet flow	[mol/h]
k	Deactivation constant	[-]
K_a	Attrition constant	[s^{-1}]
k_{c0}	Pre-exponential factor of the kinetic constant of $CaCO_3$ calcination	[m^3/mol·s]
k_c	Kinetic constant of $CaCO_3$ calcination	[m^3/mol·s]
L(t)	Cumulative sorbent specific CO_2 loading	[-]
N	Number of carbonation/calcination cycles	[-]
N_{Ca}	Solid inventory of Ca in the calciner	[mol/m^2]
N_{th}	Theoretical number of cycles	[-]
g	Acceleration of gravity	[m/s^2]
P_{CO2}	CO_2 Partial Pressure	[Pa]
$P_{CO2,eq}$	Equilibrium CO_2 Partial Pressure	[Pa]

R	Ideal gas constant	[J/molK]
Re_{mf}	Reynolds number for minimum fluidization velocity	[-]
S_g	Specific B.E.T. surface area	[cm^2/mol]
T	Temperature	[^oC]
t	Residence Time (subscript indicates the reactor)	[s]
t^*	Time required for the X_{max} to be reached	[s]
t^*_c	Time required for full calcination	[s]
U_{mf}	Minimum fluidization velocity	[m/s]
U_s	Superficial Gas Velocity	[m/s]
V_{total}	Total bed volume	[m^3]
$\overline{V_{CO2}}$	CO_2 concentration in the carbonator	[-]
$V_{CO2,eq}$	Equilibrium CO_2 Concentration in the carbonator	[-]
X_{calc}	Carbonate content of the solids after calcination	[-]
X_{carb}	Carbonate content of the solids after carbonation	[-]
X_{max}	Maximum carbonation conversion of the sorbent	[-]
$X_{max,N}$	Maximum carbonation conversion of the sorbent after N cycles	[-]
X_R	Lower Limit of the Maximum Capacity for Rapid Integration of CO_2	[-]
y_{CO2}	CO_2 concentration	[-]

Greek Symbols

Symbol	Significance	Unit
ε	void fraction in the bed	[-]
μ	Dynamic viscosity	[kg/ms]
ρ_g	Gas density	[m^3/kg]
ρ_p	Particle density	[m^3/kg]
T_{carb}	Carbonator Space Time	[s]
τ_{active}	Carbonator Active Space Time	[s]
τ_{reg}	Regenerator Space Time	[s]
τ_a	Regenerator Active Space Time	[s]

List of abbreviations

Abbreviation	Significance
ASU	Air Separation Unit
BFB	Bubbling Fluidized Bed
CCS	Carbon Capture and Sequestration
CLP	Calcium Looping Process
CFB	Circulating Fluidized Bed
COE	Cost of Electricity
DFB	Dual Fluidized Bed
EU	European Union
FB	Fluidized Bed
IGCC	Integrated Gasification Combined Cycle
O&M	Operations and Maintenance
PC	Pulverized Coal
PSD	Particle Size Distribution
RPM	Random Pore Model
SCM	Shrinking Core Model
TGA	Thermo-Gravimetric Analyzer

Chemical Compounds and Elements

Symbol	Significance
CaO	Calcium Oxide
$CaCO_3$	Calcium Carbonate
CO_2	Carbon Dioxide
H_2O	Water
N_2	Nitrogen
O_2	Oxygen
SO_2	Sulfur Dioxide

1 Introduction

1.1 Carbon Capture and Storage

Carbon Dioxide is the major greenhouse gas and it is being produced at large quantities from fossil fuel combustion, especially at power plants. Global energy demand in 2040 is expected to be increased by 30% in comparison to 2010, while 40% of energy consumption will be due to electricity generation [1]. This demand will be mostly covered by fossil fuel power plants and coal-fired power plants are responsible for 43% of the world's CO_2 emissions [2]. While renewable energy and nuclear power are the world's fastest growing energy sources coal will continue to attribute for 80% of global energy production through 2040 [3].

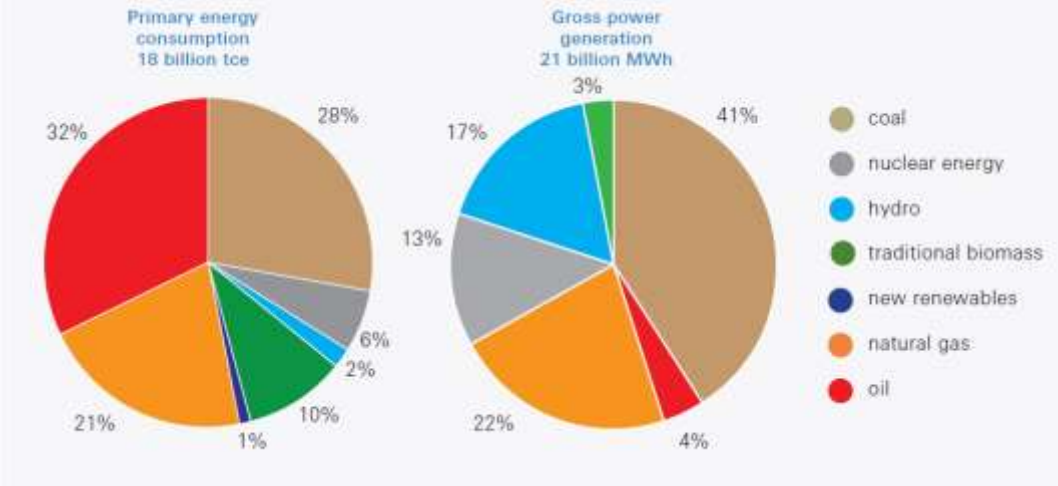

Figure 1.1: Coal's share in global primary consumption and electricity generation, 2010 [4]

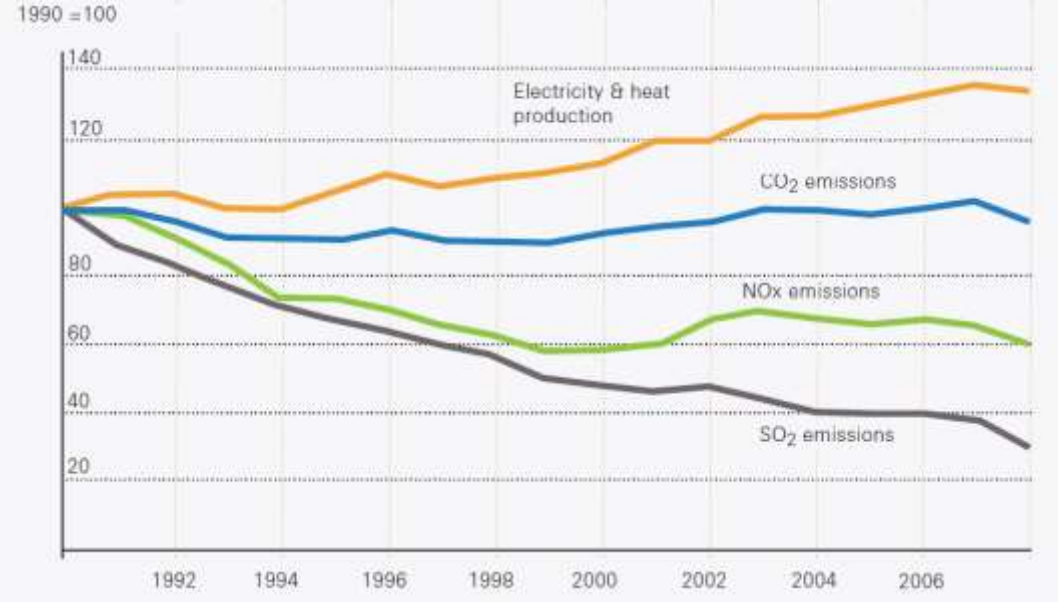

Figure 1.2: Emissions from electricity and heat production across Europe (EEA-32) 1990 - 2008 [4]

It was recently reported that CO_2 concentration levels in our atmosphere broke a new milestone of 400ppm. This milestone is expected to be broken again this year since the annual lowest value of CO_2 concentration is already behind us, recorded during October and the CO_2 levels are rising back up as shown in Fig. 1.3 [5]. According to International Energy Outlook's scenarios and projections the global temperature is expected to be increased by 6°C by the end of 2050 if the current regulations and policies are maintained and no effort is made to mitigate Greenhouse Gas emissions [6]. This makes it more apparent than ever that the need for efficient ways of making such power plants environmentally friendly is imperative and the EU has committed itself into reducing the greenhouse gas emissions in order to prevent an increase in global temperature. More specifically, the 450 scenario presented in the World Energy Outlook has set out an energy pathway consistent with the goal of limiting the global increase in temperature to 2°C by 2050, by limiting concentration of greenhouse gases in the atmosphere to around 450 parts per million of CO_2 [7].

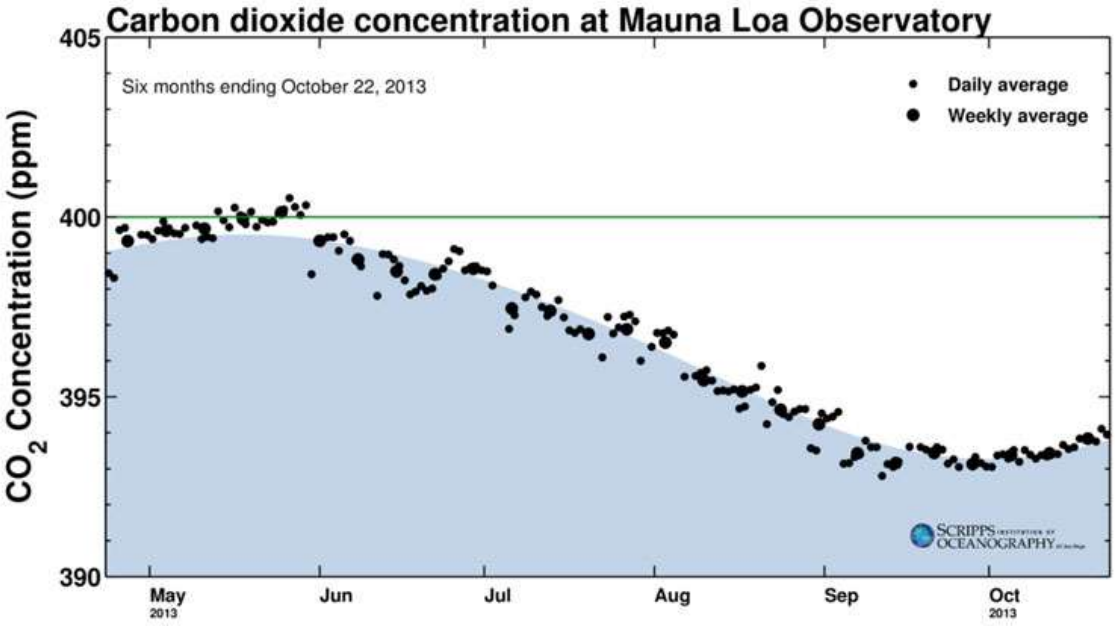

Figure 1.3: CO_2 concentration levels over the last 6 months measured at Mauna Loa Observatory [5]

Dealing with the global warming while being able to provide affordable energy is a challenge that we need to overcome and it will require a wide range of efficient and low carbon technologies. In the field of fossil fuels the only technology that is currently available for this purpose is Carbon Capture and Storage (CCS), which dictates the capture of the CO_2 that would otherwise be emitted to the atmosphere and injecting it to be stored in deep geological formations.

CCS usually involves 3 steps, capture, transportation and storage of CO_2 [2]. Economic Analyses have shown that of those 3 steps the CO_2 capture is the most expensive, which is why capture methods are being researched and developed with the goal of becoming as efficient and cost-effective as possible. There are 3 main CO_2 capture processes for CO_2 capture generation [8]:

- Pre-Combustion
- Post-Combustion
- Oxy-Fuel

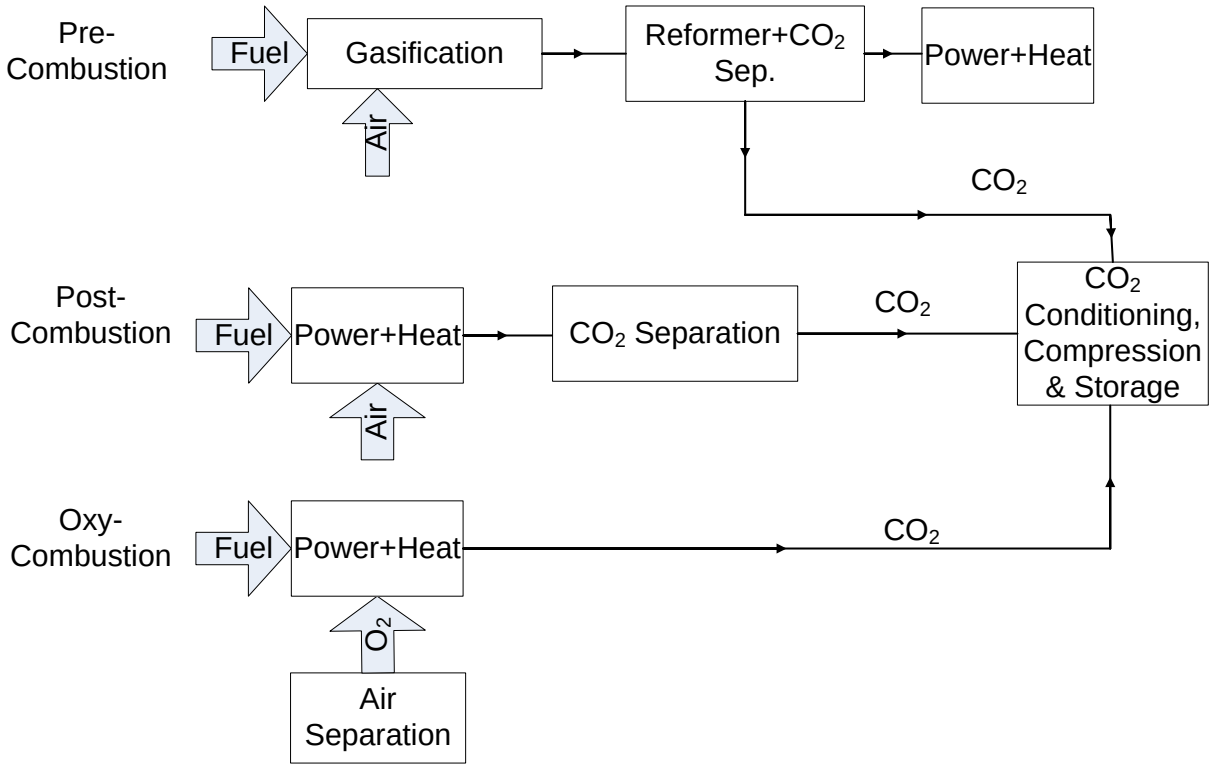

Figure 1.4: Schematic of CCS technologies

Pre-Combustion processes involve separating CO_2 before the fuel is burned via gasification of the solid or liquid fossil fuels such as coal, biomass and petroleum products. From this gasification 2 gases are produced: CO and H_2. The CO is converted to CO_2 and then removed while the H_2 is burned to produce electricity or used for other purposes. The most advanced Pre-Combustion Process is the Integrated Gasification Combined Cycle (IGCC) with CCS. This process involves partial oxidation of the fuel with pure O_2, shift of the syngas to CO_2 and H_2 and CO_2 separation with natural solvents such as the Selexol or Rectisol process [9].

Post-Combustion processes involve separating the CO_2 from flue gases after the combustion of the fuel. The properties of flue gas from coal combustion pose several key challenges that are common to all carbon capture processes and include a large total volumetric flow rate, dilute concentration of carbon dioxide in the flue gas stream, and existence of impurities. In addition, existing coal-fired power plants have further restrictions, such as size constraints and operating conditions necessary for optimal performance that increases the difficulty of developing post-combustion technologies for carbon dioxide (CO_2) capture suitable as a retrofit. The process that is in use for decades in large scale deployment is the use of Amine-based solvents, such as monoethanolamine (MEA). A CO_2 rich gas stream, such as a power plant's flue gas, is "bubbled" through an amine solution. The CO_2 bonds with the amines as it passes through the solution while other gases continue up through the flue. The CO_2 in the resulting CO_2-saturated amine solution is then removed from the amines, "captured" and is ready for carbon storage [8]. The amines themselves can be recycled and reused. This method however poses problems because amines are corrosive and increase the cost of electricity. Several other options are being investigated, including using sorbents, membrane, and chemical looping processes [2]. One of the most feasible of those methods appears to be the Calcium Looping process (CaL) which has the potential to reduce the cost and increase the efficiency of H_2 and/or electricity production from coal derived syngas by implementing the principles of process integration. This process is using a Dual Fluidized Bed system and Calcium Oxide as a sorbent that is carrying the CO_2 between a FB Carbonator and a FB Regenerator. The CO_2 contained in the power plant's flue gases, typically in a concentration of 15%, reacts with the CaO in the Carbonator and forms $CaCO_3$. This way a stream of flue gas free of CO_2 exits the carbonator. Then the newly formed $CaCO_3$ enters the Regenerator where it is separated to CaO and a pure stream of CO_2 ready for compression and storage.

Oxy-Fuel combustion (also called oxy-firing) involves the combustion of coal in pure oxygen, rather than air, to fuel a conventional steam generator. An Air Separation Unit (ASU) is used to separate the Nitrogen from the combustion air. By avoiding the introduction of nitrogen into the combustion chamber, the amount of CO_2 in the power station exhaust stream is greatly concentrated, making it easier to capture and compress. Oxy-Fuel combustion with CO_2 storage is currently at the demonstration phase.

Each of these capture options has its particular benefits. Post-combustion capture and oxy-fuel have the potential to be retrofitted to existing coal-fired power stations and new plants constructed over the next 10-20 years. Pre-combustion capture utilizing IGCC is potentially

more flexible, opening up a wider range of possibilities for coal, including a major role in a future hydrogen economy [8].

Capturing CO_2 by using any of those processes however, results in higher capital and operating costs, as well as lower efficiencies than the conventional power plants utilizing no form of CCS. This is because more equipment must be built and operated and around 10-40% more energy is required for a CCS plant.

1.2 The Calcium Looping Process

1.2.1 Process Description

Calcium Looping is a CO_2 Capture process using CaO-based sorbents to remove CO_2 from flue gases producing a concentrated stream of CO_2 suitable for storage. This procedure is based on the reaction which is fundamental to the process, the reversible carbonation of lime as shown below:

$$CaO + CO_2 \leftrightarrow CaCO_3 \quad \text{Eq. 1.1}$$

This is a reversible reaction, with the forwards step known as Carbonation, an exothermic reaction and the backwards step known as Calcination which is an endothermic reaction.

$$CaO + CO_2 \rightarrow CaCO_3 \quad \Delta H^o = -178 \text{ kJ/mol.} \quad \text{Eq. 1.2}$$

$$CaCO_3 \rightarrow CaO + CO_2 \quad \Delta H^o = +178 \text{ kJ/mol.} \quad \text{Eq. 1.3}$$

This process was initially introduced by Shimizu et al. [11] and it is designed to take place in a Dual Fluidized Bed facility. Dual Fluidized Bed (DFB) is a mature technology at a large scale which is also used for other important processes for lowering CO_2 emissions such as chemical looping combustion and gasification of coal or biomass with or without CO_2 adsorption. As presented below, out of those processes Calcium Looping seems to be the most efficient and viable way to capture CO_2 from flue gasses due to its advantages, such as utilizing a sorbent derived from cheap, abundant and environmentally benign limestone and dolomite precursors, providing additional energy to the original power plant and coupling with cement industries [12], [13].

The principle of Calcium Looping process is displayed in Figure 1.5:

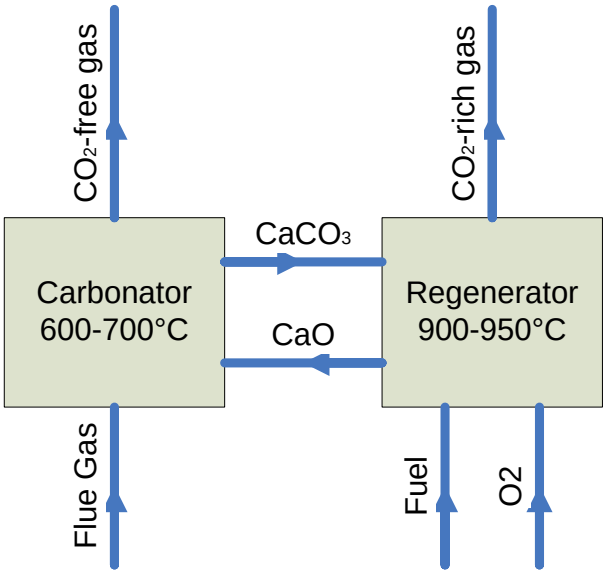

Figure 1.5: Schematic Illustration of the Calcium Looping process

A certain flue gas first enters the Carbonator containing CO_2 in a concentration of around 15%. There the CO_2 is adsorbed by CaO at temperatures of 600-700°C to form $CaCO_3$. This way a stream of almost CO_2-free lean flue gas, exits the Carbonator to be released in the atmosphere. The partially carbonated sorbent then enters the Regenerator where the CO_2 is separated from CaO at temperatures above 900°C as suggested by the following reversible reaction:

$$CaCO_3 \leftrightarrows CaO + CO_2 \qquad \text{Eq. 1.5}$$

The most common way of providing the heat required to achieve such temperatures is Oxy-Combustion of Coal, however other methods have been suggested such as providing heat using a hot stream of solids circulating from an air-fired combustor. This would alleviate the costs of the air separation unit; however such processes will need more time to be developed [14]. In the case of Oxy-Fuel Combustion O_2 is diluted with CO_2 in order to keep the temperature under control. Therefore, after the material has been calcined in the Regenerator the gas that is produced mainly consists of CO_2 and water vapour. After the gas is condensed what remains is a stream of pure CO_2 ready to be compressed and stored.

1.2.2 Pros & cons of the Calcium Looping Process

The Calcium Looping Process is not the first method proposed in order to reduce greenhouse gas emissions. Other methods include Amine Scrubbing and Chemical Looping process. Calcium Looping however appears to have distinct advantages compared to other methods:

1. Use of an integrated steam cycle for additional electricity production

The Calcium Looping Process also offers the opportunity to increase the electricity generation of the power plant it is associated to. The carbonator captures CO_2 from the power plant's flue gases at temperatures of 650^{o}C and the regenerator utilizes additional coal in order to reach temperatures as high as 900-950^{o}C. This high temperature can be used for an independent steam cycle in order to make up for the energy penalty caused by the CO_2 capture. Hawthorne et al. [12] simulated the calcium looping process treating the flue gas exiting a 1025MW_e power plant with a standard flue gas composition, i.e. y_{CO2}=15 vol-%. The simulation predicted heat streams coming out of the Carbonator and the Calciner producing a supercritical steam with a temperature of 600^{o}C and 300bar at a flow of 477kg/s. The heat required for the CaL process was about 40% of the heat input of the power plant but with the steam generation cycle increasing the electrical output by 500MW_e and resulting in overall electrical efficiency of 39.2%.

Table 1.1: Heat stream summary for Carbonate Looping steam cycle [12]

Reference Power Plant	P_{net}	1100MW_e
	η_{net}	45.6%
Carbonate Looping Process	P_{net}	724MW_e
	η_{net}	45.3%
CO_2 conditioning	$P_{CO2,comp}$	128MW_e
	P_{ASU}	115MW_e

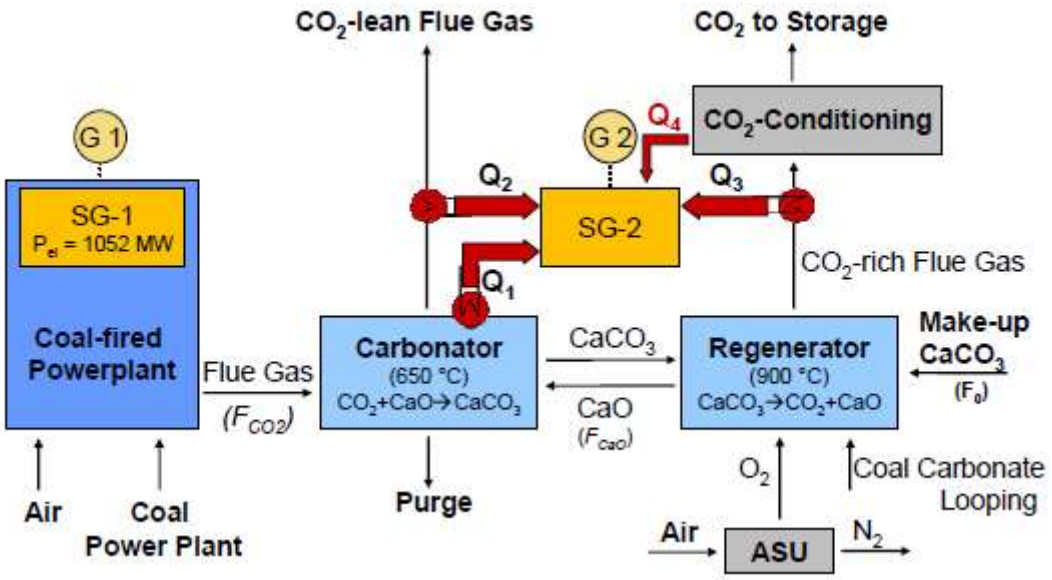

Figure 1.6: Diagram of retrofitted coal-fired power plant. Four different heat streams (Q_1-Q_4) are integrated in a new steam generator (SG2). [12]

2. Use in cement industry

The Calcium Looping process can be used to reduce CO_2 emissions from cement production plants in an efficient way, as they account for about 5% of the global man-produced CO_2 from stationary sources [13]. In cement plants with drastically reduced fuel consumption or that are biomass-fueled the majority of the CO_2 emissions comes from the calcination of limestone, since $CaCO_3$ decomposition is a major process of cement production. Implementing an Oxy-combustion calciner instead of the standard air-fired calciner is already being considered as a very promising CO_2 capture method for this purpose. This process however is not able to manage the flue gases that exit the rotary kiln where cement is produced. This is why the Calcium Looping process can reduce the amount of CO_2 released in the atmosphere even further. In addition to the CFB Oxy-calciner a CFB Carbonator reactor is also used in order to take advantage of the large amounts of active CaO that are present. Instead of leading the whole amount of Carbonated Lime in the rotary kiln, a fraction of it is diverted to the CFB carbonator which uses it to capture CO_2 from the kiln, releasing a stream of gas very low in CO_2. The $CaCO_3$ produced is then lead back into the Oxy-regenerator for the CO_2 to be released, compressed and stored.

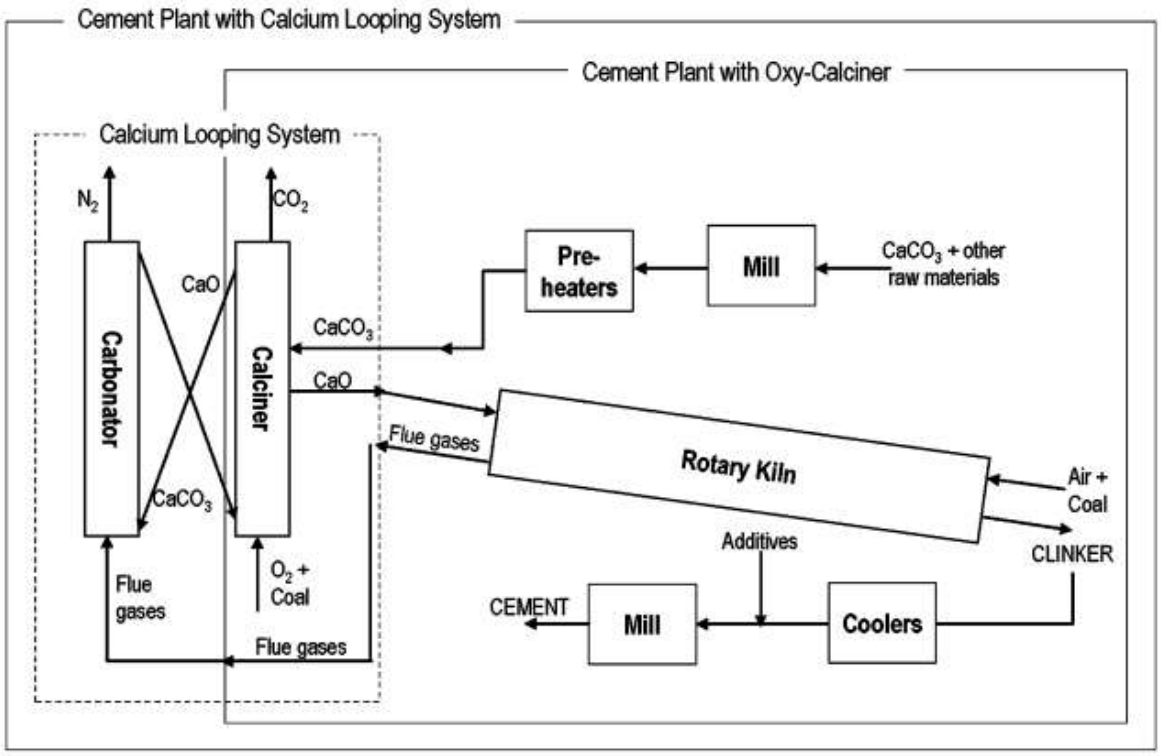

Figure 1.7: Scheme of a cement plant with oxy-fired calciner and cement plant with calcium looping system [13]

3. More Economically feasible

Current technologies present high capital costs and high power consumption. Amine scrubbing for instance when used to capture CO_2 from a new pulverized coal (PC) power plant may reduce the net electric generating capacity by approximately 30% and increase its capital cost by 80%. On the other hand, if a physical absorption process for pre-combustion CO_2 is applied to a new Integrated Gasification Power Plant the plant's net electric generating capacity is reduced by 15-25% while its capital cost is increased by 35-50% [15]. In simulations run by Cornell et al. [16] it is shown that an IGCC plant with conventional CO_2 capture methods of 90% capture capability, has a net efficiency of 32.7% whereas a CLP IGCC plant has a net efficiency of 33.1%. While this might appear as a small difference it should be kept in mind that in comparison to a conventional IGCC plant where the heat input of the plant is fed to the gasifier, the CLP plant feeds 41% of that heat input to the calciner where Pulverized Coal is used for Oxy-fuel combustion and electricity generated by PC is expected to be of much lower efficiency in comparison to an IGCC plant with CO_2 capture [16]. CLP can also be used in Coal to H_2 plants as its integrated steam cycle can offer a net electrical energy output whereas with conventional CO_2 capture methods there would be little to no energy production.

Table 1.2: Summary of economic analysis simulation results for the IGCC power plant [16] (currency: USD)

	Base Plant	CLP Plant
First-year capital ($/MWh)	$59.00	$51.20
Fixed O&M ($/MWh)	$22.38	$18.88
Coal ($/MWh)	$17.12	$16.86
CO_2 emissions ($/MWh)	$2.71	$0.15
Other variable O&M ($/MWh)	$1.76	$3.59
First-year COE	$102.97	$90.68

As the first year Cost of Electricity from this simulation suggests, it is apparent that in the IGCC power plant's case the plant with CLP integrated is at an economic advantage, as it essentially integrates an IGCC plant and a PC plant (the coal oxy-fired calciner) around a common CO_2 capture technology. It must be noted however that the simulations included a hydration stage in order to reactivate the sorbent which decays after each consecutive cycle.

4. It is based on already mature technology.

The Fluidized Bed technology has been studied for many years due to its widespread use over the industry.

5. It utilizes an easily accessible material

Lime and limestone (empirical names for CaO and $CaCO_3$ respectively) are ancient and low-cost materials without which industry as we know it would not exist. Any object in one's home has required at least one of them at some point of its manufacture, either directly or indirectly. Lime and limestone are the building blocks of commerce and industry along with iron ore, salt, sulfur, petroleum and coal. Evidence on its abundance can be provided by the fact that a high percentage of calcium and magnesium are contained in earth's crust. In terms of abundance, lime and limestone are surpassed only by oxygen, silicon, aluminum and iron [17].

As promising as the Calcium Looping Process might seem however, there are still issues that need to be dealt with before it progressing to industrial scale.

One of the main issues is the amount of heat that is required for the regenerator [18]. The decomposition of lime which takes place in the calciner is an endothermic reaction which requires temperatures over 850^{o}C according to the reaction equilibrium. For this reason oxy-combustion of coal is needed in order to provide such high temperature and even though the heat recovery in a CLP facility is relatively easy because all mass streams are at high temperature, minimizing the energy consumption even further, and thus minimizing O_2 consumption and costs associated with it such as the Air Separation Unit will always be a design target.

Another drawback is presented by sorbent attrition which leads to material losses [19]. The reduction of the particle size results in finer particles leaving the system along with the gas stream, requiring a constant flow of fresh make-up sorbent. To this make-up sorbent requirement adds the deactivation of the material. As the sorbent undergoes repeated carbonation-calcination cycles the CaO's CO_2 capture capacity decreases, reaching a residual activity which is often dictated by the quality of the material. In most cases the capture capacity drops to approximately 10-15% [20].

1.2.3 Status of the Process

Experimental work has been carried out in small scale fluidized bed pilot facilities and has been published over the last few years [14]:

Abanades et al. [21] demonstrated CO_2 capture in a DFB facility comprised of a CFB regenerator and a BFB carbonator. The process proved to be effective as long as there was sufficient active CaO.

Lu et al. also performed experiments in a 75kW$_{th}$ DFB system using a CFB combustor as a regenerator and a 2-stage fluidized bed carbonator and demonstrated its feasibility by achieving capture efficiencies of over 95% at the first cycles which was later reduced to 72% after more than 25 cycles [22]. The highest efficiencies were recorded for the lowest values of fluidization velocities, confirming that higher residence time of the sorbent in the carbonator reactor results in more effective CO_2 capture. Another parameter tested in those experiments was the carbonation temperature. It appeared that temperatures at the range of 650-700^{o}C provided unreasonably high capture efficiencies (90%) but this was addressed to the

fact that the temperature in the reactor was higher at the bottom of the bed than at the top. High CO_2 removal continued to be observed at lower temperatures until a critical value of 500^{o}C. The highest CO_2 capture efficiency achieved was 98% and it was at the range of 580-600^{o}C. Finally they confirmed the use of oxy-fuel combustion as a heat source for the calcination by extracting off-gas of CO_2 concentrations higher than 85% from the calciner.

Charitos et al. proceeded to carry out continuous Carbonation-Calcination cycle experiments in IFK's 10kW$_{th}$ DFB facility [23] in order to do a parametric investigation of the main operation variables of the BFB carbonator. What was innovative about this DFB system was a cone valve which gave much more control over the circulation rate of the solids and the calcium looping ratio. The heat required for the calcination reaction was provided by electrical heaters. Increasing the carbonation temperature proved to lead to lower capture efficiencies, which was an expected result. Charitos et al. also used a parameter called space time (τ) to characterize the Carbonator. Space time is defined as the ratio of the moles of CaO present in the carbonator and the flow of CO_2 in moles per hour in the flue gas feed and it is given from the following equation:

$$\tau = \frac{n_{Ca}}{F_{CO_2}} \qquad \text{Eq. 1.6}$$

They varied the fluidization velocity in order to achieve different space time values with a constant inlet CO_2 concentration and they found that increasing space time at a constant calcium looping ratio resulted in higher capture efficiencies with the increase being less significant for higher levels of looping ratio.

Finally, Alonso et al. [24] performed continuous experiments in a dual CFB 30MW$_{th}$ facility and achieved stable CO_2 capture efficiencies of 65-75% using deactivated, close to residual activity material, i.e. after hundreds of cycles of operation.

1.2.4 Examples of larger pilot scale facilities

The IFK's 200kW$_{th}$ Dual Fluidized Bed Facility (Stuttgart, Germany)

This is the first pilot scale facility that has carried out parametric studies and has reached capture efficiencies over 90% under steady state conditions. It was designed to operate continuously 24 hours a day so that a stationary-state with respect to sorbent (calcined limestone) activity can be obtained [25]. It consists of a CFB Carbonator and a CFB Regenerator, each 10m high and with a diameter of 0.23m and 0.15m respectively. In addition to those reactors there is a 6m high combustor serving as a flue gas generator. The schematic of the facility can be seen in Figure 1.7.

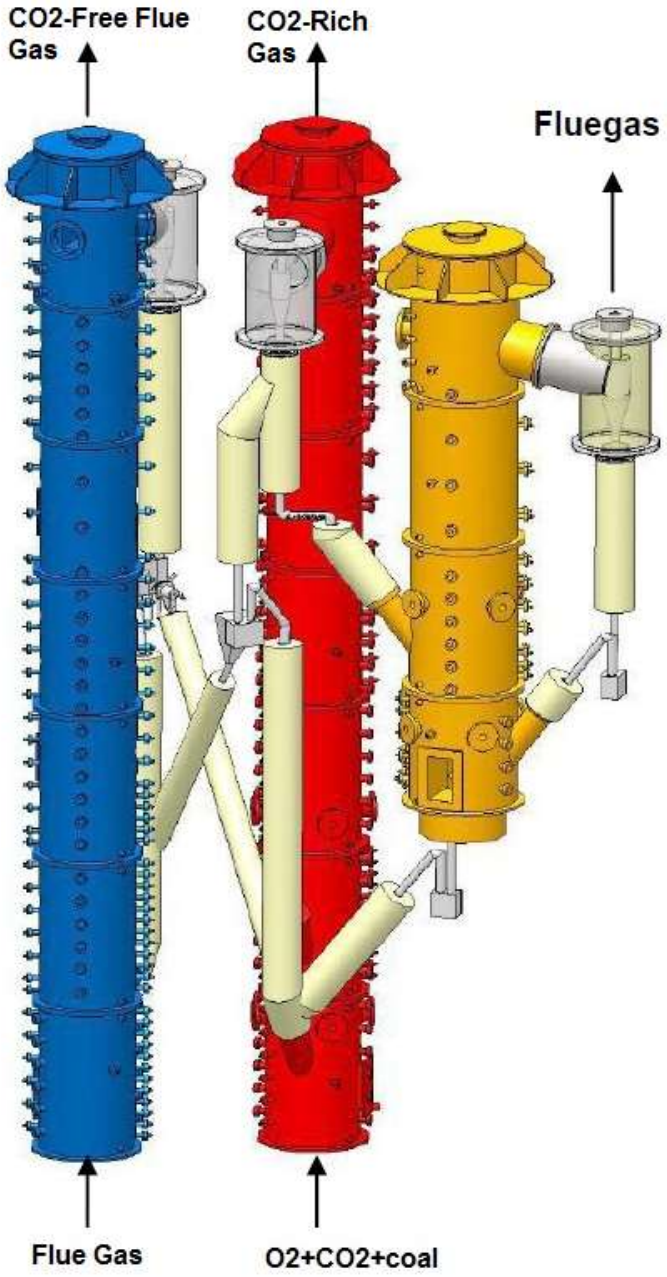

Figure 1.8: The 200kW$_{th}$ Dual Fluidized Bed facility in IFK, Stuttgart, Germany

The TU Darmstadt's 1MW$_{th}$ facility (Darmstadt, Germany)

The 1MW$_{th}$ facility at TU Darmstadt comprises of a CFB carbonator and regenerator, with height of 8.66m and 11.35m and inner diameter of 0.59m and 0.4m respectively. The heat required for the calciner is provided by combustion of either propane gas or pulverized coal. In January and February of 2012 2 separate experimental campaign took place in this facility where those 2 fuels, propane and pulverized coal were tested in terms of providing heat for the calciner while performing continuous CO_2 capture. In both experimental campaigns CO_2 capture efficiencies over 85% were recorded.

The 1.7MW_{th} pilot plant facility integrated in La Pereda Power Plant (Northern Spain)

In 2011 a large scale 1.7 MW_{th} pilot plant was built and commissioned next to the 50MW power plant in La Pereda, Spain. The facility was built in order to:

- Evaluate and optimize the concept in the 1.7 MW test facility, in operating conditions equivalent to large-scale industrial units and integrated in a commercial plant.
- To analyze the controllability and stability of the process
- To find the optimum set of operating conditions to minimize sorbent make-up flow cost.
- To measure the effects of initial particle size and attrition phenomena in the continuous circulating fluidized bed system.
- To analyze the effects of the flue gas impurities in the sorbent performance and the effects of coal ash and sulfur content

Both reactors are CFB reactors 15m high and are equipped with a startup burner. To gain operational flexibility, a mechanical system allows modifying the distribution of the solids circulation between both reactors. Moreover dimensions of some parts of the reactors can be modified to increase the range of operation. In this large scale pilot facility the Calcium Looping process has been proven successfully to be feasible with capture efficiencies over 90% and simultaneous SO_2 capture in the CFB carbonator of over 95%.

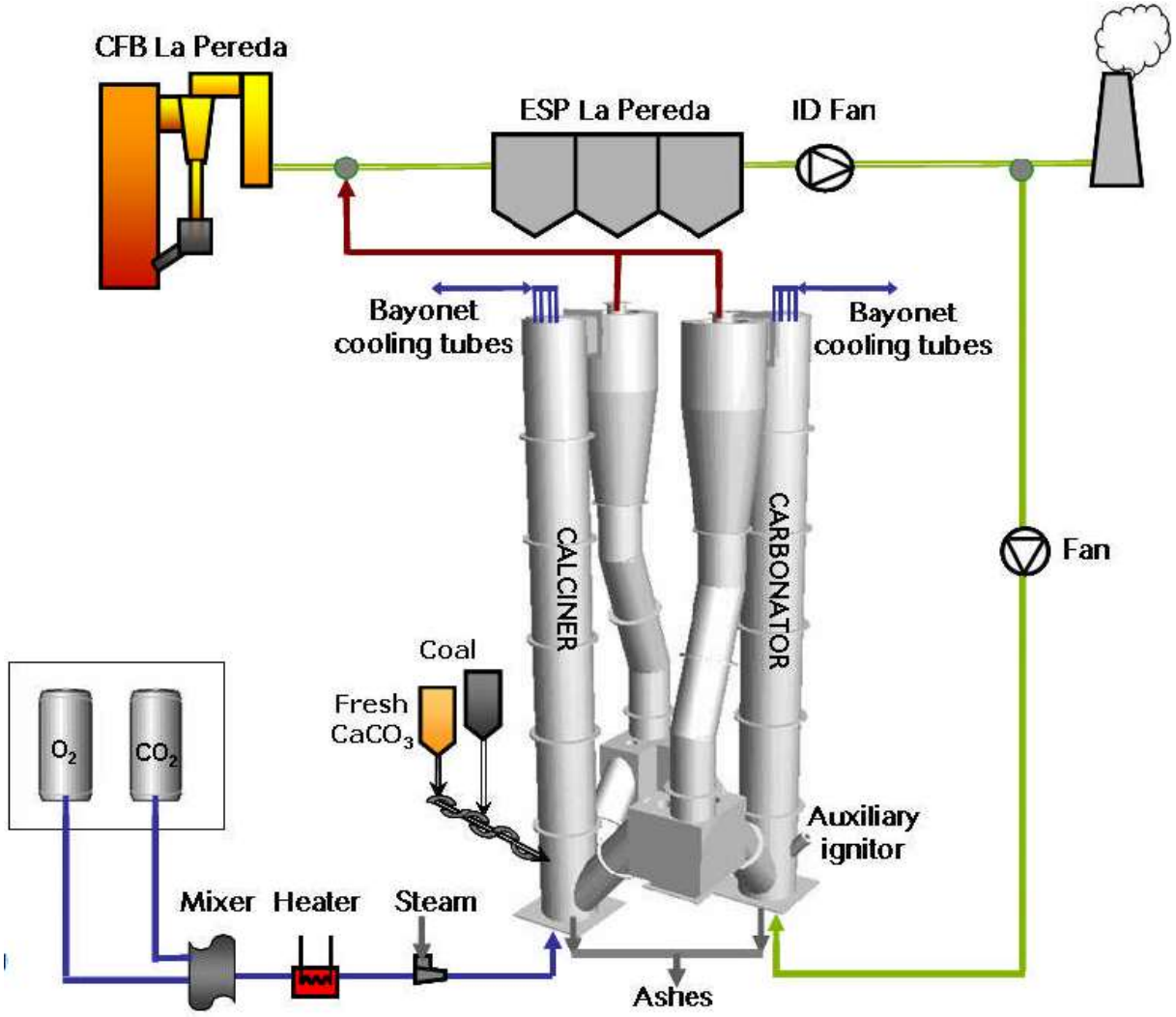

Figure 1.9: The 1.7MWth Calcium Looping pilot facility in La Pereda, Spain [26]

Table 1.3: Main Parameters of the CO_2 Capture facility in La Pereda [26]

Main Parameters in the carbonator during CO_2 capture tests	
Carbonator Temperature (^oC)	600-715
Carbonator Superficial Gas Velocity (m/s)	2.0-4.0
Inlet CO_2 volume fraction	0.12-0.14
Inlet SO_2 concentration (mg/m^3)	100-250
Inventory of solids in the Carbonator (kg)	100-1000
Maximum CO_2 carrying capacity of the solids	0.10-0.70
CO_2 capture efficiency	40-95%
SO_2 capture efficiency	95-100%

1.3 Goal of the Thesis

A significant amount of research has been carried out regarding the carbonator reactor in the Calcium Looping process. The regenerator however has not had such attention. While the decomposition of limestone is a complicated reaction and it is a subject that has been thoroughly studied over the last 50 years, this is the first time that such experiments take place in a small pilot-scale facility in order to characterize the calcination reaction for the calcium looping process. The oxy-fuel combustion that takes place in the calcium looping process in order to achieve the temperatures required for the calcination reaction imposes an environment very high in CO_2 for the reaction.

There are important issues to the calcination of $CaCO_3$ related to the Calcium Looping Process that need to be investigated. Assuming that an oxy-fired CFB combustor will be used as the regenerator, the combustion conditions will most likely result in CO_2 concentrations within the range of 50-80 vol. % [27]. For that reason the effect of CO_2 partial pressure on calcination needs to be determined for different temperatures and sorbent residence times in order to find an operating window for the process parameters that allow stable operation of an economically viable use of the regenerator, i.e. minimizing energy consumption in the calcium looping process while still providing a constant high degree of calcination. The design temperature of the reactor for instance must always be as low as possible in order to achieve effective calcination of $CaCO_3$ as well as to prevent sorbent deactivation and ash issues which are presented at temperatures higher than 950°C [27]. This Thesis will present results from an experimental campaign carried out in the $10kW_{th}$ pilot DFB facility in IFK in order to determine the effect of CO_2 partial pressure in the reactor by operating at a wide range of CO_2 inlet concentrations (0-75%) within the temperature range of 900-930^{o}C.

2 Theoretical Background

During this theoretical background review, the aspects regarding the Calcium Looping Process will be analyzed. Those include Dual Fluidized Bed technology, carbonation and calcination reaction principles and chemical properties of the material, as well as the sorbent's mechanical stability in terms of particle attrition phenomena.

2.1 Fluidized Bed Technology

The Calcium Looping Process is based on Dual Fluidized Bed technology. Fluidization is a process introduced by Fritz Winkler in 1921 [28] during which granular material is converted from a static solid-like state to a dynamic fluid-like state when a gas or liquid passes through the material. This process is now widely used and finds application in industries such as energy conversion and mineral processing. In the Calcium Looping Process the ideal setup is the use of twin CFB reactors.

2.1.1 Hydrodynamics and regimes of fluidization

In order to get a better understanding of how a fluidized bed works one can imagine a gas moving up through a bed of granular solids resting on the porous bottom of a column. As the gas velocity through the solid particles increases, a series of changes in the motion of the particles could occur. For example, at a very low velocity the particles remain stationary on the floor but at a sufficiently high velocity they are transported out of the vessel. As the gas velocity increases it changes the fluidization regime of the solids. Therefore we have the following regimes as the gas velocity increases [28], [29]:

- Packed or Fixed Bed

The solids are stationary while the gas flows through a grid they reside on. Solids in a packed bed are significantly larger than the ones in other fluidization regimes.

- Bubbling Fluidization

As the gas velocity increases it reaches a critical value after which the solids begin to act like a fluid. If the velocity increases further, the excess gas begins to flow in the form of bubbles.

- Slugging Fluidization

If the bubble size increases enough to be comparable to the width of the bed it passes through the column as a slug, resulting in frequent and large pressure fluctuations.

- Turbulent Fluidization

The bubble phase loses its identity due to rapid coalescence and breakup of bubbles. Upper surface is difficult to distinguish and there are only small amplitude pressure fluctuations.

- Fast Fluidization

There is no distinguishable upper bed surface; particles are transported out at the top and must be replaced by adding solids at the bottom, done by recirculating the particles that come out via cyclone and downcomer.

- Transport/Pneumatic Bed

There is no axial variation of solids concentration except in the bottom acceleration section.

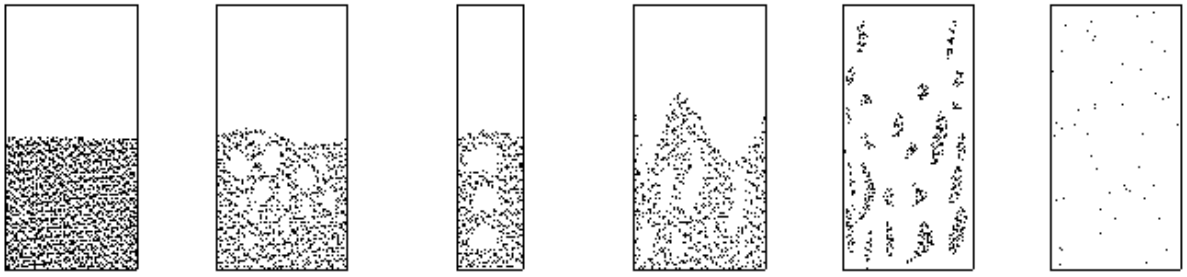

Figure 2.1: Schematic illustration of the different fluidization regimes. From left to right: Fixed/Packed bed, Bubbling, Slugging, Turbulent, Fast fluidization and Transport/Pneumatic Bed

The Fluidized Bed reactors used in the frame of this Thesis were operating under the Fast and Bubbling fluidization regimes, therefore emphasis will be given to those 2 in this chapter.

2.1.2 Bubbling Fluidized Bed

In order to characterize the operation conditions in a bubbling fluidized bed we need to take a look at the parameters affecting its fluidization. One of them is the superficial gas velocity, and it is the artificial velocity that is calculated as if the fluid is the only thing present in the reactor while disregarding all other solids and gases completely. The superficial gas velocity is used because it has a consistent value while the real gas velocity is not stable throughout the reactor and its mean value cannot be measured in a reliable way.

The superficial gas velocity is given by the following formula:

$$U_s = \frac{\dot{V}}{A} \cdot 3600 \qquad \text{Eq. 2.1}$$

In order for the bed solids to start behaving like a fluid the superficial gas velocity must reach a critical value. This value is called Minimum Fluidization Velocity or U_{mf} and it is given by the following equation:

$$Re_{mf} = \frac{U_{mf} d_p \rho_g}{\mu} = [C_1^2 - C_2 Ar]^{0.5} - C_1 \qquad \text{Eq. 2.2}$$

Where Ar is the Archimedes number:

$$\mathrm{Ar} = \frac{\rho_g(\rho_p - \rho_g) g d_p^3}{\mu^2} \qquad \text{Eq. 2.3}$$

And d_p is the surface-volume mean diameter of particles.

The values of the constants C_1 and C_2 are taken from experiments [28] and are 27.2 and 0.0408, respectively.

For the sorbent particles used in the Calcium Looping process, when the gas velocity exceeds the aforementioned minimum fluidization velocity, the excess gas begins to flow through the reactor in the form of bubbles. Bubbles are basically gas voids that rise through the reactor while by-passing the emulsion phase thereby expanding the bed. The emulsion phase is the phase of gas-solid suspension that surrounds the bubbles and rises to the surface of the bed with an absolute velocity of $U=(U_s-U_{mf})$. The bubbles themselves rise through the emulsion phase with a diameter that increases along the height of the reactor. Figure 2.2 presents a simple schematic of the concept of the emulsion phase and the bubble phase.

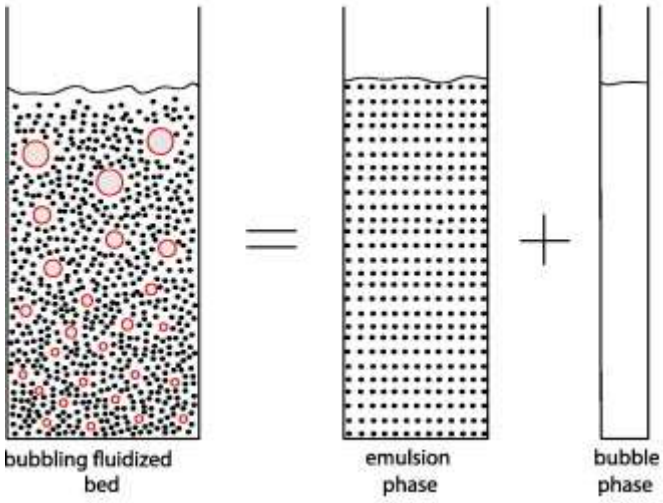

Figure 2.2: Illustration of the emulsion and the bubble phase in a bubbling fluidized bed [30]

Table 2.1: Properties of operation under Bubbling Fluidization Regime [28]

Property	Bubbling Fluidization Regime
Application	Bubbling Fluidized Bed
Mean Particle Diameter(mm)	0.03-3
Gas velocity in the combustion zone (m/s)	0.5-2.5
Overall Voidage	0.5-0.85
Temperature gradient	Very Small
Typical Bed-to-surface heat Transfer coefficient(W/m^2K)	200-550

2.1.3 Circulating Fluidized Bed

A Circulating Fluidized bed operates under the Fast fluidization regime. In a typical fast fluidized bed, one observes a non-uniform suspension of slender particle agglomerates or clusters moving up and down in a dilute, upwardly flowing gas–solid continuum. The main features that characterize this regime are high slip velocity between the gas and solids, formation and disintegration of particle agglomerates and excellent mixing [28].

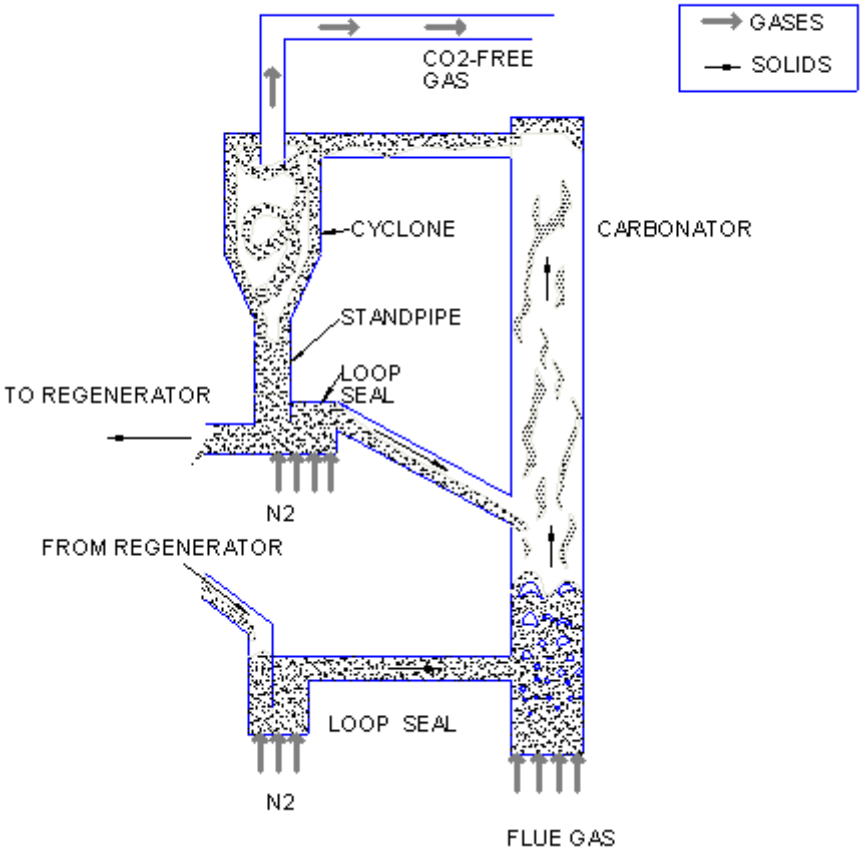

Figure 2.3: A CFB Carbonator as part of the Calcium Looping Process

Table 2.2: Properties of operation under Circulating Fluidization Regime [28]

Property	Fast Fluidization Regime
Application	Circulating Fluidized Bed
Mean Particle Diameter(mm)	0.05-0.5
Gas velocity in the combustion zone (m/s)	4-6
Overall Voidage	0.85-0.99
Temperature gradient	Small
Typical Bed-to-surface heat Transfer coefficient(W/m^2K)	100-200

2.1.4 Dual Fluidized Bed Technology

A Dual Fluidized Bed reactor usually comprises of 2 interconnected Circulating Fluidized Beds or a Circulating Fluidized Bed riser and a Bubbling fluidized bed [31]. The two reactors are connected through a valve, which is why it is often called 'interconnected circulating fluidized bed reactor'. Apart from the Calcium Looping process, the DFB technology is widely used in the industry. Applications of this technology include but are not limited to the Dual Fluidized Bed Gasifier and the Chemical Looping Process.

The experimental setups described in literature through which the calcium looping process has been validated have varied from CFB carbonator-BFB regenerator and vice versa, to 2 interconnected CFB reactors. In terms of the carbonator reactor, it is more likely to be a CFB, i.e. operate under the fast fluidization regime due to better gas-solid contacting conditions. More specifically, Charitos et al. [32] compared 3 different fluidization regimes for the operation of the carbonator reactor, namely the bubbling, turbulent and fast fluidization. Operation under all 3 conditions gave satisfactory results and capture efficiencies over 90% and very close to the maximum allowed by the equilibrium were achieved. It was shown however that for the same values of active space time, the capture efficiencies and gas-solid contacting were significantly lower in the case of the bubbling fluidization regime [33].

2.2 The Carbonation-Calcination equilibrium

The chemical reaction upon which the Calcium looping Process is based is the following: $\mathrm{CaO} + \mathrm{CO_2} \rightleftarrows \mathrm{CaCO_3}$. As mentioned in Chapter 1 the forwards step is known as carbonation (Eq. 1.2) and it is an exothermic reaction while the backwards step is called calcination (Eq. 1.3) and it is endothermic, meaning that it requires heat intake to take place. For the carbonation reaction to occur, the partial pressure of CO_2 in the gas above the solid surface is higher than the decomposition pressure of the $CaCO_3$. This decomposition pressure is determined by equilibrium thermodynamic considerations and it is given by the equation of Baker (Eq. 2.4). This equation was calculated using experimental data with temperatures above 1170K and CO_2 pressures above 101kPa and it correlates well with data presented for these conditions with some deviation occurring for lower values of dissociation temperature and partial pressures of CO_2 [20].

$$\log \mathrm{P_{eq}} = 7.079 - \frac{8308}{\mathrm{T_{carb}}} \qquad \text{Eq. 2.4}$$

Fig. 2.4 depicts the P_{eq} plotted vs Temperature as calculated from Eq. 2.4

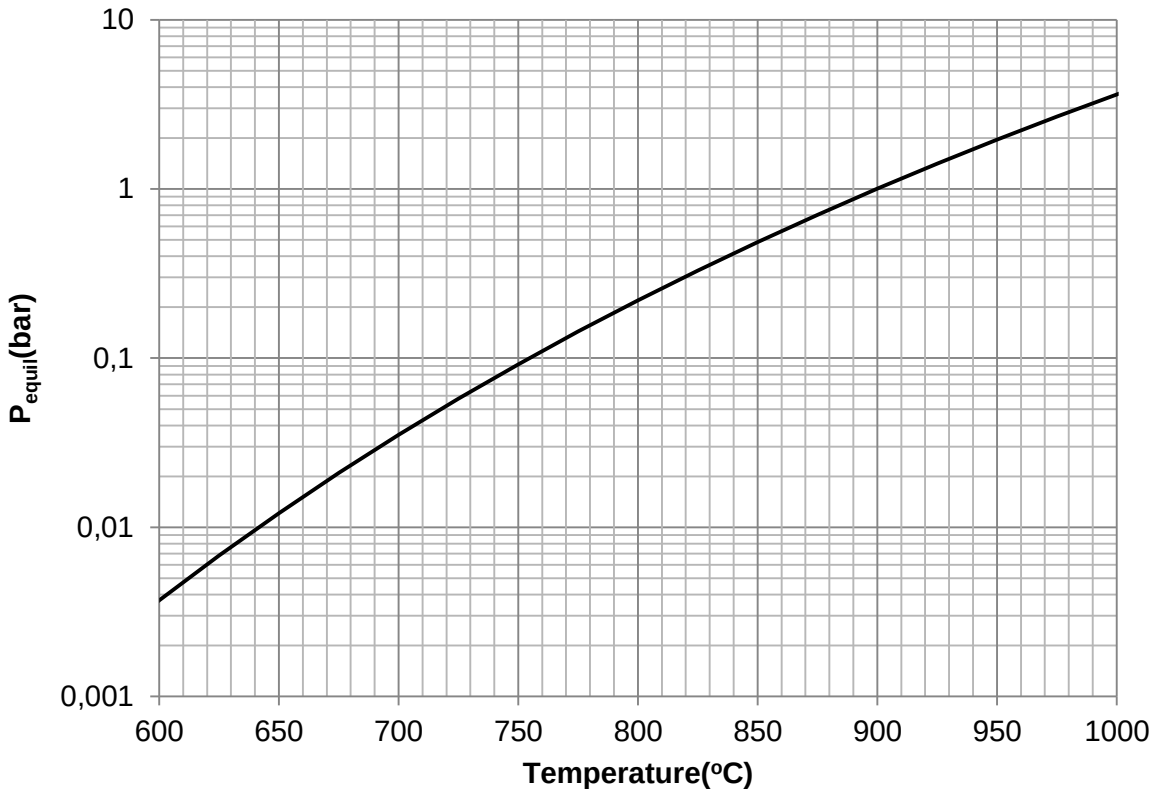

Figure 2.4: CO_2 partial pressure plotted vs. temperature as proposed by Eq. 2.4

According to Figure 2.4, points below the Equilibrium line are representing calcination while the ones above it represent the carbonation reaction. We can see that for an increasing value of CO_2 partial pressure higher temperatures are needed in order for the decomposition of $CaCO_3$ to be achieved.

Another important parameter related to the carbonation-calcination equilibrium is the CO_2 equilibrium concentration ($C_{CO2,eq}$) which defines the maximum capture efficiency (E_{eq}) that can be achieved in the Calcium Looping Process. C_{CO2} can be calculated from Eq. 2.5.

$$\mathrm{C_{CO2,eq}} = \frac{1.462 \cdot 10^{11}}{\mathrm{T_{carb}}} \cdot \exp\left(\frac{-19130}{\mathrm{T_{carb}}}\right) \qquad \text{Eq. 2.5}$$

And the maximum CO_2 capture efficiency dictated by the equilibrium is:

$$\mathrm{E_{eq}} = 1 - \frac{\mathrm{P}_{eq}\left(1 - y_{CO2,in}\right)}{y_{CO2,in}\left(P_{total} - \mathrm{P}_{eq}\right)} \qquad \text{Eq. 2.6}$$

2.3 The Carbonation reaction

The Carbonation is the forward step of the aforementioned equilibrium during which the CO_2 is captured by CaO. In the calcium looping process it takes place in a Fluidized Bed reactor at a temperature of approximately 650°C.

The carbonation reaction is split into two stages. When it starts it is controlled by surface kinetics and is progressing rapidly. This is called the Fast carbonation stage. After a certain point the $CaCO_3$ that forms on the surface of CaO occupies a large molar volume, creating a layer of carbonate which impedes transport of carbon dioxide making the reaction follow a diffusion controlled mechanism, resulting in a slow carbonation stage [20]. The point at which the reaction shifts from the fast carbonation stage to the slow carbonation stage is defined as the maximum carbonation conversion of the sorbent carrying capacity (X_{max}) [9].

2.4 The calcination reaction

The decomposition of $CaCO_3$, also known as Calcination is a very important reaction to the Calcium Looping process as it releases the CO_2 captured in the Carbonator by separating it from the CaO. It is a reaction which has been studied extensively over the years because of its multiple practical and industrial applications such as cement production and desulphurization in coal-based power plants. The essential factors in the kinetics of calcination are the following [17]:

- The material must be heated to the dissociation temperature of the carbonates and this minimum temperature must be maintained for a certain duration
- The CO_2 released during the reaction must be removed.

According to existing literature, solid-state decomposition processes such as calcination are difficult to obtain reliable kinetic and mechanistic data for, because of the product gas (in this case CO_2) being released in close proximity to the decomposing material in such a reversible reaction [20].

Martinez et al. in recently published work studied the calcination of $CaCO_3$ in immediate relation to the Calcium Looping process, namely taking in consideration the conditions imposed by it such as temperature and CO_2 partial pressure. After conducting experiments in a TGA [27] they proposed an equation which calculates the calcination reaction rate:

$$\frac{d(X_{carb} - X_{calc})}{dt} = k_c \cdot \left(1 - \frac{X_{carb} - X_{calc}}{X_{carb}}\right)^{2/3} \cdot (C_{eq} - C_{CO_2}) \qquad \text{Eq. 2.7}$$

C_{eq} and C_{CO2} are the equilibrium CO_2 concentration and the CO_2 concentration in the gas phase respectively. The kinetic constant k_c is calculated according to the Arrhenius equation:

$$k_c = k_{c0}\exp\left(\frac{-E_{ac}}{RT}\right) \quad \text{Eq. 2.8}$$

Where k_{c0} and E_{ac} are a pre-exponential factor and activation energy respectively which depend on the type of limestone used.

By integrating the Eq. 2.8 they then calculated the time required to achieve full calcination:

$$t_c^* = \frac{3X_{carb}}{k_c \cdot (C_{eq} - C_{CO_2})} \quad \text{Eq. 2.9}$$

The same set of experiments also led to the conclusion that the calcination reaction is chemically controlled and is affected primarily by calcination temperature and CO_2 partial pressure, whereas factors such as $CaCO_3$ content and particle lifetime do not affect the reaction rate.

Using this model, Martinez et al. in a subsequent paper [34] proposed a formula which evaluates the regenerator's efficiency demonstrating how it is affected by characteristics such as calcination temperature, CO_2 partial pressure, solid inventory, solids circulation rate and the content in $CaCO_3$ from the material coming from the carbonator.

$$E_{calc} = \frac{f_a}{\ln\left(\frac{1}{1-f_a}\right)} \quad \text{Eq. 2.10}$$

Where f_a is the fraction of particles in the regenerator that are still reacting, i.e. with a reaction time lower than t^*_C and is defined as:

$$f_a = 1 - \exp\left(-\frac{t_c^*}{\tau}\right) \quad \text{Eq. 2.11}$$

Where τ is the average residence time of the particles and can be calculated as follows:

$$\tau = \frac{N_{Ca}}{F_{Ca} + F_0} \quad \text{Eq. 2.12}$$

2.4.1 CO_2 partial pressure: an important parameter affecting the reaction

As proposed by the reaction equilibrium and can be seen by Fig. 2.4, higher partial pressures of CO_2 would favor the carbonation step rather than the calcination. Research has been conducted over the last decades in order to determine the effect of CO_2 on the calcination rate with many different results being stated. Ingraham and Marier [35] came to the conclusion that the reaction rate has a linear dependence on the difference between the CO_2 partial pressure and the CO_2 equilibrium pressure. Other authors proposed that it's inversely proportional to the CO_2 partial pressure [36]. Hashimoto [36] found that the rate dependency was linear at lower temperatures but non-linear at higher temperatures while Darroudi and Searcy [37] proposed that CO_2 only plays a role when its partial pressure is relatively high, namely higher than $10^{-2}P_{eq}$, presenting a parabolic dependency which becomes linear when the partial pressure gets closer to the equilibrium pressure. Garcia-Labiano et al. also performed

experiments using a TGA [36] and came to the conclusion that the calcination rate is indeed reduced by higher CO_2 concentrations. A more abrupt decrease in the reaction rate was noted at the highest CO_2 concentration environments.

Khinast et al. [38] performed TGA experiments on 2mg samples in order to determine the effect of CO_2 partial pressure within the range of 0-6.5%. This is a short range of concentrations [36] and in contrast to authors who proposed a linear correlation between the reaction rate and P_{CO2} they suggested that the reaction rate decays exponentially, by using a modified Random Pore Model. They addressed the reported linear dependency which had been proposed in literature to incorrectly neglecting mass transport in the sample.

Garcia-Labiano et al. [36] also researched the effect of P_{CO2} in $CaCO_3$ decomposition using a TGA and 2 different limestones with sample weights ranging from 10mg to 75mg and particle size ranging from 0.4mm and 2mm. The CO_2 concentration ranged from 0% to 80%. The results showed that as partial pressure increased the $CaCO_3$ decomposition was getting slower. In order to come up with a model that predicts the reaction's behavior they used a modified Lamguir adsorption isotherm as shown in Eq. 2.13. An adsorption isotherm describes the equilibrium of the sorption of a material at a surface (more general at a surface boundary) at constant temperature. It represents the amount of material bound at the surface (the sorbate) as a function of the material present in the gas phase and/or in the solution. Sorption isotherms are often used as empirical models which do not make statements about the underlying mechanisms and measured variables. They are obtained from measured data by means of regression analysis.

$$\theta = \frac{\left(K_A P_{CO_2}\right)^{1/n}}{1 + \left(K_A P_{CO_2}\right)^{1/n}} \qquad \text{Eq. 2.13}$$

with the exponent n ranging from 0.5 to 2.

Where θ is the fraction of active sites occupied by CO_2. This proved to be accurate for lower values of CO_2 concentrations but wasn't reliable at the highest partial pressures.

After that, the Freundlich isotherm was used:

$$\theta = c P_{CO_2}^{1/n} \qquad \text{Eq. 2.14}$$

The best fit was found for n=2 and it proved to be in agreement with experimental results and therefore deemed valid to describe the calcination reaction in a broad range of CO_2 partial pressures.

Stanmore and Gillot in a published literature review [39] also suggested the following equation to describe the limestone decomposition rate:

$$R_r = K_D \cdot \left(P^* - P_{CO_2}\right) = \left[A \cdot \exp\left(\frac{-E}{RT}\right)\right] \cdot \left(P^* - P_{CO_2}\right) \quad \text{Eq. 2.15}$$

Where P_{CO_2} is the partial pressure of CO_2 in the experiment and P^* is the equilibrium CO_2 pressure of the decomposition of $CaCO_3$. A is the Frequency factor while E is the activation energy. As it can be seen in this equation the Reaction rate is proportional to the difference $\left(P^* - P_{CO_2}\right)$ under constant temperature. CO_2 partial pressure also seems to enhance sintering effects as shown by Borgwardt [40].

2.4.2 The role of Calcination temperature and residence time

In order for the calcination reaction to take place, the material needs to reach a certain dissociation temperature and that temperature must be maintained for the duration of the reaction. According to literature and as it can be seen in Figure 2.4, the typical dissociation temperature for calcite under 100% CO_2 environment at 1° atm is approximately 898°C [17]. This minimum temperature however is dependent on the type of limestone. Especially in the case of dolomitic limestone with a high $MgCO_3$ content it falls as low as 400°C. Naturally, as proposed by Figure 2.4, a change in one of the two parameters presented will affect the reaction, moving it towards the carbonation or the calcination step. In the case of temperature, an increase in its value at the same levels of CO_2 concentration will result in a better calcination. This effect has been proven by several authors: Borgwardt [41] performed experiments in a TGA which show higher temperatures to have a positive effect on the reaction rate. This was also shown by Garcia-Labiano et al. in 2002 [36] when they also attempted modeling the reaction for different values of CO_2 concentration. Wang et al. performed experiments in a bubbling fluidized bed regenerator in order to determine the effect of temperature on calcination. In a case where the solids had a residence time of 70min the temperature varied from 1193K to 1293K [42]. It was observed that conversion to CaO was indeed dependent on the fluidized bed temperature. The magnitude of the effect however decreased as the temperature increased. In the same set of experiments the effect of the solids' residence time was also determined. The conversion to CaO proved to increase by increasing the average residence time in the reactor. The effect however was not in the same scale as the one of the temperature.

2.5 Mechanical and Chemical degradation of the sorbent

One of the disadvantages of the Calcium Looping process is the need for a make-up sorbent flow. This need derives from the mechanical and chemical degradation of the sorbent. The first manifests itself as attrition, where the particles break, the size decreases and a number of finer ones are produced and they are carried away by the cyclone. Chemical degradation on the other hand refers to the ability of the sorbent to capture CO_2 in the carbonator.

2.5.1 Particle attrition

In the calcium looping process particle attrition results in material loss from the circulation as the finer particles leave the cyclone along with the gas stream. This material loss, in addition to increasing the amount of the required make-up fresh sorbent flow, it also adds to sorbent deactivation [19]. While literature concerning attrition in the Calcium Looping process is limited, the material available about attrition in fluidized beds is abundant. The attrition mechanisms that have been identified are the following:

- Primary fragmentation
- Secondary fragmentation
- Attrition by abrasion

Primary fragmentation takes place immediately when the material is added to the reactor while operating at a high temperature, due to the thermal shock caused by the fast heating of the particles and due to internal overpressures caused from the CO_2 release from calcination and results in both coarse and fine particles. Secondary fragmentation and attrition by abrasion take place due to collisions among particles themselves and with the interior of the reactor. Secondary fragmentation results in generation of coarse particles while attrition by abrasion produces finer ones.

Attrition in fluidized bed systems leads primarily to a loss of bed material since the cyclones, which are mostly used for the collection of entrained material, are not able to keep the attrition-produced debris inside the fluidized bed system. The material loss through the cyclone is, therefore, usually taken as the attrition rate. This means that among the attrition mechanisms listed above, namely fragmentation and abrasion, it is abrasion which is the attrition mechanism of interest for fluidized bed systems [43]. In a fluidized bed system the main sources of attrition can be:

- The gas distributor at the bottom of the bed. The particles are entrained by the gas jets that exit the distributor and are accelerated at high velocities, resulting in impacts with the fluidized bed suspension.

- The motion created by the rising bubbles and their coalescence. This results in low velocity impact between the particles. In addition, the eruption of the bubbles at the top of the bed can also lead to stresses due high velocity impact between the particles.
- Cyclones. The cyclones are mainly used for gas-solid separation and the elutriated fines resulted from attrition leave the system. However, those fines are the sum of both the ones that initially entered the cyclone and fines that are actually produced inside it.

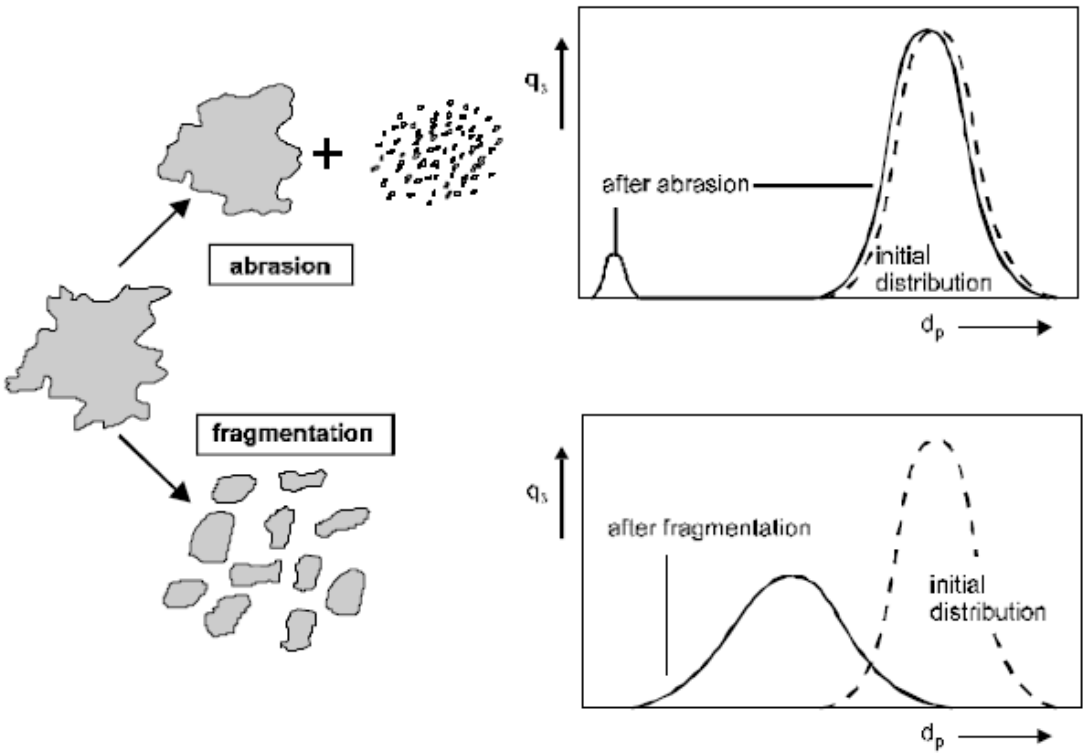

Figure 2.5: Schematic of attrition by fragmentation and attrition by abrasion [43]

Charitos et al. [23] in their experimental campaign showed that as the process goes on the number of fine particles increases, indicating attrition and sintering of the sorbent. The first is due to the high gas velocities that are present in a DFB environment while the second is due to the repeated carbonation-calcination cycles. Reduction of the particle size is important because it results in material loss, since fine particles do not continue the DFB loop but are collected in the cyclones and candle filters.

The factors affecting attrition in fluidized beds can be divided into 2 major groups. One of them is the properties of the material itself and the other is the process conditions [43].

Factors related to material properties: Apart from the type of the material used, which in this case is CaO and $CaCO_3$, the other major factor affecting mechanical degradation is the initial particle size distribution of the sorbent. Larger particles contain more faults than the smaller ones therefore they are more susceptible to breakage. This is why coarser particles tend to fragmentation while smaller ones have a higher inclination towards abrasion.

Depending on the **conditions of a process**, particle degradation can be caused by either stress that will be generated upon the individual particles of the material or the material's properties being affected. The stress may be a mechanical one due to compression, impact or shear, a thermal one owing to evaporation of moisture or temperature shock, or a chemical one by molecular volume change or partial conversion of the solid into the gas phase. In most cases a combination of these types will occur. The factors that will have to be dealt with in the scope of the current thesis are more likely to be the following:

- **Gas and solid velocity:** Higher gas velocities lead to stronger and more frequent interparticle collisions as well as collisions of particles with the reactor walls, therefore increasing the attrition rate of the sorbent. An example of the effect of gas velocity on particle attrition can be seen in a paper by Chen et al. [44] where it is shown that increasing the superficial gas velocity in a small circulating fluidized bed increases the attrition rate of the material as well as the generation of fine particles (<100μm). More specifically, the factor that appeared to matter the most was the squared excess gas velocity, namely the difference between the superficial gas velocity and the minimum fluidization velocity$\left(U - U_{mf}\right)^2$. More detail on this correlation will be provided in the results section.
- **Residence time of the solids:** The relation of particle attrition with the solids' residence time is generally non-linear. The extent of attrition is at higher levels initially and it falls off with time. The reason is most likely because the fresh particles are irregular in shape and contain a lot of faults, so as the particles break the edges and those faults are quickly knocked off and dealt with. As the process continues the particles become smoother and rounder in shape. An example of this can be seen in recent published work of Gonzalez et al. [45] in which the mean particle diameter of limestone was presented to reach a steady-state like phase after a few hours of operation.
- **Temperature:** The temperature under which the process is taking place can affect the mechanical stability of the material in 3 different ways: providing stress under thermal shock, changing the chemical properties of the material and changing the density of the gas. In general, at lower temperatures the particles become brittle and

easier to break. The phenomenon of lower temperatures leading to higher attrition rates can also be seen in experiments shown in published papers [44] [46]. In the frame of the calcium looping process however, the temperature at both reactors is relatively high, at approx. 600°C and 900°C in the carbonator and regenerator respectively, which means that the temperature-related mechanism most expected to affect particle degradation is the stress induced by thermal shock when cold particles enter the hot reactors.

- **Chemical Reaction:** The chemical reaction of particulate material that takes place in the bed generates stresses within the particle that can lead to fracture. In relation to the calcium looping process, the general consensus is that the reaction responsible for the bigger part of particle attrition and fines generation is the calcination that takes place in the regenerator [45].

2.5.2 Sorbent deactivation

The carbonation-calcination cycle happens multiple times and as the number of cycles keeps increasing it is shown that the maximum carbonation conversion (X_{max}) is reduced, ultimately reaching a practically constant value determining the sorbent's residual activity. According to literature, there are 2 main reasons for this to be happening. One is the closure of small pores during the carbonation, that do not reopen. The other reason is the sintering of the sorbent. In the context of the Calcium Looping process, sintering means change of the pore shape, pore shrinkage and grain growth. Sintering of the sorbent happens almost exclusively during calcination and increases at higher values of calcination temperature and residence time, as well as at high partial pressures of CO_2. Carbonation on the other hand has been found to have little to no effect on sintering of the particle [20] [47]. In experiments performed mentioned in literature, highly sintering environments (high CO_2 partial pressure, high calcination temperatures, presence of H_2O) have been proven to accelerate the decay of the sorbent's carrying capacity [20].

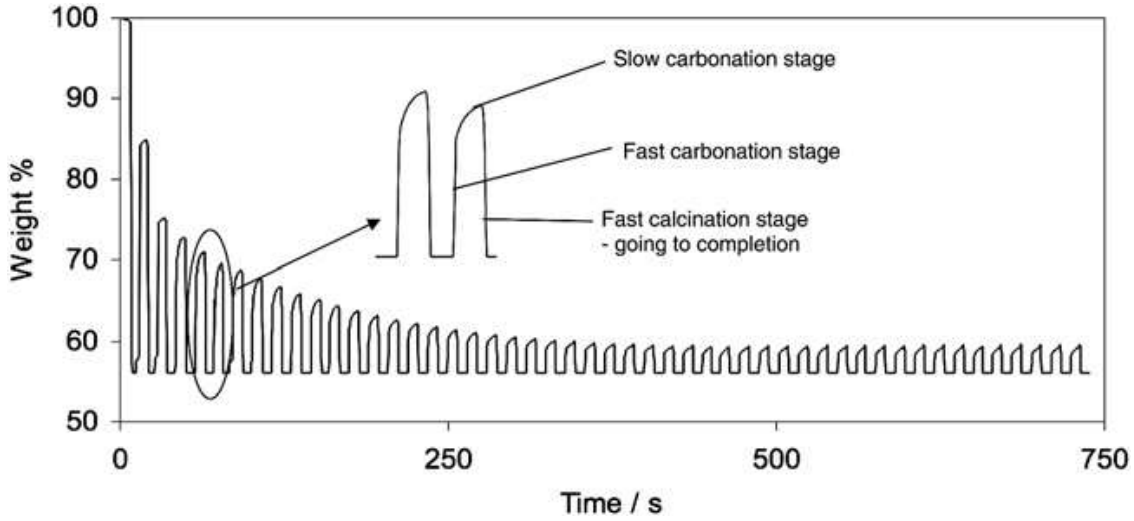

Figure 2.6: Repeated Carbonation-Calcination cycles in a TGA [20]

As it has been proposed, the trend of this decay for up to 500 cycles can be predicted by the equation proposed by [48]:

$$X_{max,N} = \frac{1}{\frac{1}{1 - X_R} + kN} + X_R \qquad \text{Eq. 2.16}$$

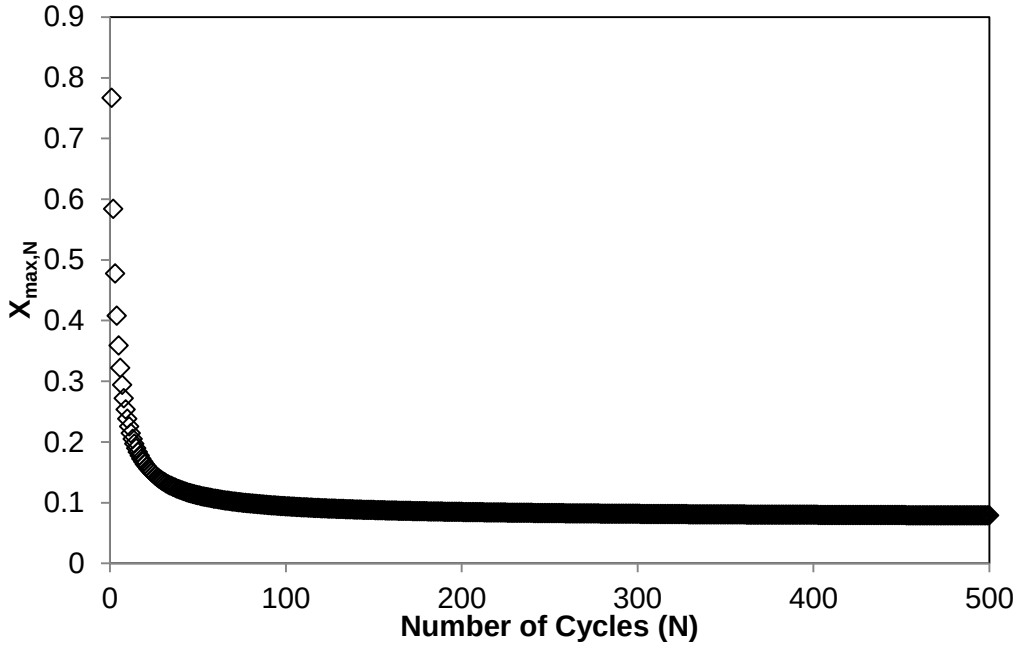

Figure 2.7: Maximum carbonation conversion ($X_{max,N}$) over 500 cycles for X_R=0,075 and k=0,52 [49]

This equation takes two factors into consideration. One is the rate of decay which is represented by the constant k and the other, X_R, is the residual activity, namely the value of X_{max} after a large amount of carbonation-calcination cycles. The constant k has been referred to as a link to sintering which the sorbent undergoes during calcination [20], therefore it is subject to change for different experimental conditions. In the aforementioned example the value of the k constant corresponds to a calcination temperature less than 950°C and a CO_2 inlet concentration of approximately 15%.

This deactivation effect is very important as it compromises the Calcium Looping Process's economic viability by requiring large sorbent purge and makeup rates [16]. Charitos et al., using data provided from experiments performed in IFK's $10kW_{th}$ facility, attempted to monitor the evolution of the maximum carbonation conversion under realistic conditions and continuous carbonation-calcination cycles [50]. Because the number of cycles is not easily distinguishable as in the case of TGA experiments, they expressed the X_{max} as a function of a parameter they called theoretical number of cycles (N_{th}). This parameter expresses the amount of times that the moles of CO_2 captured could carbonate the bed inventory up to its CO_2 carrying capacity (X_{max}).

A number of solutions however have been found in order to improve consecutive carbonation-calcination cycles as much as possible. Ronald Barker, who was the first to study the reversibility of the reaction and the sorbent's behavior after multiple cycles [51] proposed use of particles with a diameter less than 44nm. This however is not a feasible solution as very small particles can result in huge material losses from the cyclones [23]. The most promising method appears to be hydration of the sorbent [52] on an intermediate stage, just before reentering the carbonator reactor. Ramkumar and Fan showed that a sorbent undergoing liquid water or steam hydration after the calcination reaction will essentially restore its original activity as shown in Fig. 2.8.

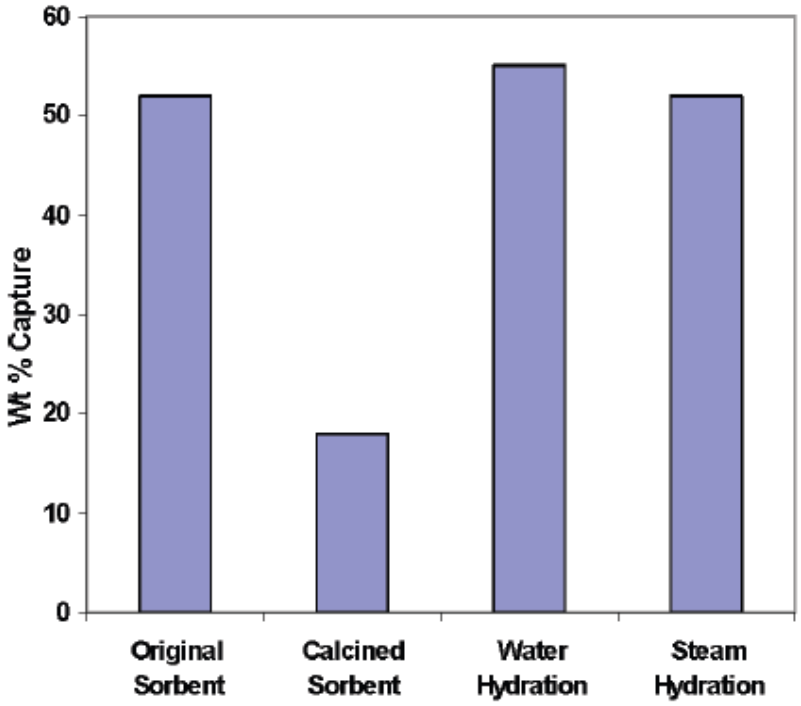

Figure 2.8: Effect of water and steam hydration on the sorbent's reactivity as presented by Ramkumar and Fan [52]

2.6 Mass Balance of the DFB system

The molar balance of Calcium Looping is demonstrated in Fig. 2.9. Before going into further detail it is important to review certain important values that characterize the sorbent which have already been proposed by and used in recent published work. Those values are the carbonate content of the material as it leaves the carbonator and the regenerator and are symbolized as X_{carb} and X_{calc} respectively. X_{carb} and X_{calc} indicate the fraction of the $CaCO_3$ that is contained in the CaO particles.

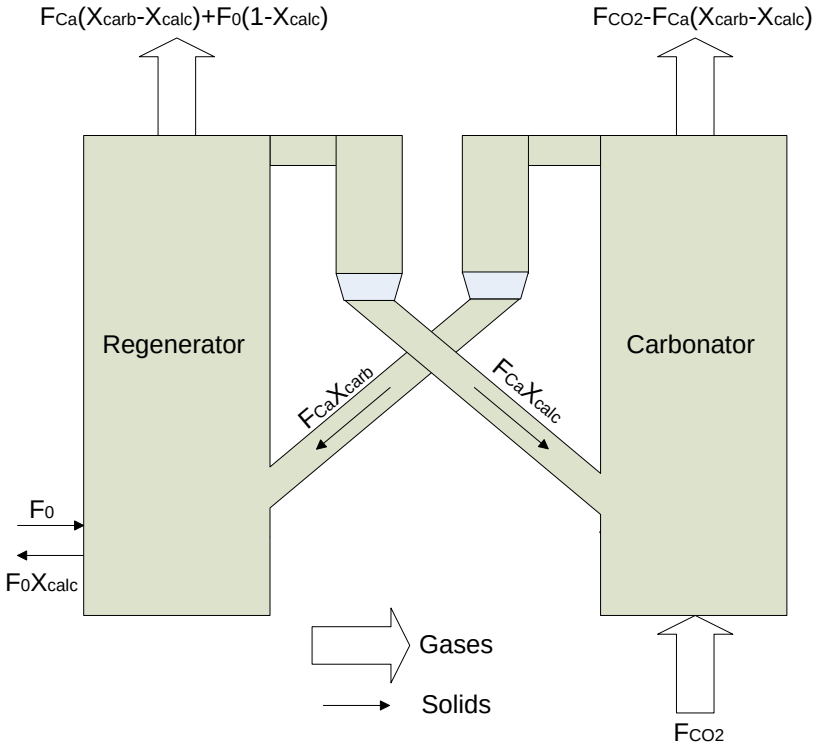

Figure 2.9: Illustration of the mass balance in a Calcium Looping schematic

The CaO in the carbonator adsorbs the CO_2 and a stream of flue gas is produced with a content in CO_2 equal to F_{CO2}-F_{Ca}(X_{carb}-X_{calc}). The fraction of the solids that is carbonated then enters the calciner ($F_{Ca}X_{carb}$) along with a stream of make-up fresh $CaCO_3$ in order to compensate for the sorbent's deactivation after multiple cycles. The mixture of carbonated CaO and fresh limestone are then calcined in the Regenerator releasing a flow of CO_2 equal to F_{Ca}·(X_{carb}-X_{calc})+F_0·(1-X_{calc}) and a stream of solids with a carbonate content of X_{calc} is then led back to the Carbonator.

The most significant means of evaluating the performance of the Carbonator is its CO_2 capture efficiency, which is defined by the ratio of the moles of CO_2 captured during the carbonation process to the total inlet flow of CO_2 and it is given by the equation below:

$$\mathrm{E_{CO_2}} = 1 - \frac{\mathrm{F_{CO2out}}}{\mathrm{F_{CO2in}}} \qquad \text{Eq. 2.17}$$

The regenerator performance is expressed through the regenerator efficiency (E_{reg}). The regenerator efficiency is defined by the ratio of the CO_2 released from each particle to the carbonate content of the particles entering the calciner. The E_{reg} is given in Eq. 2.11 based on the carbonation conversion of the incoming (X_{carb}) and outgoing (X_{calc}) sorbent in regard to the regenerator.

$$\mathrm{E_{reg}} = \frac{\mathrm{X_{carb}} - \mathrm{X_{calc}}}{\mathrm{X_{carb}}} \qquad \text{Eq. 2.18}$$

This practically means that the regenerator's efficiency is optimized when the X_{calc} is as close to 0 as possible. This would mean that the sorbent was fully calcined and all the CO_2 captured from carbonation along with the one in the fresh $CaCO_3$ was removed. If the X_{calc} is close to the value of the X_{carb} of the solids entering the calciner this would mean that the sorbent was not calcined at all.

For the carbonator mass balance to be satisfied the CO_2 removed from the gas phase must be equal to that adsorbed by the bed and equal to the increase of the moles of $CaCO_3$ after leaving the carbonator.
In mathematical terms this is expressed by Eq. 2.19:

$$F_{CO_2} E_{CO_2} = F_{Ca}(X_{carb} - X_{calc}) \qquad \text{Eq. 2.19}$$

3 Experimental Approach

3.1 Goal of the experiments

The goal of the experimental campaign was to determine the effect of CO_2 partial pressure and temperature on the efficiency of the regenerator, the impact on the CO_2 capture efficiency of the carbonator and the sorbent's performance regarding chemical deactivation and mechanical stability, i.e. attrition phenomena and losses. Under realistic conditions, the heat required for the calcination reaction will most likely be provided by oxy-combustion of coal, and to regulate the temperature flue gas recirculation will be required. This will result in the reaction taking place in a high CO_2 environment, at approx. 50-80 vol.-%. According to literature presented in the previous chapter, increasing the CO_2 partial pressure will worsen the calcination efficiency ($CaCO_3$ to CaO conversion) while increasing the temperature will be beneficial as long as it is kept below 950°C, since above that there are expected to be problems related to ash and sintering [34].

3.2 Description of the IFK 10kW$_{th}$ Dual Fluidized Bed Facility

The IFK 10kW$_{th}$ DFB facility consists of 2 Fluidized bed reactors, a CFB which is used as the Carbonator and a BFB which is used as the regenerator. It is known [53] that a pair of CFB reactors for the Calcium Looping process is the ideal setup; however this is a limitation imposed by the facility. The Carbonator is 12.4m high with a diameter of 71mm while the regenerator's diameter is 150mm. The required heat was supplied from electrical heaters and the temperature was controlled by N type thermocouples. The solid circulation rate between the beds was adjusted via a cone valve. The procedure goes as follows: A mixture of N_2 and CO_2 enter the carbonator (1) and the CO_2 reacts with the CaO in the CFB. The carbonated CaO then makes its way to the Regenerator (2) through the upper loop seal (6) which is controlled with the cone valve (5). The material is then calcined at 900-930^{o}C while being fluidized by a mixture of N_2 and CO_2 as well with the CO_2 partial pressure varying from 0% to 75%. The calcined material then circulates back to the Carbonator through the Overflow (7) which leads the material through the Lower Loop Seal (8). The gas exiting the carbonator is led to the Cyclones where it gets separated from solids and then goes through the Candle Filter and ultimately to the gas analyzer. The solids after being separated from the carbonator off-gas are led to the Upper standpipe and then to the upper loop seal where the opening of the cone valve dictates how much of it will be led to the BFB regenerator while the rest of it will return to the riser. The necessary gas flows for fluidization are supplied and controlled by MFCs. Multiple pressure and temperature sensors are spread from top to bottom of each reactor. Pressure sensors are also flushed with N_2, which will also be considered during the

evaluation of the results. The entire process was being monitored by the program Lab-View2011 which provides excel sheets containing all the raw data with all values being measured in 3 second intervals.

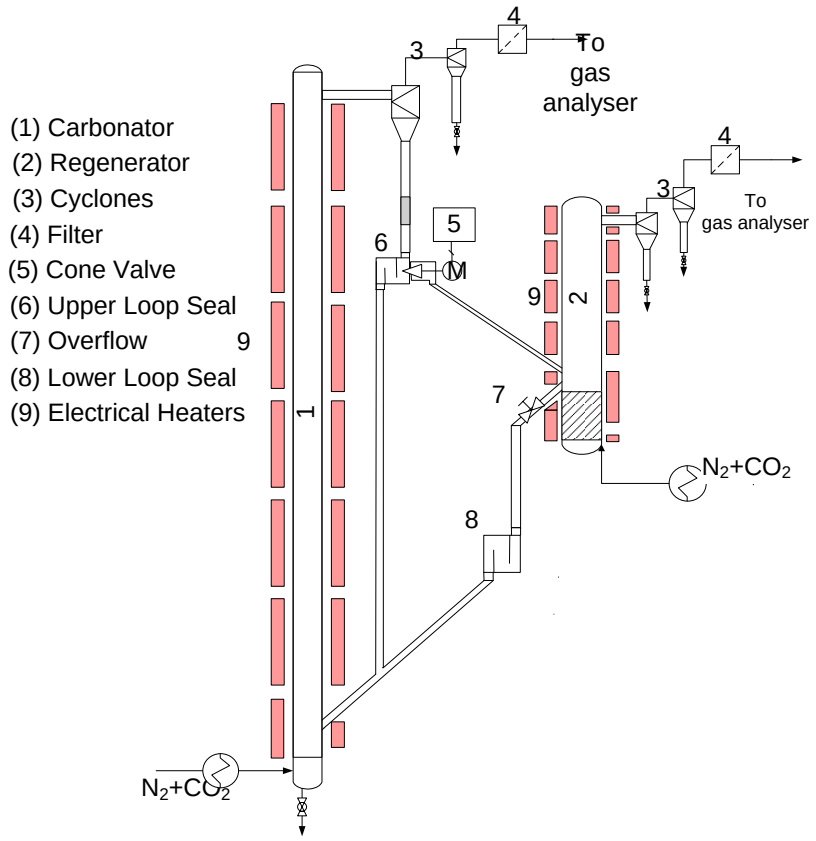

Figure 3.1: Schematic of the 10KW$_{th}$ Calcium Looping DFB facility in IFK

3.3 Materials

The limestone used for the experiment is originated from south Germany and its chemical composition is presented in the following table:

Table 3.1: Chemical composition of the limestone used for the experiments.

CaO	SiO_2	MgO	Al_2O_3	Fe_2O_3	Na_2O	TiO_2	CO_2
56,01	0,3	0,26	0,13	0,08	0,02	0,01	43,19

3.4 Experimental procedure

3.4.1 Procedure description

Heating up: The temperature in the reactors was raised slowly (approx. 100°C every 10min) using the LabView 2011 software, from room temperature to 900°C and 630°C in the case of the regenerator and carbonator respectively.

Solids: The limestone was always pre-calcined at 900^{o}C before being used for the experiments. The calcined material was fed to both reactors and standpipes adding up to a total of approx. 20kg. Afterwards the Upper Loop seal valve was opened in order to begin internal circulation in the carbonator. Once the carbonator was hydrodynamically stable the cone valve in the double-exit loop seal, as well as the butterfly valve used to isolate the regenerator from the carbonator would be opened and dual circulation would commence.

Gases: Initially, N_2 was introduced in both reactors and Loop Seals. After the solids procedure was completed and the reactors were coupled the inlet gas composition was changed to a N_2/CO_2 mixture for the carbonator and regenerator. The CO_2 inlet concentration in the carbonator was kept stable at 12% while in the regenerator it varied within the range of 0-75%.

3.4.2 Steady States

With dual operation in work and when the whole system had achieved hydrodynamic stability it was possible to start taking measurements. However, the gas phase data would not immediately stabilize to a new value as soon as parameters such as temperature or CO_2 inlet concentration, were changed. Measurements were only taken during Steady States. Steady State is defined as a period of time lasting at least 10 minutes for which the operational parameters such as gas phase variables (inlet and outlet CO_2 concentrations), reactor temperatures, solid circulation rate and pressures would remain stable. During each Steady State 2 samples from each reactor would be collected and the Calcium Looping rate would be calculated by measuring the circulation rate. One of the samples would be used to determine the carbonate content (X_{carb}) and maximum carbonation conversion (X_{max}) of the material that exited the carbonator and the carbonate content of the material that exited the Regenerator (X_{calc}). The other was used for Particle Size Distribution (PSD) analysis.

3.4.3 Experimental plan

The experimental campaign was planned in regards to determining the effect of CO_2 partial pressure and the regenerator temperature on the calcination reaction. For that to be achieved all parameters regarding the carbonator were kept as stable as possible. Those were the CO_2 inlet concentration, fluidization velocity, reactor temperature and calcium looping ratio. The latter however was not as easy to maintain as the rest of the variables. As stated above, it was controlled via the opening of the cone valve in the Upper Loop Seal, and in many cases it was required to be altered in order to maintain the hydrodynamic stability of the DFB system. Therefore, the steady states were achieved by mostly varying the desired parameters on the regenerator reactor, namely inlet gas composition and temperature. On each experimental day the first steady state was always at 0% CO_2 partial pressure. After this steady state was achieved the variables were changed as follows:

- CO_2 Partial Pressure: In order to increase the CO_2 partial pressure, we increased the CO_2 inlet flow via MFC while decreasing the N_2 flow accordingly so that the overall gas velocity remained unchanged. Steady states were taken at approximately 0, 12.5, 25, 37.5, 50, 62.5 and 75% CO_2 partial pressure.
- Temperature: In order to be able to determine the effect of temperature during the analysis of the results, steady states were taken with similar CO_2 inlet concentration but with higher or lower temperature. The planned temperature regions were 900°C and 930°C.

Table 3.1: Experimental plan table. a) Regenerator

Parameter	Value
T_{calc}	900°C; 915°C; 930°C
y_{CO2in}	0%; 12.5%; 25%; 37.5%; 50%; 62.5%; 75%
Space Time	0.6-1.1h
Solids' Residence time	5-9min
Fluidization Regime	Bubbling (~0.4m/s)

b) Carbonator

Parameter	Value
T_{carb}	630°C
y_{CO2in}	12%
Space Time	0.35-0.6h
Solids' Residence time	5-6min
Fluidization Regime	Fast (~6m/s)

3.4.4 Measured Parameters

- Temperature

The temperature in the reactors was measured with and controlled by N type thermocouples.

- Pressure

The pressure was measured at many different points across the height of the carbonator, the regenerator and each of the 2 standpipes.

- Gas Outlet

The carbonator outlet gases were measured with an ABB Advance Optima 2020 analyzer while for the regenerator an ABB Easy Line 3020 analyzer was used.

- Velocity-Fluidization regime

All gas flows were measured and controlled with Mass Flow Controllers (MFCs). The gas velocity in the regenerator which operated under the bubbling regime was 0.6m/s or 4Nm^3/h while the in the carbonator which operated under the fast fluidization regime it was approx. 5.8m/s or 18Nm^3/h.

The flows in the Upper and Lower loop seal were 30lpm and 15lpm respectively.

- Circulation Rate

The circulation rate was controlled by a cone valve and was measured manually with the following method: The solid flow was stopped by closing a butterfly valve after the exit of the upper loop seal and measured the time the sorbent took to fill up a specific volume and that time was used to calculate the circulation rate.

3.4.5 Basic Calculated Parameters

- Bed Mass

The Bed Mass is calculated by the pressure drop between the top and bottom of each reactor with the following formula:

$$m = \frac{\Delta P \cdot \pi \cdot d^2}{4 \cdot g} \qquad \text{Eq. 3.1}$$

Where ΔP is the pressure drop, d is the diameter of the reactor and g the acceleration of gravity.

- Residence Time

The residence time in the regenerator is the ratio of the bed mass (kg) to the solid circulation rate (kg/h) and it is measured in minutes:

$$t = \frac{m}{F_{CaO} \cdot 60}\,[\mathrm{min}] \qquad \text{Eq. 3.2}$$

- Calcium Looping Ratio

The Calcium Looping Ratio is defined as the fraction of molar flow of Ca (F_{Ca}) and CO_2 (F_{CO2}) in mol/h (F_{Ca}/F_{CO2}). High Looping ratios result in massive energy costs as more heat will be required to calcine the circulating sorbent thus the amount of fuel consumed in the oxy-fuel combustor which provides this heat will be significantly increased.

- CO_2 capture efficiency

The CO_2 capture efficiency of the carbonator is defined as the molar fraction of the difference CO_2 outlet flow minus CO_2 inlet flow to the CO_2 inlet flow as shown in Eq. 3.3:

$$E_{CO2} = \frac{F_{CO_2,in} - F_{CO_2,out}}{F_{CO_2,in}} \quad \text{Eq. 3.3}$$

- Regenerator efficiency

The efficiency of the regenerator is calculated based on the amount of CO_2 released from the carbonated CaO that comes from the carbonator normalized by the carbonate content of the incoming material. It is defined as shown by Eq. 3.4:

$$E_{reg} = \frac{X_{carb} - X_{calc}}{X_{carb}} \quad \text{Eq. 3.4}$$

- Space time

For both reactors a characteristic space time parameter was used. For the carbonator reactor that space time is defined by the ratio of the moles of CaO present in the reactor to the CO_2 flow as shown in Eq. 1.6. In the case of the regenerator the space time is defined as the ratio of the residence time of the solids in the reactor to the carbonate content of the incoming sorbent from the carbonator and it is given by Eq. 3.5:

$$\tau_{reg} = \frac{t_{reg}}{X_{carb}} \quad \text{Eq. 3.5}$$

3.4.6 Sampling

Samples were collected after each steady state from the upper and lower loop seal and were given for TGA and PSD analysis.

- TGA analysis

The carbonate content of the samples was measured with a TGA at IFK laboratory. In order to determine the X_{max} of the samples we used a TG analyser developed by the IFK in cooperation with the company Linseis Thermal Analysis. 10mg of each sample was placed in the TGA and they underwent a full calcination-carbonation cycle. The calcination occurred under 850^{o}C and a gas flow of pure N_2. The amount of CO_2 released after that calcination determined the carbonate content of the material leaving the Carbonator (X_{carb}) or of the material leaving the regenerator (X_{calc}) depending on the sample, in order to confirm the results pro-

vided by the aforementioned TGA analysis and make sure that the sample is representative of the respective steady state.

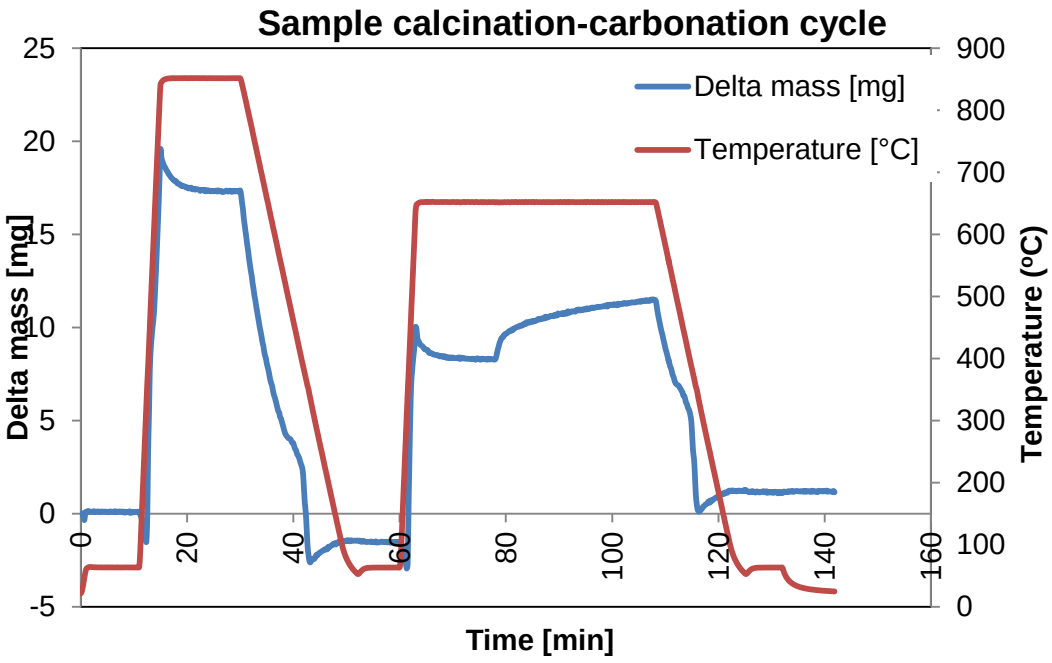

Figure 3.2: Example of a Carbonation-Calcination cycle of a carbonator sample in the TGA. Calcination under 850°C and 0% CO_2 and Carbonation under 650°C and 10% CO_2.

The carbonation was performed under a temperature of 650°C and a mixture of N_2 and CO_2. The fast reaction region was used to determine the maximum carbonation conversion of the material leaving the carbonator. As a demonstration of the method used to estimate the X_{max} is presented in Figure 3.3. The sample in question shows an X_{max} of approximately 13%

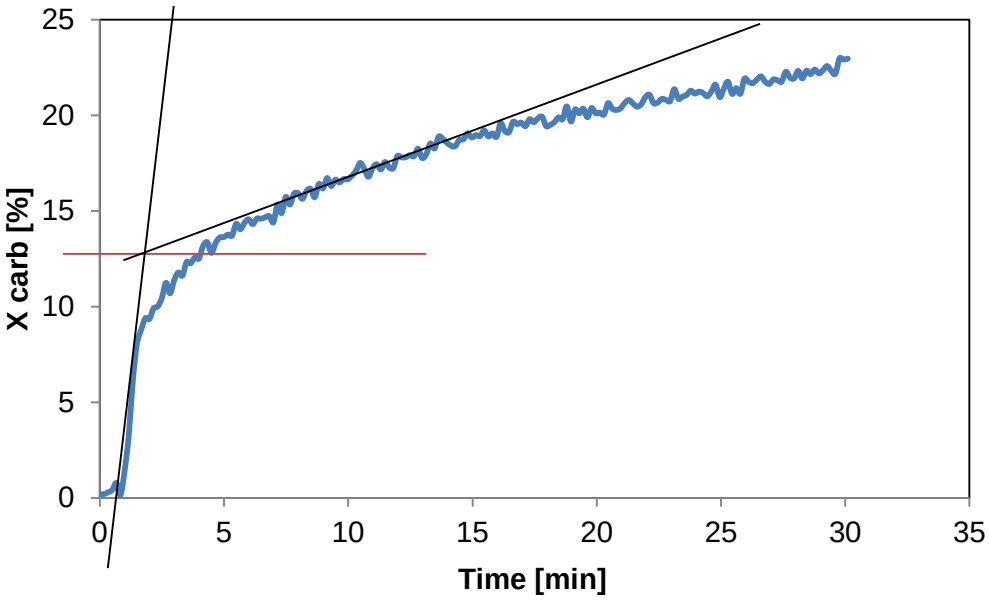

Figure 3.3: Example of X_{max} calculation of a ULS sample right after TGA analysis

- PSD analysis

Particle Size Distribution analysis was performed by the method of Sieve Analysis in IFK. The PSD is of high importance because it is used to determine the particle attrition and sintering effects. Particle attrition results in generation of fine particles which are carried away by the flue gas in the cyclone thus requiring more fresh make-up material.

4 Results and discussion

In this chapter the analysis of 20 steady states achieved in this experimental campaign will be presented. This will include both reactors' performance, namely the calcination efficiency in the regenerator as well as the CO_2 capture efficiency, and the performance of the sorbent in terms of chemical degradation and mechanical stability. The carbonator's capture efficiency is evaluated through the parameters of Calcium Looping Ratio, Space Time, and Active space time, while the regenerator's efficiency will be correlated to CO_2 concentration inside the reactor, Space Time, Active Space Time, reactor temperature and residence time of the solids. It must be noted here that the CO_2 concentration that was used to characterize the regenerator is the sum of both the CO_2 introduced via MFC and the CO_2 released from solids during calcination.

4.1 Data validation

The first step after receiving the results from the experiment as well as the ones from sample analysis was to close the mass balance in order to test their validity. In order for the mass balance of the carbonator to close the criteria which need to be met is the CO_2 captured in the carbonator being equal to the CO_2 released in the regenerator.
This is represented by Eq. 4.1:

$$\mathrm{F_{CO_2}} \cdot \mathrm{E_{CO_2}} = \mathrm{F_{Ca}} \cdot (\mathrm{X_{carb}} - \mathrm{X_{calc}}) \qquad \text{Eq. 4.1}$$

$\mathrm{F_{CO_2}} \cdot \mathrm{E_{CO_2}}$represents the amount of CO_2 captured where F_{CO2} is the molar flow of CO_2 entering the carbonator and E_{CO2} is the Carbonator capture efficiency, namely the percentage of CO_2 captured in the reactor and $\mathrm{F_{Ca}} \cdot (\mathrm{X_{carb}} - \mathrm{X_{calc}})$ represents the amount of CO_2 released from the solids in the regenerator where $\mathrm{F_{Ca}}$ is the molar flow of the sorbent entering the regenerator and $\mathrm{X_{carb}}$ and $\mathrm{X_{calc}}$ the carbonate content of the solids exiting the carbonator and regenerator respectively.

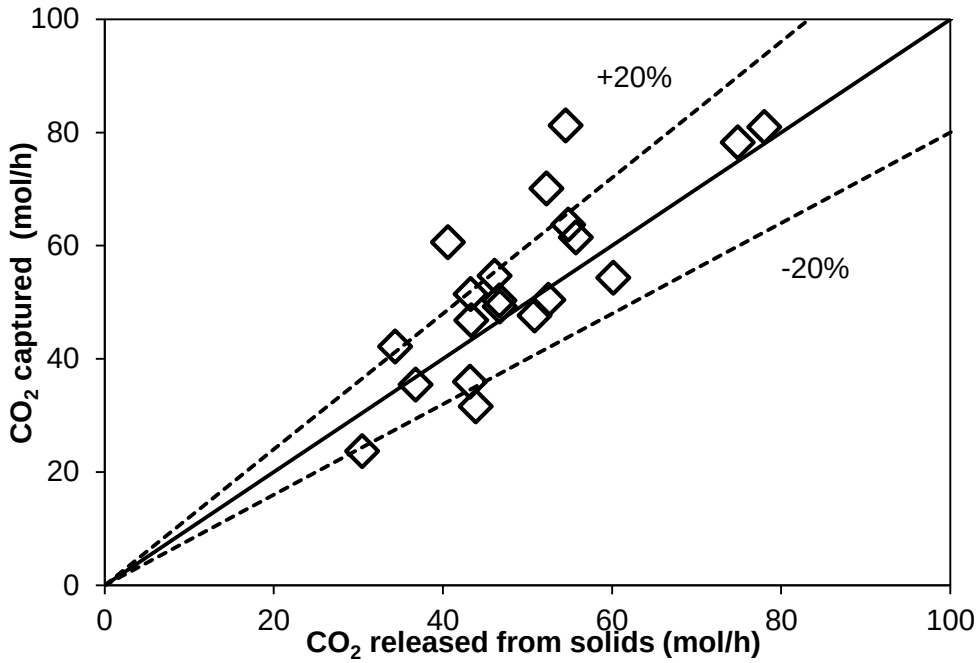

Figure 4.1: Mass balance closure in the carbonator [54]. The CO_2 inlet concentration was 12% and the carbonation temperature was 630°C.

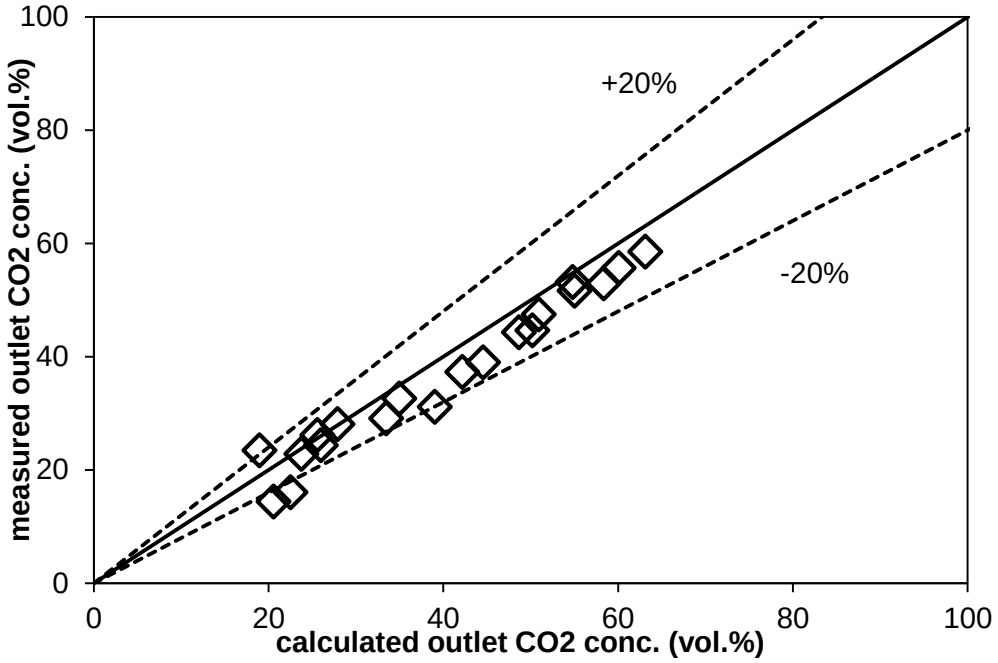

Figure 4.2: Mass Balance closure in the Regenerator [54]. The CO_2 inlet concentration ranged from 0-75% and the calcination temperature ranged from 900-930°C.

In order to validate the mass balance closure in the regenerator we calculated the molar flow of CO_2 that was released from the calcination reaction as shown in Eq. 3.4 and 3.5. This value was compared to the CO_2 outlet concentration given by the gas analyzer. As it can be

seen in Figure 4.1 and Figure 4.2 the mass balance closes successfully for our experimental results. There is only a small fraction of the experimental points that appears to be outside the acceptable range and this can be addressed to errors during sampling or measurement of the circulation rate as well as during analysis of the sorbent.

4.2 Example of a Steady State

In fig 4.3 we can see a diagram showing a steady state in terms of CO_2 concentrations and reactor temperatures. The steady state presented in figure 4.3 has a mean CO_2 capture efficiency of approximately 78% and a regenerator efficiency of 80% for a looping ratio of 5.8 and space time of 0.75h. . The experimental results presented in this topic have been derived from studying 20 10-minute long steady states without any effects from presence of steam, sorbent make-up flow or presence of SO_2.

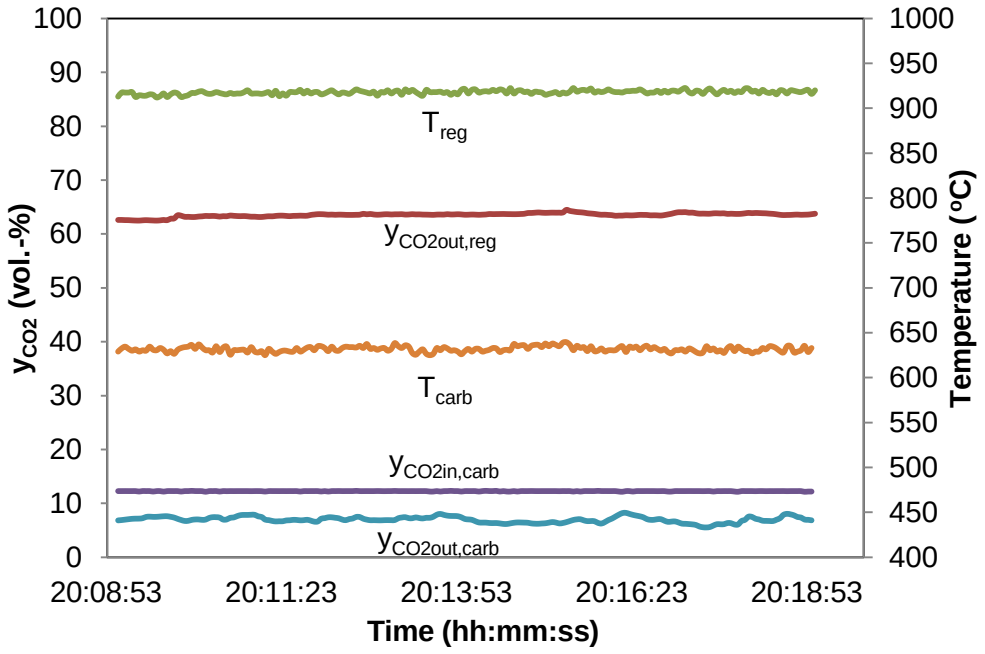

Figure 4.3: Steady state example.

In figures 4.4 and 4.5 we can see the temperature and pressure profile in the carbonator reactor and the pressure profile and CO_2 inlet & outlet concentrations in the regenerator reactor for the first steady state. From the pressure profile in figure 4.4 we can observe from the high pressure indications that the lower parts of the reactor contain the majority of the sorbent. According to previous work regarding this specific facility a different pressure profile is expected [55]. The difference can be addressed to malfunction of the measuring instrument. After the dense region, which corresponds to the bottom 3 meters where the most amount of the material is located, we expect a lean-core annulus region with a steady decline of pres-

sure until it reaches the top of the reactor where the pressure drop becomes zero. As far as the temperature profile is concerned, we can see that for the first 4 meters the temperature is considerably higher, due to the most of the carbonation reaction taking place there. As shown in Eq. 1.2, the carbonation is an exothermic reaction, releasing heat and thus resulting in higher temperature readings.

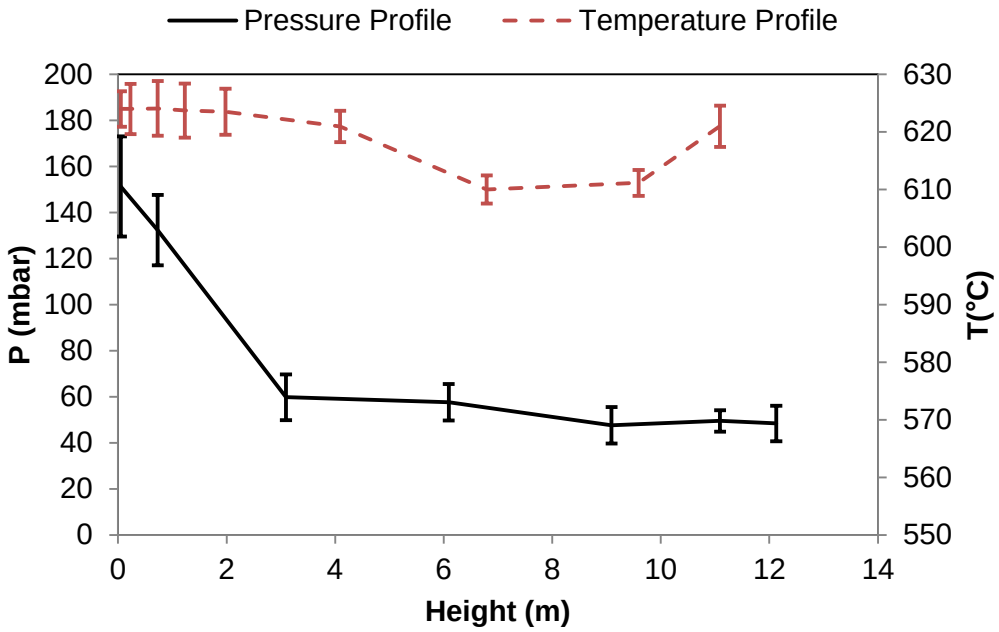

Figure 4.4: Pressure profile of the carbonator of the Steady State shown in Figure 4.3. Pressure drop (ΔP) is plotted against the reactor height. Inlet y_{CO2} in the regenerator is 0% and the calcination temperature is 900°C

By observing the regenerator's pressure profile in figure 4.5 we can see that the majority of the material resides at the bottom of the reactor, filling up to about 1.5m. This is to be expected because this is a bubbling fluidized bed and the gas velocities are just above the minimum fluidization velocity. Unlike the Carbonator which operates under the fast fluidization regime, in the Regenerator a core-annulus region is not to be expected.

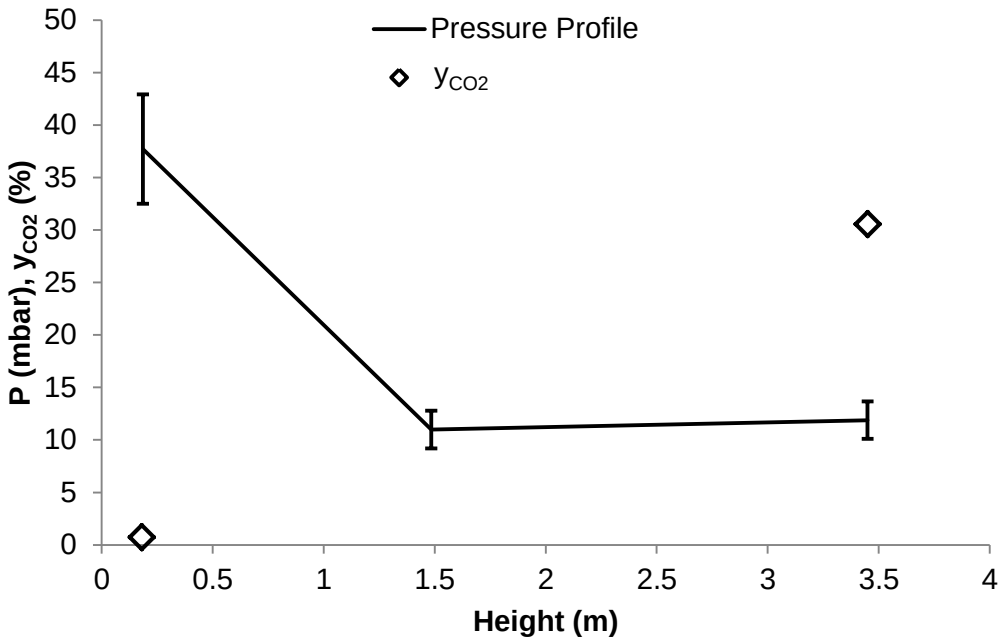

Figure 4.5: Pressure profile of the regenerator of the Steady State shown in Figure 4.3. Pressure drop (ΔP) is plotted against the reactor height. The y_{CO2} is also shown at the bottom and exit of the reactor.

4.3 Carbonator analysis

In this section the analysis of the data regarding the carbonator is presented. The capture efficiencies achieved were in the range of 35-80%.

4.3.1 Effect of Active Space Time

As part of the carbonator analysis we compared the experimental results with the model that has been proposed in by Charitos et al. [50] According to this model, the CO_2 capture efficiency of the reactor can be predicted as a function of active space time (τ_{active}) by knowing the kinetic characteristics of the limestone used, i.e. a kinetic constant derived from TGA, the carbonation temperature and the CO_2 inlet concentration in the reactor. This approach assumes that only a fraction of the particles in the carbonator are reacting in the fast regime, symbolized as f_{active}. Those particles have a residence time less than t* which is the time needed for the X_{calc} of the particles to reach the X_{max}. After this time, the reaction rate becomes zero. For residence time values lower than t* the reaction rate is given by Eq.4.2:

$$\left(\frac{dX}{dt}\right) = k_s \varphi X_{max}\left(\overline{V_{CO_2}} - V_{eq}\right) \qquad \text{Eq. 4.2}$$

In order to determine the limestone's kinetic constant k_s, the samples taken from the carbonator underwent TG analysis during which they were fully calcined and then carbonated again under 10% CO_2 inlet concentration and 650°C. This way we were able to determine the X_{max} graphically, as shown in the experimental section. The slope of the curve (dX/dt) until the

conversion to $CaCO_3$ reached the X_{max} was used in order to derive the value of the kinetic constant k_s using Eq. 4.3:

$$k_s = \frac{\frac{dX}{dt}}{X_{max}\left(\overline{V_{CO_2}} - V_{eq}\right)} \ [s^{-1}] \qquad \text{Eq. 4.3}$$

The k_s derived for the limestone used was $0.33s^{-1}$. On the other hand, φ is an effective fitting constant of the experimental data with the model equation. This factor has already been derived equal to 0.8 from previous work [50] indicating great gas-solid contacting in the CFB reactor. This results in a $k_s\varphi$ value of $0.264s^{-1}$.

Using Eq. 2.1 to calculate the reaction rate we can express the E_{CO2} using the mass balance of the reactor:

$$F_{CO_2}E_{CO_2} = \frac{dX}{dt}n_{Ca} \rightarrow E_{CO_2} = k_s\varphi f_{active}\tau X_{max}\left(\overline{V_{CO_2}} - V_{eq}\right) \qquad \text{Eq. 4.4}$$

The expression of Eq. 4.4 has the important advantage of correlating the average activity of the carbonator solids with their residence time distribution in the bed. This is because the fraction of active particles, f_{active}, reacting in the fast reaction regime corresponds to the fraction of particles with a residence time below a critical reaction time t* which is the time needed for the particles to increase their carbonate content from X_{calc} to X_{max}. The f_{active} and t* are given by the following equations:

$$f_{active} = 1 - e^{-\frac{t^*}{n_{Ca}F_{Ca}}} \qquad \text{Eq. 4.5}$$

$$t^* = \frac{X_{max} - X_{calc}}{k_s\varphi X_{max}\left(\overline{V_{CO_2}} - V_{eq}\right)} \qquad \text{Eq. 4.6}$$

Furthermore, the active space time was defined as the product of space time (τ), f_{active} and the maximum carbonation conversion X_{max} as shown in Eq. 4.7.

$$\tau_{active} = \tau X_{max} f_{active} \qquad \text{Eq. 4.7}$$

Thus, Eq. 4.4 is written as follows:

$$E_{CO_2} = k_s\varphi\tau_{active}\left(\overline{V_{CO_2}} - V_{eq}\right) \qquad \text{Eq. 4.8}$$

Space time, as mentioned earlier is defined as the ratio of molar inventory in the carbonator to the CO_2 molar flow in the reactor and expresses the bed inventory for a specific F_{CO2}. For a specific carbonator reactor operating at given fluidization conditions, limestone type, temperature, and inlet CO_2 vol.-% the active space time is the single parameter determining the CO_2 capture efficiency, as shown in eq. 4.8. With the goal of validating this model with the experimental points acquired, the following figure is presented.

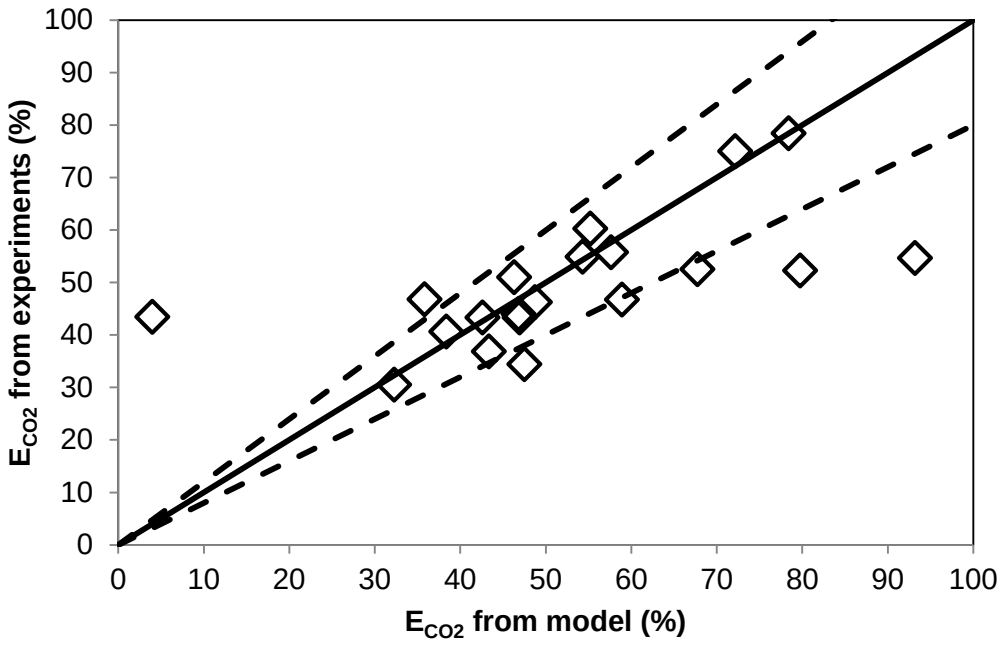

Figure 4.6: Model validation via mass balance. Carbonator conditions: Temperature: 630°C, y_{CO2in}: 12%. Regenerator conditions: Temperature: 900-930°C, y_{CO2in}=0-75%

Figure 4.6 depicts the CO_2 capture efficiency resulted from our experimental points vs. the one predicted from the model presented in eq. 4.8. As it can be seen, most of the points fit the balance within acceptable error. There is one point deviating from the norm by an unacceptable margin which can be justified by errors during sampling and TGA analysis because it presents a value of X_{calc} as high as 11%, which would imply that the material was not calcined at all in the regenerator. This is false because according to the experimental values the CO_2 capture efficiency of this steady state was at approximately 42% which would have been nearly impossible if the material had not been previously calcined. This successful mass balance closure means that the Eq. 4.4 is fulfilled to a satisfactory extent thus validating the constant k_s and φ values used.

In figure 4.7 we can see the E_{CO2} plotted vs. the active space time.

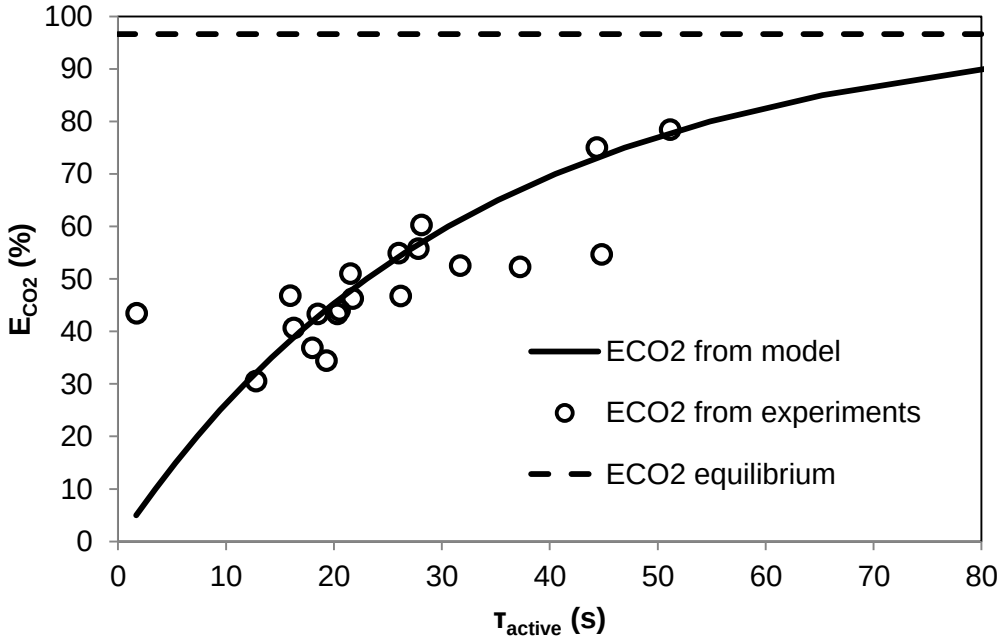

Figure 4.7: Capture efficiency plotted vs. Active Space Time as resulted from the experiments and as predicted from the model. Carbonator: 630°C, y_{CO2in}=12%. Regenerator: 900-930°C, y_{CO2in}=0-75%

The continuous line represents the E_{CO2} predicted by the model whereas the circles represent the experimental points. It can be once again observed that the experimental results and the model are in good agreement. It is also apparent that the CO_2 capture efficiency of the reactor increases with the increase of active space time, confirming it as a characteristic carbonator parameter. It is important therefore to have a better understanding of what this parameter means in terms of designing a carbonator reactor. Apart from the X_{max}, the maximum carbonation conversion of the sorbent which will be more or less defined by the material, the active space time is going to be dependent on the space time and f_a, which are both linked to the residence time of the sorbent in the reactor, and therefore the reactor's inventory, as well as the looping ratio. As an example, in order to achieve a capture efficiency of 85% a critical value of active space time is observed, which is approximately 60s or 0.017h. This means that in order to design a facility where the goal is at least 85% CO_2 capture efficiency it should be designed so that the looping ratio and the residence time of the solids inside the reactor are high enough for the active space time to be at least 0.017h.

4.3.2 Calcium Looping Ratio

The Calcium Looping Ratio is a very important parameter since it is directly correlated to O_2 consumption in the regenerator and therefore drastically affects the cost. For this reason it is important to confirm its impact on the CO_2 capture efficiency. It has previously been shown [23] that the looping ratio has a significant effect on E_{CO2}, namely increasing the F_{Ca}/F_{CO2} results in an increase of the capture efficiency of the carbonator. While in the current experimental campaign the aim was to maintain stable low values of looping ratio, varying it proved inevitable in order to achieve hydrodynamic stability. This variation was achieved by increasing or decreasing the opening of the cone valve in the upper loop seal.

In Figure 4.8 we can see the normalized capture efficiency plotted vs. the Calcium Looping ratio in 3 cases: The first case corresponds to data from a previous experimental campaign run by Charitos et al. where calcination took place under air-fired conditions [23]. The 2nd and 3rd case correspond to our experimental points for low CO_2 and high CO_2 conditions respectively. In all those cases the space time of the carbonator is within the range of 0.42-0.52h.

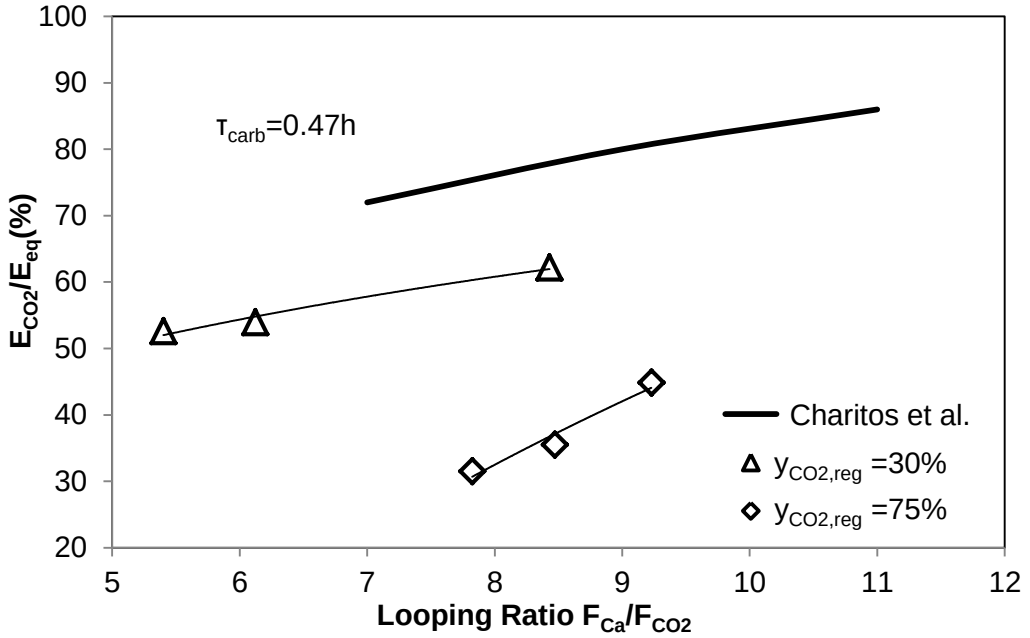

Figure 4.8: Normalized CO_2 capture efficiency plotted vs. the Calcium Looping Ratio. Carbonator: 630°C, y_{CO2in}=12%. Charitos et al. case [23]: Carbonator: 660°C, y_{CO2in}: 15%. Regenerator: 850°C, y_{CO2in}=30%.

In all cases it can be seen that the trend shows an improvement of the CO_2 capture efficiency of the carbonator. This physically means that as the circulation rate of the sorbent increases, assuming that there is a constant flow of CO_2 in the flue gas entering the carbonator, so does the capture efficiency of the reactor. Consequently, the regenerator will have a larger flow of $CaCO_3$ to calcine and will need more fuel to combust, as well as more oxygen which will increase the costs associated with the ASU.

We can observe that the highest efficiencies are achieved in the first 2 cases in which regeneration of the sorbent took place under low CO_2 conditions and the lowest efficiencies are presented in the high CO_2 case. It is known from the mass balance equation that due to the term (X_{carb}-X_{calc}), the CO_2 capture efficiency can be affected by the degree of calcination in the regenerator. This can be seen in case 3 where, as shown in the regenerator analysis, high CO_2 partial pressures result in a lower degree of calcination, lowering in turn the capture efficiency of the carbonator.

4.4 Regenerator Analysis

In this section the aspects of the BFB regenerator reactor are investigated where the effects of altering operating conditions such as CO_2 partial pressure, temperature and residence time are shown. In addition to those, the attempt of modeling the reactor based on work published by Martinez et al. [34] is discussed.

4.4.1 Effect of Space Time

A regenerator operating in a DFB Calcium Looping system is different to a standalone reactor. This is because the solids entering the CaL regenerator come from the carbonator and their carbonate content is within the range of 10-18%. For this reason the parameter of space time (τ_{reg}) was used to characterize the reactor. This parameter is defined as the ratio of the residence time of the solids in the reactor to the carbonate content of the sorbent entering the regenerator as seen in Eq. 3.8. This way we can successfully correlate the reactor's efficiency to the quality of the sorbent as well as the residence time of the material, which has an impact on the reactor's dimensions since for higher residence times a larger reactor will be needed. Practically the regenerator space time suggests the amount of time a material of a certain achievable X_{carb} will need to spend in the regenerator in order to achieve the desired calcination efficiency.

In Figure 4.9 we can see the efficiency of the regenerator plotted vs. the space time for 3 different cases: an air-fired case from a previous experimental campaign (Data were obtained from the experiment described in [56]) where the CO_2 inlet concentration was 30% and 2 different cases from the experiments carried out for this Thesis, a low CO_2 case where the CO_2 concentration is approx. 30% and a high CO_2 case where the CO_2 concentration was around 65%.

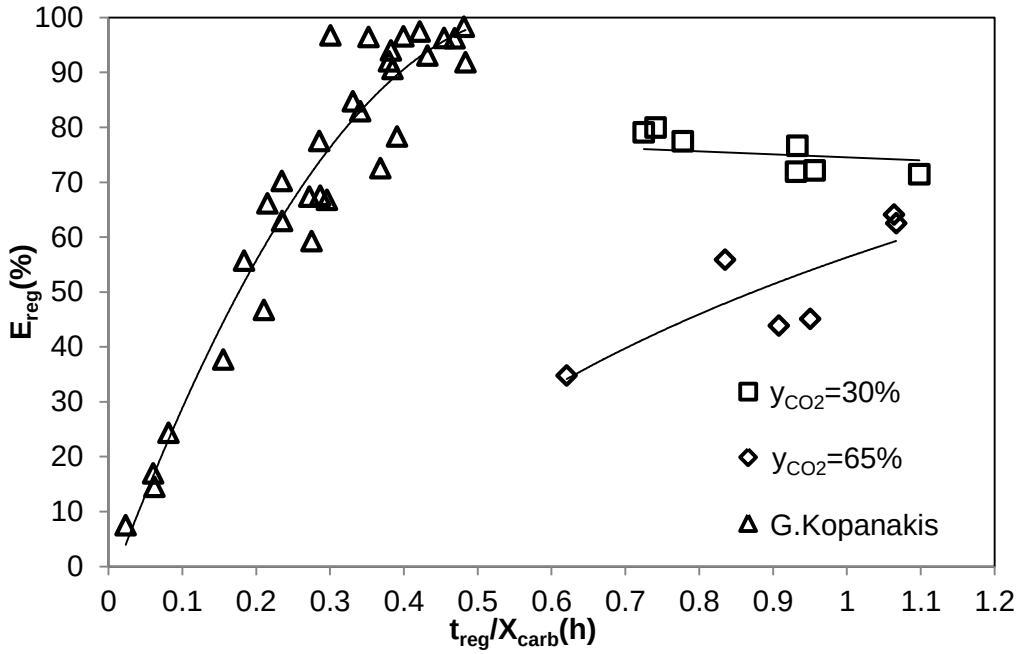

Figure 4.9: Reg. efficiency plotted vs. reg. space time (t/X_{carb}). G. Kopanakis case [56]: Carbonator: 630-700°C, y_{CO2in}: 15%. Regenerator: 900°C, y_{CO2}=30%.

We can see that the increase of space time appears to have a positive effect on the regenerator's efficiency. This practically means that in order to achieve high calcination efficiencies for a material with a high CO_2 capture capacity the solids need to remain for a longer time in the regenerator, thus requiring a larger reactor. Taking one of the last 2 points of the high-CO_2 case as an example, for a sorbent with a residual activity of 11%, in order to reach 65% calcination efficiency, the material will need to have a residence time in the reactor of approximately 7 minutes. This information can be used to estimate the size of the reactor required. It is important to note here that 7 minutes of residence time would be an absurdly large number in a realistic situation at an industrial scale. As explained below however, there were limitations imposed by the facility which kept the regenerator efficiency at consistently lower values and this lead to requiring higher residence times in order to achieve a better calcination.

If we compare the 2 sets of data from our experiment we can observe that in the air-fired case where the CO_2 inlet concentration is within the 0-25% range the calcination efficiency is higher than the one in the 50-60% case, which comes in accordance to previous literature

with the fact that an increased CO_2 partial pressure will result in lower calcination efficiencies. This means that for high CO_2 conditions a higher space time is required in order to reach the same level of efficiency as in low CO_2 conditions.

Finally, an important observation can be made by comparing the 2 experimental campaigns. In the case of [56] it is seen that the efficiency of the calciner is much higher for lower values of space time and ultimately reaches the levels of 100% for a space time as low as 0.4h while in both sets of our data the regenerator's efficiency appears to hit a limit at approx. 75-80% in one case and 60% in the other. This can be explained by the low gas velocities in order to operate under the bubbling fluidization regime, in contrast to the turbulent fluidization regime that was used for the previous experimental campaign. As we can see the turbulent fluidization regime allowed for calcination efficiencies very close to 100%, meaning that the material leaving the regenerator had little to no $CaCO_3$ content, while the carbonate content of the material at the regenerator's exit under bubbling fluidization was relatively high as the bubbling bed appears to be allowing higher local values of P_{CO2} within the reactor, since even with an inlet gas with low CO_2 complete calcination could still not be achieved. Another reason for the lower calcination efficiencies can be the quality of heat provided by the electrical heaters, as it appears that there were temperature differences in the different areas of the bed. In contrast, in the previous experimental case CH_4 combustion took place which provided heat of better quality, in addition to introducing some steam (H_2O) in the reactor which is known to be beneficial to the calcination reaction. Lastly, as seen in table 2.1 the temperature gradient in the case of a bubbling fluidized bed is very small, which means that the temperature changes at a relatively smaller rate within the bed. Especially in the low CO_2 case we can see that all the points are in the 70-80% area even under favourable conditions. For this reason we assume that in this low-CO_2 case we achieved the maximum regenerator efficiency allowed by this experimental setup. However, we do not have the actual curve due to lack of experimental points in lower space times.

4.4.2 Effect of CO_2 concentration

CO_2 partial pressure is a significant factor that affects the calcination reaction and studying this effect is very important since in realistic scenarios the CO_2 concentration will be at the levels of 50-80 vol. % [27]. This is due to the oxy-fuel combustion needed to provide the temperature required to carry out the calcination reaction and the CO_2 recirculation associated with it. A large amount of studies recorded in the literature has shown that higher CO_2 partial pressure inhibits the calcination reaction [47], [34], [36] - [39]. In figure 4.12 we can see the E_{reg} plotted vs. the CO_2 concentration of the gas inside the BFB reactor. As explained

in the experimental section, E_{reg} is the regenerator efficiency, i.e. the fraction of the CO_2 captured in the carbonator which was released in the regenerator given by Eq. 3.4. As expected from literature, the CO_2 released from calcination shows a clear decline with the increase of CO_2 partial pressure in the regenerator.

Figure 4.10 depicts the regenerator efficiency as the CO_2 concentration increases for a space time of 0.91h and a calcination temperature of 910°C. It can be seen that the regeneration efficiency decreases from an initial 78% at 30% CO_2 concentration to approximately 30% as the CO_2 concentration reaches the levels of realistic Oxy-fuel conditions.

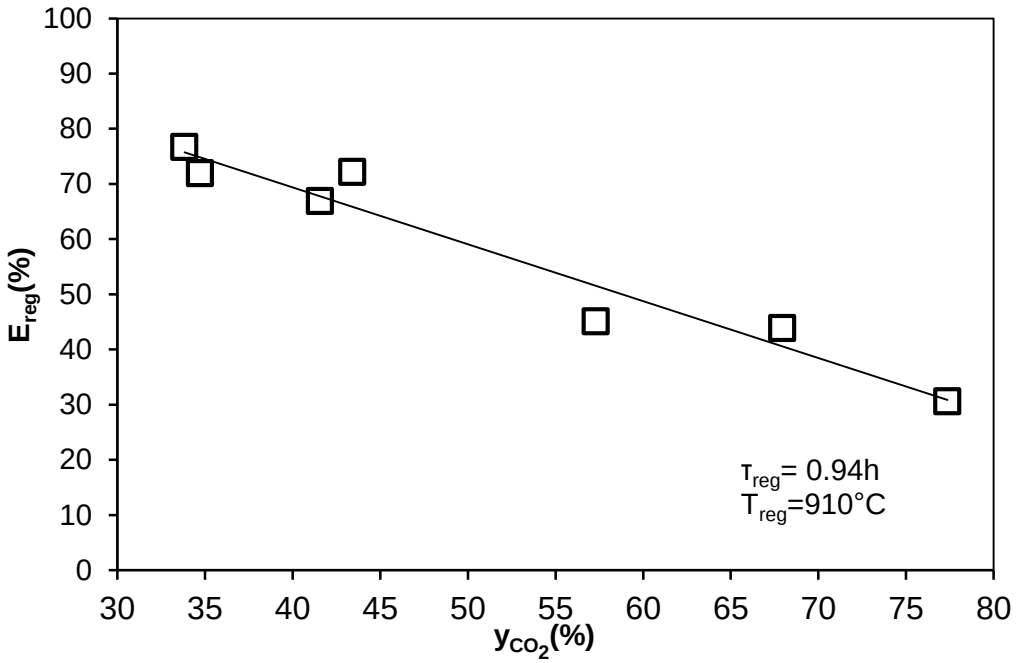

Figure 4.10: Efficiency of the regenerator vs. the CO_2 concentration inside the reactor.

4.4.3 Effect of Temperature

The calcination temperature is a very important aspect of the process. Higher temperatures mean higher fuel consumption therefore we need to determine how the reaction is affected by this parameter. Literature has reported higher calcination efficiencies for higher temperatures.

In figure 4.11 we can see the efficiency of the regenerator plotted vs. the temperature in the reactor. The illustrated points are divided in 3 categories depending on the average CO_2 concentration: 30%, 55% and 75%.

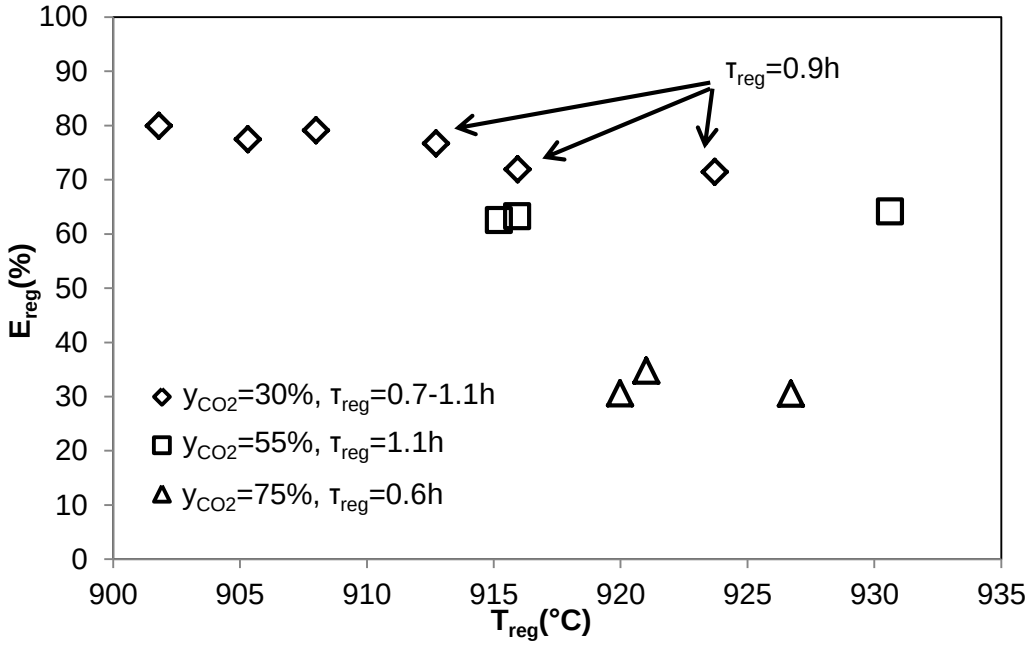

Figure 4.11: Regenerator efficiency vs. calcination temperature for different values of y_{CO2} and space time.

In this diagram the calcination temperature does not appear to play a significant role on the efficiency of the regenerator. The points corresponding to 30% CO_2 concentration appear to be close to 70-80% efficiency regardless of temperature and space time. The points corresponding to 55% CO_2 concentration show lower efficiencies as expected because of the high CO_2 partial pressure. Those points exhibit the same value of space time, approximately 1.1h and while there is a temperature gap between them the efficiency remains stable. Lastly, the 3rd set of points corresponding to very high CO_2 concentrations, namely 75%, exhibits the lowest efficiencies, at approximately 30-40% for a space time of 0.6h while the temperature gap is too small to draw conclusions. The fact that the temperature does not appear to have a significant effect on the regenerator efficiency overall, at least in this range of 900-930°C is very important because it might mean that 900°C could potentially be sufficient to achieve satisfactory calcination efficiencies without excessive energy penalties related to increasing the regenerator temperature in a realistic case scenario where the limitations imposed by this facility discussed earlier do not exist, since there will be combustion taking place as well as much higher gas velocities.

In this figure something peculiar is observed: When the CO_2 partial pressure increases from 30% to 55%, the regenerator efficiency only drops by approx. 10%. When it increases from 55% to 75% however the reduction of the efficiency is much more prominent, approx. 25-30%. This can be explained by taking into consideration the parameter of space time. The space time of the experimental points that correspond to the low-CO_2 conditions, especially

in the range of 915-930°C is lower than that of the points below them which correspond to 55% CO_2. More specifically, the 3 last points of the 30% CO_2 case have a space time of 0.9h while the points representing the 55% CO_2 case have a space time of 1.1h. On the other hand, in the case of 75% CO_2, the space time is approximately 0.6h. For this reason, while the CO_2 partial pressure increases from 30% to 55%, the efficiency drop appears to be less significant due to the space time increasing at the same time. When it increases from 55% to 75% however, a drop in the space time is also noted, resulting in a much bigger "gap" between the 2 cases.

4.4.4 Effect of Particle residence time

The effect of the particles' residence time in the reactor can be observed in figure 4.12, where the Xcarb-Xcalc plotted vs. the CO_2 concentration for 2 different values of residence time at 910°C. As it can be seen when the residence time is approx. 2.5 minutes longer better calcination is achieved. While the space time parameter is ideal when working with the E_{reg} since they are both normalized as per X_{carb}, the residence time is reliable when it comes to comparing X_{carb}-X_{calc} values which represent the amount of CO_2 released during calcination. We can also once again observe the importance of CO_2 partial pressure since there is an evident declining trend as the CO_2 concentration increases.

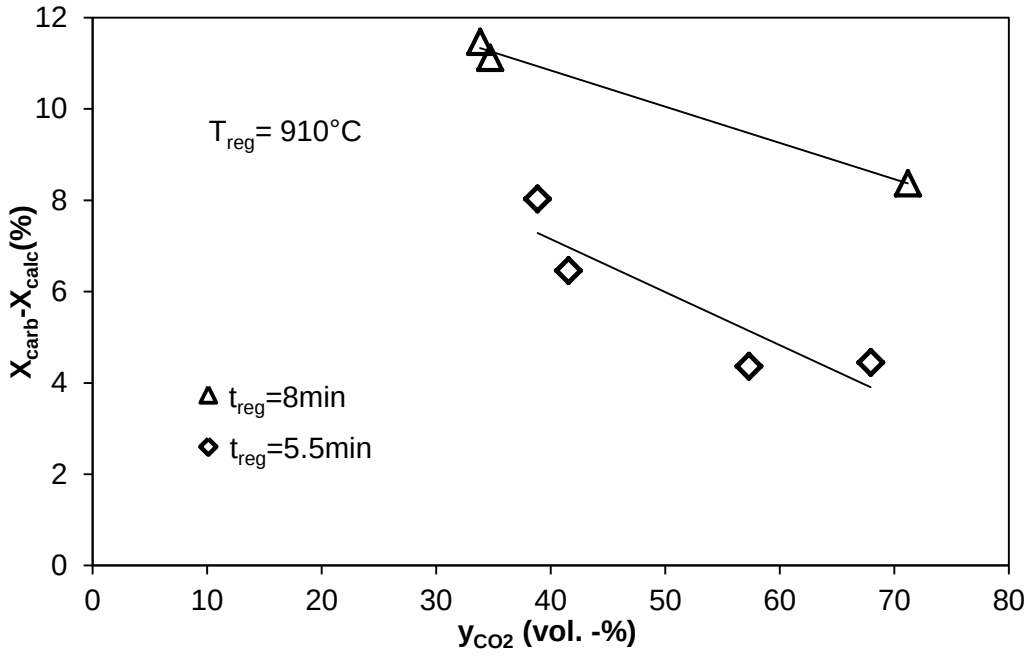

Figure 4.12: X_{carb}-X_{calc} vs. y_{CO2} for 2 different values of residence time

4.4.5 Effect of Active Space Time

As part of the regenerator analysis modeling of the reactor was attempted via the approach of Martinez et al. [34] In a similar manner to the carbonator, we used a parameter f_a which represents the fraction of particles that are not fully calcined, as the equivalent of the f_{active} in the carbonator which represented the fraction of active particles reacting in the fast carbonation stage. As mentioned earlier in Eq. 2.13 it is possible to derive the time required for full calcination. This fraction f_a of the particles has a residence time less than t^*_c and has a reaction rate r_{calc} and is given by Eq. 2.11. The regenerator's efficiency given by Eq. 2.10 can be expressed as shown in Eq 4.9:

$$E_{reg} = N_{Ca} f_a \frac{k_c\left(C_{eq} - C_{CO_2}\right)}{3X_{carb}} \qquad \text{Eq. 4.9}$$

Where k_c is a kinetic constant which characterizes the material.

As proposed by Martinez et al. we adopted the concept of active space time, which relates the fraction of $CaCO_3$ ($N_{Ca}{\cdot}f_a$) in the calciner reacting to the molar flow of $CaCO_3$ entering the reactor ($F_{Ca}{\cdot}X_{carb}$) and is given by eq 4.10:

$$\tau_a = \frac{N_{Ca} f_a}{F_{Ca} X_{carb}} \qquad \text{Eq. 4.10}$$

By using the active space time the regenerator's efficiency can be written as follows:

$$E_{reg} = \tau_a \frac{k_c\left(C_{eq} - C_{CO_2}\right)}{3} \qquad \text{Eq. 4.11}$$

In order to use Eq. 4.11 to calculate the E_{reg} predicted by the model for each experimental point a k_c value was needed. This is provided by the TGA by calcining samples taken from steady states under low CO_2 conditions (10% CO_2 inlet concentration) and high CO_2 conditions (50% CO_2 inlet concentration). The reaction rate is first measured from the calcination graph and then Eq. 2.11 is solved as per k_c. The k_c derived was $3.2{\cdot}10^{-4} m^3/mol{\cdot}s$ for low CO_2 conditions and $1.6{\cdot}10^{-4} m^3/mol{\cdot}s$ for high CO_2 conditions. In addition to this k_c another constant was implemented, φ_{reg} which, similarly to the carbonator's contact factor is related to the specific regenerator reactor and the bubbling regime under which it operated, taking into account the limitations imposed by the facility which were mentioned earlier. This φ_{reg} proved to be equal to 0.42. Figure 4.13 shows the Regenerator's efficiency which was calculated using the calciner model proposed by Martinez et al. vs. the efficiency which was derived from our experimental points for a $k_c\varphi_{reg}$ of $1.34{\cdot}10^{-4} m^3/mol{\cdot}s$ and $6.89{\cdot}10^{-5} m^3/mol{\cdot}s$ for low CO_2 and high CO_2 conditions respectively. It can be seen that the balance closes successfully with the majority of the experimental points being within acceptable error.

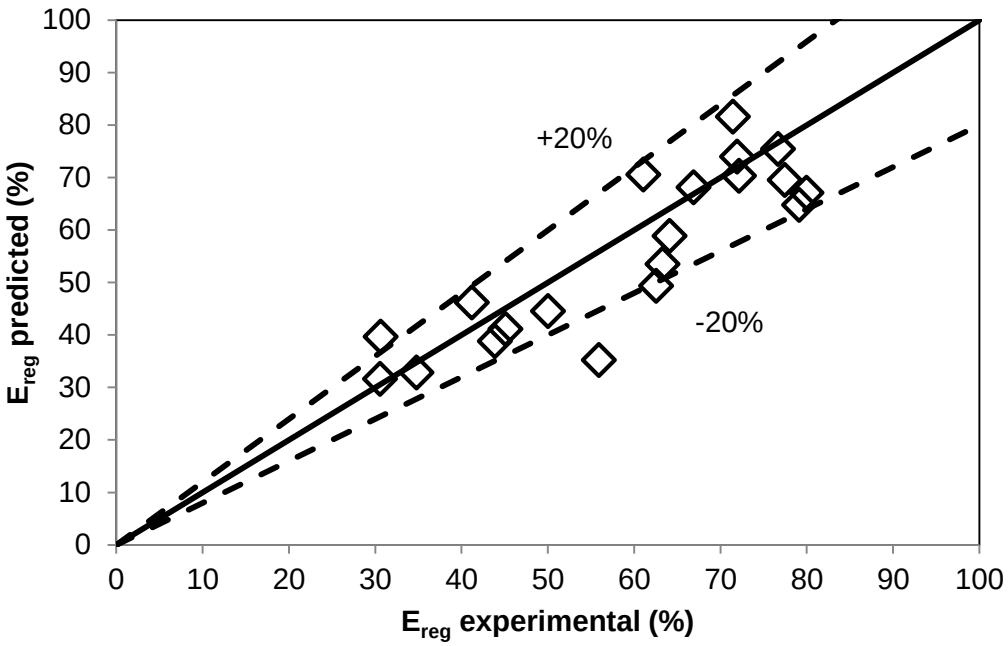

Figure 4.13: Regenerator model validation via mass balance. Carbonator conditions: Temperature: 630°C, y_{CO2in}: 12%. Regenerator conditions: Temperature: 900-930°C, y_{CO2in}=0-75%

Figure 4.14 shows the regenerator efficiency plotted vs. the active space time as predicted by the model as well as the experimental points. The continuous line results from Eq. 4.11 for a CO_2 inlet concentration of 9% and temperature of 910°C while the dashed line shows a high-CO_2 case and it results from Eq. 4.11 for CO_2 inlet concentration of 50% and temperature of 920°C. As we can see the 2 lines are in good agreement with the experimental results with acceptable deviations. Those deviations can be explained because the model line was drawn for a specific value of CO_2 inlet concentration and temperature while for the experimental points those are 0-25% CO_2 inlet conc. in the low CO_2 case and 35-75% in the high CO_2 case whereas the temperature varied between 900-930°C in both cases. In fig. 4.14 the legend that corresponds to the points shows the average CO_2 concentration inside the reactor in each case.

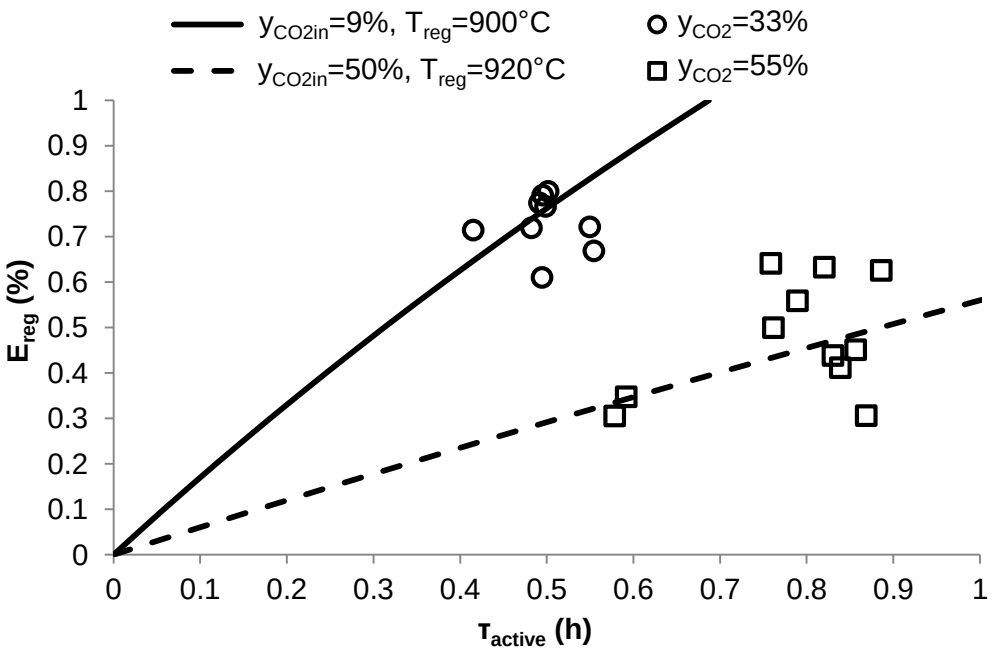

Figure 4.14: Regenerator efficiency plotted vs. Active Space time. Low CO_2 case: Temperature:900-930°C, y_{CO2in}=33%, High CO_2 case::900-930°C, y_{CO2in}=55%

4.5 Sorbent decay

As part of the TGA analysis the X_{max} was measured. This is defined as the maximum CO_2 the CaO particle can capture until the end of the fast carbonation stage..

In figures 4.15 and 4.16 the chemical activity of the sorbent is presented as far as the X_{max} is concerned. These figures depict the decay of the maximum carbonation conversion of the material over the course of the experiment in respect to 2 different variables:

- Time elapsed since the start of the experiment (Figure 4.15)
- Theoretical number of cycles (Figure 4.16)

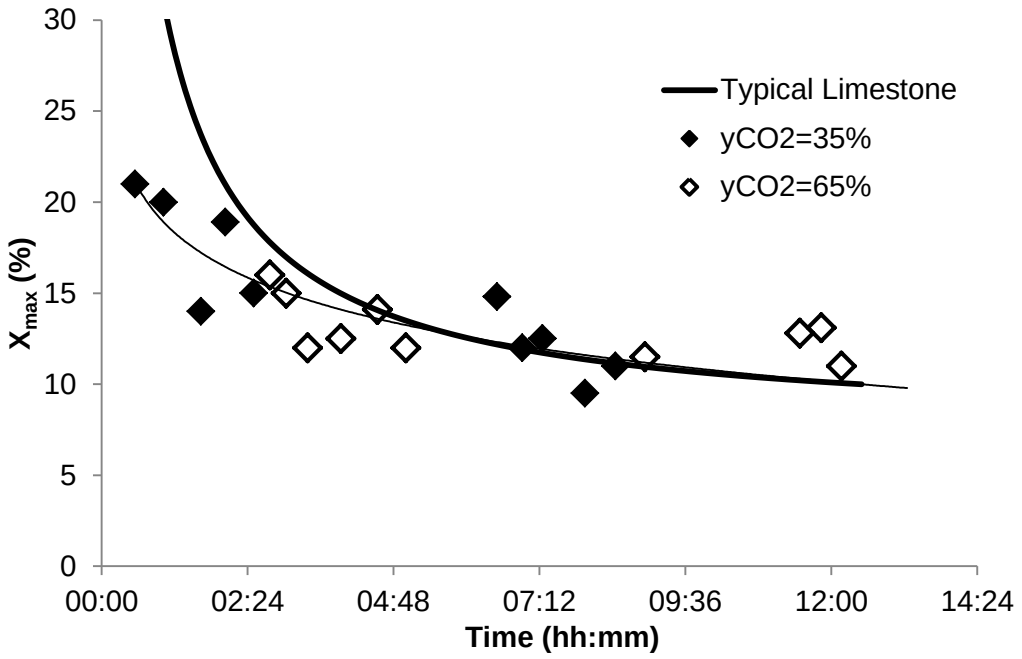

Figure 4.15: Maximum Carbonation Conversion (X_{max}) plotted vs. time. Carbonator: 630°C, y_{CO2in}=12%. Regenerator: 900-930°C.

Figure 4.15 shows the chemical activity of the sorbent by presenting the decay of the maximum carbonation conversion (X_{max}) over the total time elapsed since the start of the experiment for 2 different values of CO_2 concentration in the regenerator reactor. Since there is no constant make-up material flow or any other means to regenerate the sorbent's capture capacity we can observe a steady decline of the X_{max} towards a residual activity of approximately 10%. It should also be noted here that the CO_2 concentration of the regenerator's inlet gas does not seem to affect the X_{max}. In this figure we also compare the decay of X_{max} with the theoretical deactivation curve of a typical limestone according to Eq. 2.16 for an equivalent amount of time. We can see that the curve appears in good agreement with the trend provided by our data with a notable deviation for the first experimental hours. This deviation can be explained by the fact that our material underwent pre-calcination at a high temperature (900°C) prior to the experiment taking place which could have resulted in sintering of the sorbent. Another explanation can be the fact that in a real DFB system partial carbonation and rapid particle heating-cooling rates may lead to different sintering patterns than in the TGA [56].

The evolution of the X_{max} during the course of the experiment in respect to the theoretical number of carbonation-calcination cycles is presented in Figure 4.16.

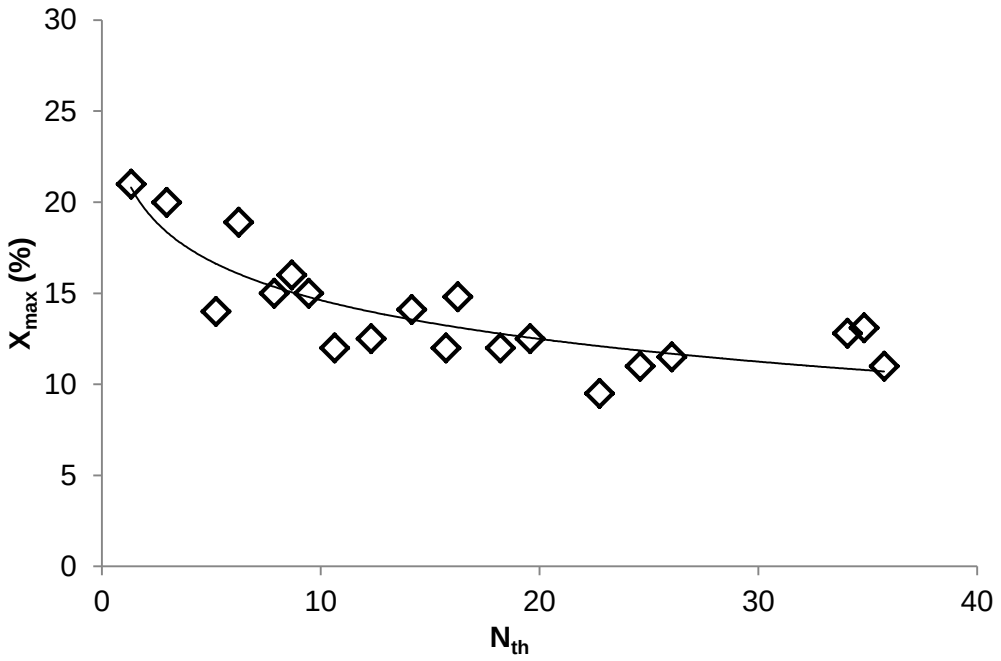

Figure 4.16: X_{max} vs. theoretical number of cycles (N_{th}). Carbonator: 630°C, y_{CO2in}=12%. Regenerator: 900-930°C, y_{CO2in}=0-75%

The theoretical number of cycles (N_{th}) is plotted in the x-axis and is given in the following equation:

$$N_{th} = \int_0^t \frac{E_{CO_2}(t) \cdot F_{CO_2}}{X_{max} \cdot n_{Ca,total}} dt \qquad \text{Eq. 4.11}$$

Where $E_{CO2}(t)$ represents once again the instantaneous CO_2 capture efficiency, while $n_{Ca,total}$ stands for the total inventory in the DFB system. The N_{th} expresses the amount of times that the moles of CO_2 captured could carbonate the bed inventory ($n_{Ca,total}$) up to its CO_2 carrying capacity (X_{max}). Once again it can be noticed that the value of the X_{max} is reduced for each theoretical cycle and appears to be reaching a residual activity of X_{max} equal to 12%.

4.6 Mechanical Stability of the sorbent

Particle Size Distribution analysis provided information on the sorbent's mechanical stability. It is expected from the particles' size to decrease over the course of the experiment.

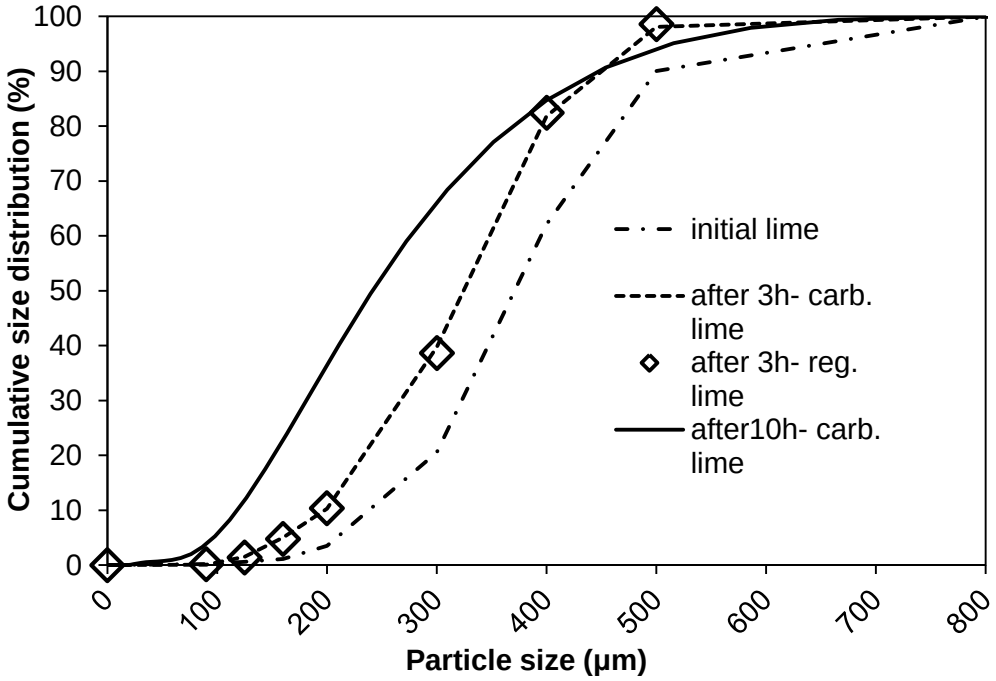

Figure 4.17: Cumulative particle size distribution of the solids at 3 different timestamps [54]. Carbonator: 630°C, y_{CO2in}=12%. Regenerator: 900-930°C, y_{CO2in}=0-75%

In figure 4.17 we can see the evolution of particle size at the start of the experiment and after 3 and 10 hours of operation. As predicted by literature, the overall particle size decreased over the course of the experiment. It is important to note however that the difference between the particles entering and the ones exiting the calciner as presented after 3 hours of operation is non-existent when the calcined material should be presenting a smaller particle size. One possible explanation for this observation is the bubbling fluidization regime. The gas velocity is lower thus collisions are not as intense as they would be in the turbulent or fast fluidization regimes where much higher gas velocities are introduced. This assumption is also backed up by existing literature where it is presented that gas velocity plays a significant role in particle attrition [46].

In figure 4.18 we can see the dp10, dp50 and dp90 of the samples collected throughout the experiment for 3 different samples. One from the initial lime after the first calcination, one after 3h of operation and one at the end of the experiment, after 10 hours out of the carbonator reactor.

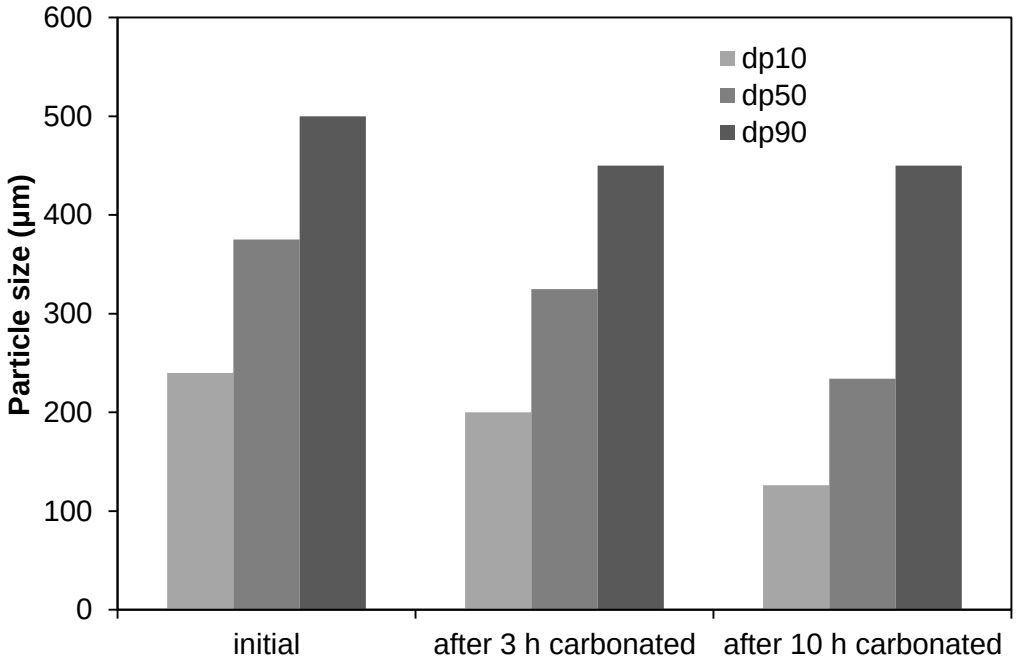

Figure 4.18: Particle size distribution of the solids for 3 different timestamps [54]. Carbonator: 630°C, y_{CO2in}=12%. Regenerator: 900-930°C, y_{CO2in}=0-75%

Dp10, 50 and 90 stand for the size of the 10th, 50th and 90th percentile of the particles in a specific sample respectively. This means that 10, 50 and 90% of the particles of the sample have a size between 0 and the value of dp10, dp50 and dp90 respectively. We can observe that throughout the course of the experiment the overall particle size decreased, as proposed in literature, with the only exception being the dp90 of the sample taken after 10 hours of operation which remained the same as the dp90 of the sample after 3hours. This can be explained by the addition of fresh material which took place approximately 3.5 to 4h after the start of the experiment. The losses calculated through the pressure drop of the reactors (as well as confirmed through the mass balance at the end of the experiment) are measured to be around 0.8wt%/h which is significantly less than numbers recorded in previous experiments in the same facility, namely 2wt%/h [23]. This difference can be explained by the fluidization regime. In our experimental campaign the regenerator operated under the bubbling fluidization regime whereas operating under turbulent fluidization would mean significantly higher fluidization velocities and, in turn, more collisions of the particles reducing the overall particle size. It should be noted here that presence of CO_2 also enhances sintering effects [20] which harden the particle surface. This effect was more prominent in the current experimental campaign because of the difference in the CO_2 concentration of the gas inside the reactor. While in the previous experiment the CO_2 was provided by CH_4 combustion and was approximately 30% of the inlet gas, in our case the CO_2 inlet concentration was controlled and was often at values as high as 50-75%.

Those differences can also be presented in the following diagrams: In Figure 4.19 we can see the limestone Cumulative Size Distribution of the material only in the beginning and the end of the experiment, namely after 10h of operation. In comparison, the Cumulative Size Distribution of the material used by Charitos et al. is presented. The range of the particle size in that case was 0-400μm.

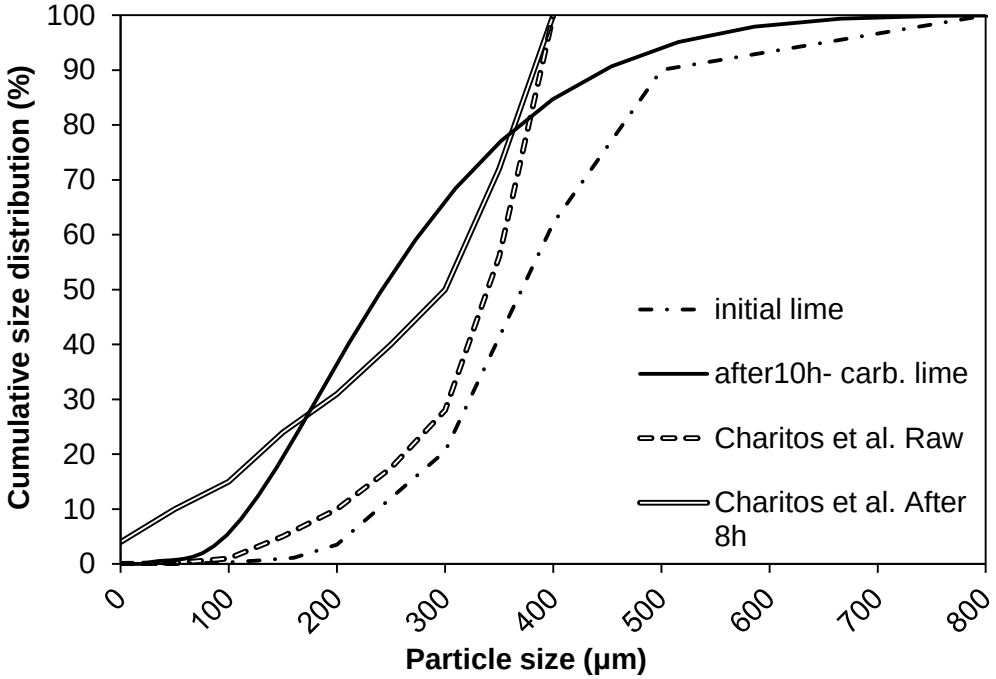

Figure 4.19: Cumulative Size Distribution at the beginning and the end of the experiment. Carbonator: 630°C, y_{CO2in}=12%. Regenerator: 900-930°C, y_{CO2in}=0-75%. Charitos et al. [23]: Carbonator: 630-700°C, y_{CO2in}=15%. Regenerator: 850°C, y_{CO2}=30%.

We can observe that the amount of fine particles, namely the ones with a size within the 0-100μm region, generated in the case of Charitos et al. is much bigger than the ones in the current experimental campaign, justifying the recorded material losses of 2wt.%.

This difference in fine generation can also be shown by the particle size distribution. In Figure 4.20 the dp10, 50 and 90 of the PSD as reported in [23] are presented.

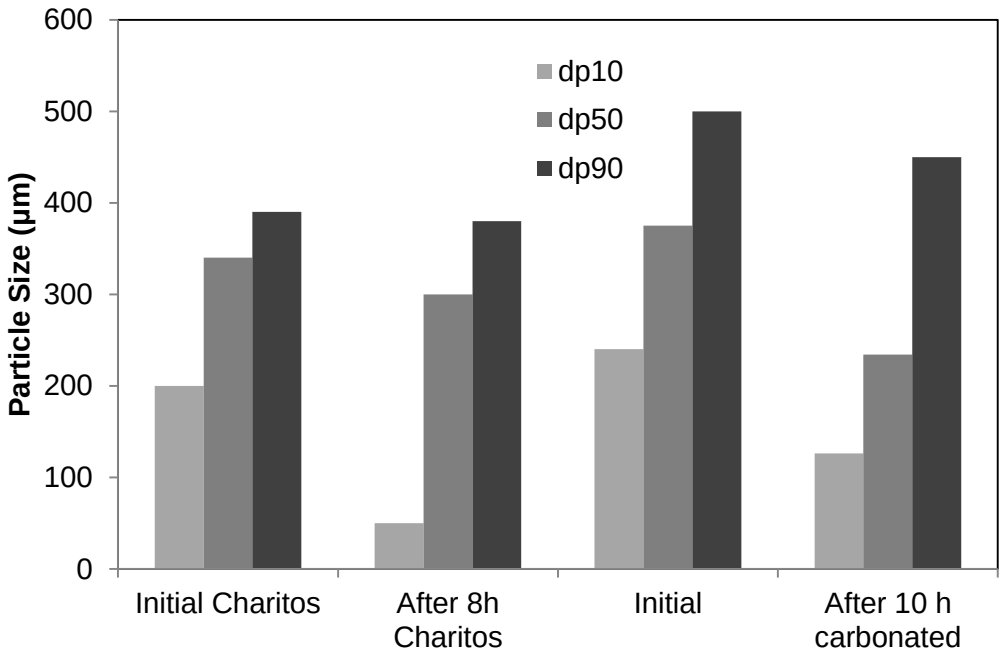

Figure 4.20: Particle Size Distribution for the beginning and end of the experiment. Carbonator: 630°C, y_{CO2in}=12%. Regenerator: 900-930°C, y_{CO2in}=0-75%. Charitos et al. [23]: Carbonator: 630-700°C, y_{CO2in}=15%. Regenerator: 850°C, y_{CO2}=30%.

We can see that while the dp50 and dp90 only decrease by a small amount, there is a significant decrease in the dp10, indicating excessive generation of finer particles since it shows that 10% of the particles have a size of 50µm or less. In comparison, after 10h of operation in this experimental campaign, the dp10 is 125µm.

Using the PSD we were also able to study the evolution of mean particle size over the course of the experiment in order to determine the level of attrition taking place during multiple carbonation-calcination cycles. The mean particle size was calculated using Eq. 4.13:

$$d = \frac{1}{\sum \frac{w_i}{d_i}} \qquad \text{Eq. 4.13}$$

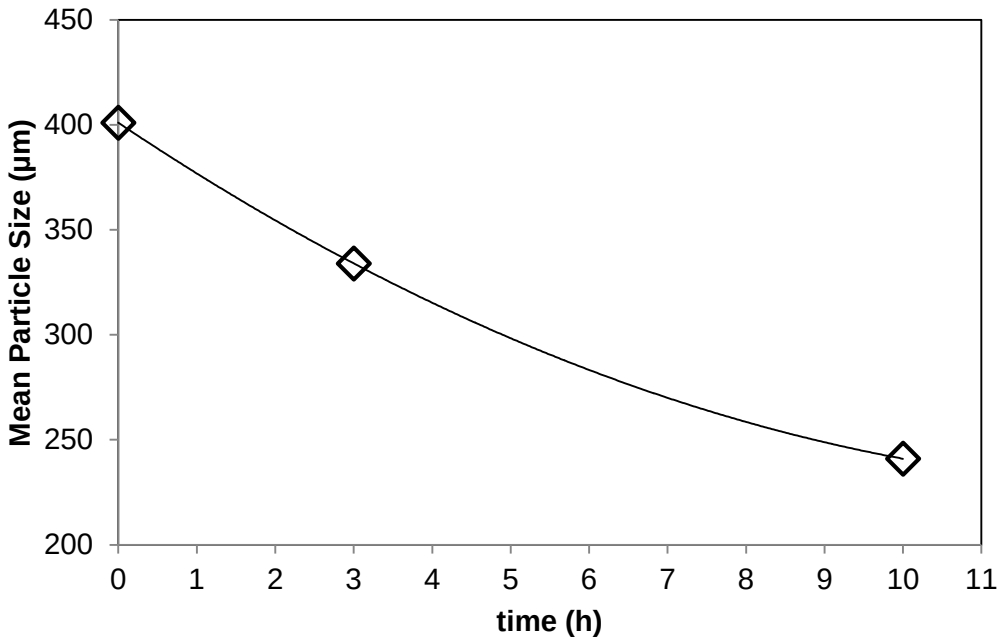

Figure 4.21: Mean particle size over time. Carbonator: 630°C, y_{CO2in}=12%. Regenerator: 900-930°C, y_{CO2in}=0-75%.

In Figure 4.21 it can be seen that the rate of attrition is decreasing with time. The reason is that at the beginning, the fresh sorbent particles are very irregular. This results in a high rate of initial particle degradation during which the particles break and their edges and asperities are knocked off. With progressing time the particles become smaller, rounder and smoother and the number of their weak points decreases. The elutriation rate, therefore, decreases continuously with time and tends to a more or less constant value which can be interpreted as some kind of a steady-state level where only abrasion takes place [43]. This behavior is also confirmed by Gonzalez et al. who conducted experiments with continuous DFB operation under similar experimental conditions [45]. The samples' average particle size they extracted from the carbonator and regenerator was decreasing rapidly with time during the first experimental hours and after that it proved to remain at a constant value for the remaining hours of operation.

Chen et al. [44] proposed a simple model to describe the evolution of the average particle size of a batch of solids in a circulating fluidized bed of lime. This model suggests that average particle size varies linearly with cumulative attrition time according to the following linear relation with time:

$$\frac{d_0}{d_t} = k_a t + 1 \qquad \text{Eq. 4.14}$$

where d_0 is the initial average particle size, d_t is the size after the cumulative attrition time and k_a is the attrition rate constant, from which detailed semi empirical correlations can be

derived. Figure 4.22 shows the ratio d_0/d_t plotted vs. time for our experimental data providing a k_a value of 0.0663 h^{-1} or $1.84 \cdot 10^{-5}$ s^{-1}.

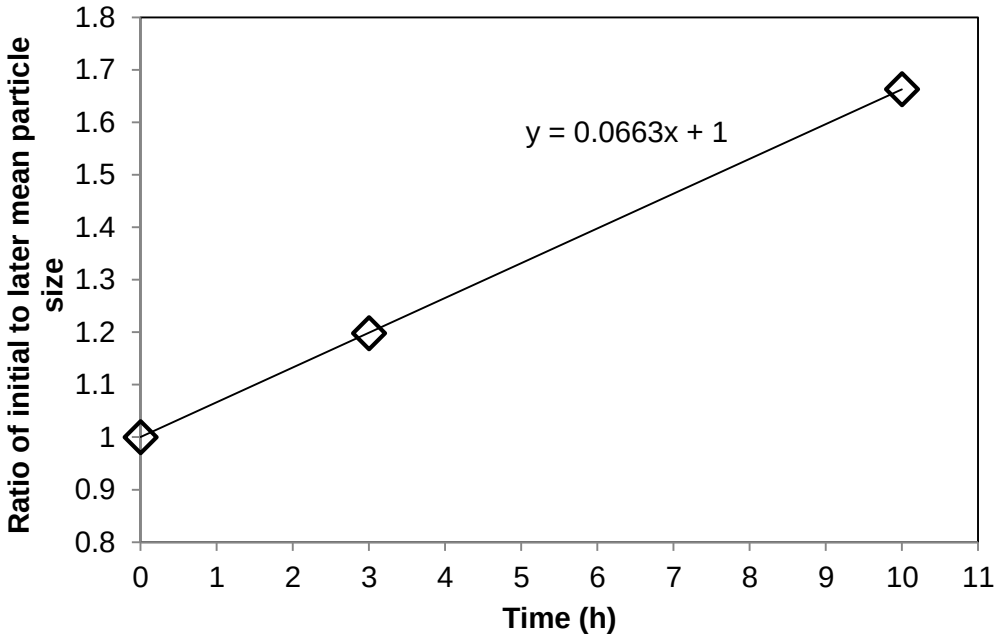

Figure 4.22: Ratio of initial to later mean particle size over time. Carbonator: 630°C, y_{CO2in}=12%. Regenerator: 900-930°C, y_{CO2in}=0-75%.

In another attempt to interpret the PSD analysis results, a second order model proposed by Cook et al. was used. With this model we can predict the evolution of mean particle size over the course of the process. This model has already been validated by Gonzalez et al. [45] under similar experimental conditions but for lower fluidization velocities, namely 2m/s while in our case they were approximately 5.8-6 m/s. For this model the concept of the W_{min} was introduced:

$$\frac{dW}{dt} = -k_a\left(W^2 - W_{min}^2\right) \qquad \text{Eq. 4.15}$$

W_{min} is the minimum material weight after which attrition is negligible, i.e. after long attrition times. Based on our experimental results this W_{min} corresponds to a mean particle diameter dp_{min} of approximately 200µm.

After integrating Eq. 4.15 the following equation is obtained:

$$\frac{(U - U_{mf})^2}{2W_{min}}\left[\ln\left(\frac{W_0 - W_{min}}{W_0 + W_{min}}\right) - \ln\left(\frac{W - W_{min}}{W + W_{min}}\right)\right] = K_a t \qquad \text{Eq. 4.16}$$

And if we assume that the particles are spherical and that the density remains constant we get Eq. 4.17:

$$\frac{(U-U_{mf})^2}{2\left(\frac{d_{p\,min}}{d_{p0}}\right)}\left[\ln\left(\frac{1+\left(\frac{d_{p\,min}}{d_{p0}}\right)^3}{1-\left(\frac{d_{p\,min}}{d_{p0}}\right)^3}\right)-\ln\left(\frac{\left(\frac{d_p}{d_{p0}}\right)^3+\left(\frac{d_{p\,min}}{d_{p0}}\right)^3}{\left(\frac{d_p}{d_{p0}}\right)^3-\left(\frac{d_{p\,min}}{d_{p0}}\right)^3}\right)\right]=K_a t \qquad \text{Eq. 4.17}$$

We should note here that the attrition constant k_a was modified in order to include the term $(U\text{-}U_{mf})^2$. U_{mf} was calculated using equations 2.2 and 2.3.

In figure 4.23 we can see the plot of the left hand side of Eq. 4.17 vs. time from which we obtain a K_a value of $0.0034 m^2 s^{-3}$.

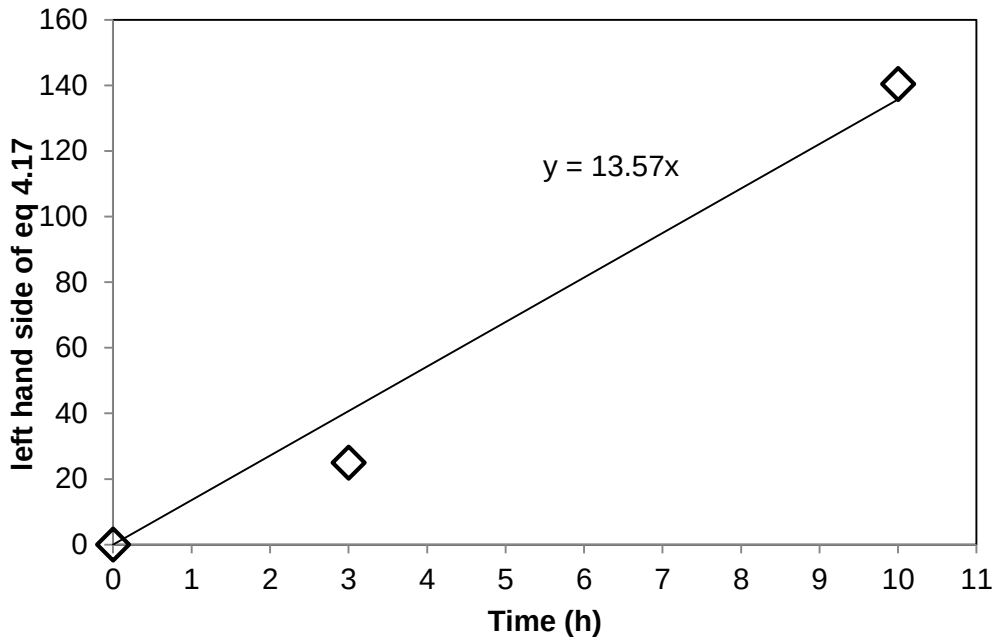

Figure 4.23: Result of left hand side of Eq 4.17 vs. time. Carbonator: 630°C, y_{CO2in}=12%. Regenerator: 900-930°C, y_{CO2in}=0-75%.

Using this value of K_a we can then solve Eq. 4.17 as per d_p in order to complete the model which will predict the evolution of the mean particle size:

$$d_p = d_{p0}\left[\frac{\left(\frac{d_{p\,min}}{d_{p0}}\right)^3\left(\left(1-e^{\frac{2d_{p\,min}^3}{d_{p0}^3(U-U_{mf})^2}K_a t}\right)-\left(1+e^{\frac{2d_{p\,min}^3}{d_{p0}^3(U-U_{mf})^2}K_a t}\right)\right)}{1-\left(\frac{d_{p\,min}}{d_{p0}}\right)^3-e^{\frac{2d_{p\,min}^3}{d_{p0}^3(U-U_{mf})^2}K_a t}\left(1+\left(\frac{d_{p\,min}}{d_{p0}}\right)^3\right)}\right]^{1/3} \qquad \text{Eq. 4.18}$$

By plotting d_p vs. time we obtain the model line which appears to be in good agreement with our experimental results, as shown in figure 4.24.

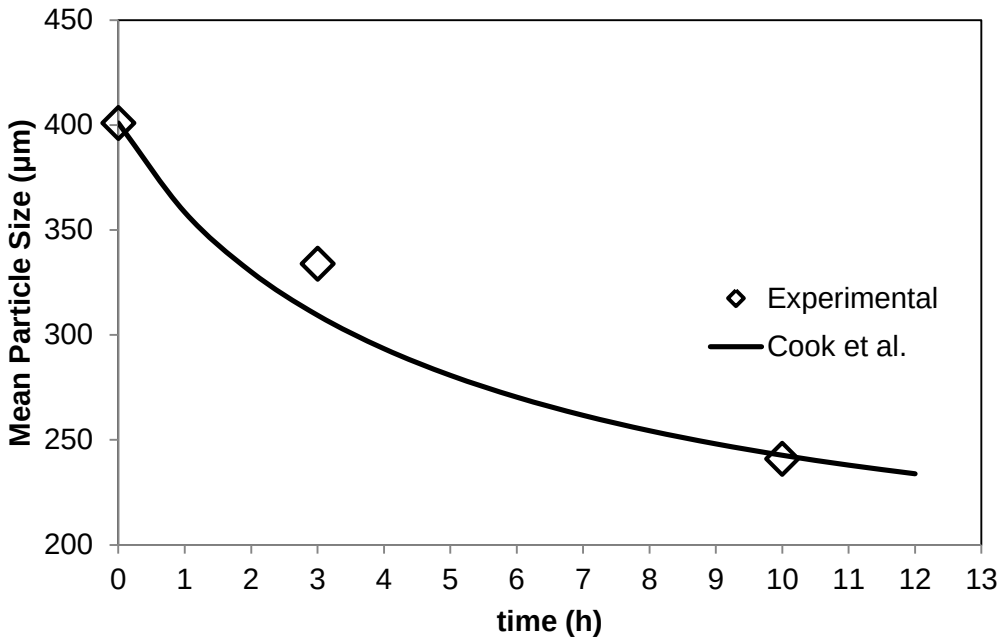

Figure 4.24: Mean Particle size plotted vs. time as resulted from the experiments and as predicted by the model of Cook et al. Carbonator: 630°C, y_{CO2in}=12%. Regenerator: 900-930°C, y_{CO2in}=0-75%.

Gonzalez et al. also attempted to fit the same model to their experimental results [45]. By comparing their attrition constant K_a, $4.53 \cdot 10^{-4} s^{-1}$ with the one that was obtained in the current experimental campaign, $3.05 \cdot 10^{-3} s^{-1}$, we can see that the material we used was more fragile. This can be explained by the fact that our material had a much bigger mean particle size. Smaller particles are more difficult to break than larger ones, mainly because they tend to contain fewer faults [43]. It should be noted here that this method depends heavily on existing experimental data in order to determine the attrition rate constant K_a as well as the d_{pmin}. However, simple tests can be performed in order to measure those parameters independently and predict the attrition behavior of sorbents on larger scale CO_2 capture systems [45].

5 Conclusions & summary

Experiments took place in the IFK 10KW$_{th}$ Facility provided results in order to validate existing work regarding the Carbonator as well as to further expand the knowledge on the regenerator's function in a small pilot scale DFB facility under continuous dual circulation. Through those results the efficiency of calcination under high CO_2 partial pressure was determined, as well as for different values of calcination temperature and residence times of the sorbent in the reactor. The space time parameter was also shown to be a reliable means of characterizing the reactor's performance. This parameter offers the opportunity to establish a link between the reactor's performance and the sorbent's quality as well as the reactor's dimensions, which is of great importance when talking about industrial scale facilities. Mechanical stability and chemical activity of the sorbent were also determined under those parameters. CO_2 predictably proved to inhibit the calcination reaction, while the calcination temperature's effect on the performance of the reactor proved to be of little significance, especially when compared to Space Time. Lastly, when the sorbent had a higher residence time in the regenerator the value of X_{carb}-X_{calc} which represents the amount of CO_2 released appeared to be at higher levels indicating a better quality of calcination. There were however limitations imposed by the facility due to operation under bubbling fluidization and heat transfer through electrical heating which prevented the limestone from calcining completely, leading to lower calcination efficiencies than those recorded in previous experimental campaigns. As far as the mechanical stability of the sorbent is concerned, a continuous decay of the mean particle size were recorded while very few fines were generated. The overall losses measured are approximately 0.8wt.%/h which was significantly lower than a previous experimental campaign presenting losses of 2wt.%/h. Lastly, CO_2 partial pressure inside the regenerator reactor did not appear to have an effect on the chemical activity of the sorbent since the maximum carbonation conversion reached a predicted residual activity of 10% regardless of the CO_2 inlet concentration.

As far as the validation of the experimental data is concerned, the mass balance closure was successful with only a few points slightly deviating from the norm, something which can be explained through errors occurring during sampling and analysis of the sorbent as well as during the measurement of the circulation rate.

6 Literature

[1] Exxonmobil, "The Outlook for Energy: A View to 2040," 2012.

[2] W. Wang, S. Ramkumar and L.-S. Fan, "Energy penalty of CO2 capture for the Carbonation-Calcination Reaction (CCR) Process: Parametric effects and comparisons with alternative processes.," *Fuel 104,* pp. 561-574, 2013.

[3] A. Sieminski, "International Energy Outlook 2013," Washington, DC, 2013.

[4] European Association for Coal and Lignite AISBL, "A strategy for green coal," 2012.

[5] Scripps Institution of Oceanography, "The Annual Rise in CO2 Levels Has Begun," 2013. [Online]. Available: http://keelingcurve.ucsd.edu/the-annual-rise-in-co2-levels-has-begun/.

[6] International Energy Agency, "Scenarios and Projections," 2013. [Online]. Available: http://www.iea.org/publications/scenariosandprojections/.

[7] International Energy Agency, "World Energy Outlook 2010 (WEO 2010)," Paris, France, 2010.

[8] World Coal Association, "Carbon Capture & Storage Technologies," [Online]. Available: http://www.worldcoal.org/coal-the-environment/carbon-capture-use--storage/ccs-technologies/.

[9] A. Charitos, "Experimental Characterization of the Calcium Looping Process for CO2 capture," 2011.

[10] E. H. Baker, "The calcium oxide-carbon dioxide system in the pressure range 1-300 atmospheres," *J. Chem. Soc. Vol. 70,* pp. 464-470, 1962.

[11] T. Shimizu, T. Hirama, H. Hosoda, K. Kitano, M. Inagaki and K. Tejima, "A twin fluid-bed reactor for removal of CO2 from combustion processes.," *Trans IChemE Vol 77, Part A,* pp. 62-68, January 1999.

[12] C.Hawthorne, M. Trossmann, P. G. Cifre, A. Schuster and G. Scheffknecht, "Simulation of the carbonate looping power cycle.," *Energy Procedia 1,* pp. 1387-1394, 2009.

[13] N. Rodriguez, R. Murillo and J. C. Abanades, "CO2 Capture from Cement Plants Using Oxyfired Precalcination and/or Calcium Looping.," *Environmental Science & Technology 46,* pp. 2460-2466, 2012.

[14] A. Sanchez-Biezma, J. Ballesteros, L.Diaz, E. d. Yarraga, F. Alvarez, B. A. J.Lopez, G.Grasa and J. Abanades, "Postcombustion CO2 capture with CaO. Status of the technology and next steps towards large scale demonstration.," *Energy Procedia 4,* pp.

852-859, 2011.

[15] National Energy Technology Laboratory, "Cost and Performance Baseline for Fossil Energy Plants Volume 1: Bituminous Coal and Natural Gas to Electricity," 2010.

[16] D. P. Connell, D. A. Lewandowski, S. Ramkumar, i. Phalak, R. M. Statnick and L.-S. Fan, "Process simulation and economic analysis of the Calcium Looping Process (CLP) for hydrogen and electricity production from coal and natural gas.," *Fuel 105,* pp. 383-396, 2013.

[17] R. S. Boynton, Chemistry and Technology of Lime and Limestone, 1980.

[18] R. N., M. Alonso, G. Grasa and J. Abanades, "2008 Heat requirements in a calciner of CaCO3 integrated in a CO2 capture system using CaO.," *Chem. Eng. Journal, 138,* pp. 148-154, 2008.

[19] A. Coppola, F. Montagnaro, P. Salatino and F. Scala, "Attrition of limestone during co2 capture in a fluidized bed calcium looping process," Chia Laguna, Cagliari, Sardinia, Italy, 2011.

[20] J. Blamey, E. Anthony, J. Wang and P. Fenell, "The calcium looping cycle for large-scale CO2 capture.," *Progress in Energy and Combustion Science Volume 36, Issue 2,* p. 260–279, 2010.

[21] C. Salvador, D. Y. Lu, E. J. Anthony and J. C. Abanades, "Capture of CO2 with CaO in a pilot fluidized bed carbonator experimental results and reactor model," in *Greenhouse Gas Control Technologies 7*, Vancouver, Canada, 2004.

[22] D. Z. Lu, R. W. Hughes and E. J. Anthony, "Ca-Based sorbent looping combustion for CO2 capture in pilot-scale dual fluidized beds.," *Fuel Processing Technology,* pp. 1386-1395, 2008.

[23] A. Charitos, C. Hawthorne, A. Bidwe, S. Sivalingam, A. Schuster, H. Spielthoff and G. Scheffknecht, "Parametric investigation of the calcium looping process for CO2 capture in a 10KWth dual fluidized bed.," *International Journal of Gas Control 4,* pp. 776-884, 2010.

[24] M. Alonso, N. Rodrigzez, B.Gonzalez, G. Grasa, R. Murillo and J. Abanades, "Carbon dioxide capture from combustion flue gases with a calcium oxide chemical loop. Experimental results and process development.," *International Journal of Gas Control 4,* pp. 167-173, 2010.

[25] C. Hawthorne, H. Dieter, A. Bidwe, A. Schuster, G. Scheffknecht, S. Unterberger and M. Käß, "CO2 Capture with CaO in a 200 kWth Dual Fluidized Bed Pilot Plant," *Energy Procedia,* no. 4, pp. 441-448, 2011.

[26] A. Sánchez-Biezma, L. Diaz, J. López, B. Arias, J. Paniagua, M.Lorenzo, J. Álvarez and J. Abanades, "CaOling Project - First experiences on the 1,7Mwt calcium looping pilot in La Pereda," 2012.

[27] I. Martinez, G.Grasa, R. Murillo, B. Arias and J. Abanades, "Kinetics of Calcination of Partially Carbonated Particles in a Ca-Looping System for CO2 Capture," *Energy Fuels,* vol. 2, pp. 1432-1440, 2012.

[28] P. Basu, Combustion and Gasification in Fluidized Beds, 2006.

[29] A. Manettas, "Experimental investigation of the oxyfuel combustion in a 150kWth circulating fluidized bed combustor," 2012.

[30] X. lv, H. Li and Q. Zhu, "Simulation of gas-solid flow in 2D/3D bubbling fluidized beds by combining the two-fluid model with structure-based drag model," *Chemical Engineering Journal,* 2013.

[31] M. W. Seo, T. D. Nguyen, Y. I. Lim, S. D. Kim, S. Park, B. H. Song and Y. J. Kim, "Solid circulation and loop-seal characteristics of a dual circulating fluidized bed: Experiments and CFD simulation," *Chemical Engineering Journal 168,* p. 803–811, 2011.

[32] N. Rodrígueza, M. Alonso, J. C. Abanades, A. Charitos, C. Hawthorne, G. Scheffknecht, D. Y. Lu and E. J. Anthony, "Comparison of experimental results from three dual fluidized bed test facilities capturing CO2 with CaO," *Energy Procedia,* no. 4, p. 393–401, 2011.

[33] H. Dieter, C. Hawthorne, M. Zieba and G. Scheffknecht, "Progress in Calcium Looping Post Combustion CO2 Capture: Successful Pilot Scale Demonstration," *Energy Procedia,* no. 37, p. 48 – 56, 2013.

[34] I.Martínez, G. Grasa, R. Murillo, B. Arias and J. Abanades, "Modelling the continuous calcination of CaCO3 in a Ca-looping system," *Chemical Engineering Journal 215-216,* pp. 174-181, 2013.

[35] J. R. Ingraham and P. Marier, "Kinetic studies on the thermal decomposition of calcium carbonate," *Canadian Journal of Chemical Engineering,* pp. 170-173, 1963.

[36] F. García-Labiano, A.Abad, L. d. Diego, P. Gayán and J. Adánez, "Calcination of calcium-based sorbents at pressure in a broad range of CO2 concentrations," *Chemical Engineering Science Volume 57, Issue 13,* pp. 2381-2393, 2002.

[37] T. Darroudi and A. W. Searcy, "Effect of CO2 pressure on the rate of decomposition of calcite," *J. Phys. Chem.,* pp. 3971-3974, 1981.

[38] J. Khinast, G. Krammer, C. Brunner and G. Staudinger, "Decomposition of Limestone: The influence of CO2 and particle size on the reaction rate," *Chemical Engineering*

Science vol.51. No. 4, pp. 623-634, 1996.

[39] B. Stanmore and P. Gilot, "Review—calcination and carbonation of limestone during thermal cycling for CO2 sequestration," *Fuel Processing Technology 86,* pp. 1707-1743, 2005.

[40] R. Borgwardt, "Sintering of nascent calcium oxide".

[41] R. Borgwardt, "Calcination Kinetics and Surface Area of Dispersed Limestone Particles," *AlChE Journal Vol. 31, No.1,* pp. 103-111, 1985.

[42] Y. Wang, S. Lin and Y. Suzuki, "Study of Limestone Calcination with CO2 Capture: Decomposition Behavior in a CO2 Atmosphere," *Energy & Fuels, 21,* pp. 3317-3321, 2007.

[43] J. Werther and J. Reppenhagen, "Attrition in Fluidized Beds and Pneumatic Conveying Lines," 1998.

[44] Z. Chen, J. R. Grace and C. J. Lim, "Limestone particle attrition and size distribution in a small circulating fluidized bed," *Fuel,* no. 87, pp. 1360-1371, 2008.

[45] B. Gonzalez, M. Alonso and J. C. Abanades, "Sorbent attrition in a carbonation/calcination pilot plant for capturing CO2 from flue gases," *Fuel,* no. 89, pp. 2918-2924, 2010.

[46] Z. Chen, C. J. Lim and J. R. Grace, "Study of limestone particle impact attrition.," *Chemical Engineering Science 62,* pp. 867-877, 2007.

[47] R. H. Borgwardt, "Calcium Oxide Sintering in Atmospheres containing Water and Carbon Dioxide.," *Ind. Eng. Chem. Res. 28,* pp. 493-500, 1989.

[48] G. S. Grasa and J. C. Abanades, "CO2 Capture Capacity of CaO in Long Series of Carbonation/Calcination Cycles," no. 45, p. 8846–8851, 2006.

[49] G. S. Grasa and J. C. Abanades, "CO2 Capture Capacity of CaO in Long Series of Carbonation/Calcination Cycles," *Ind. Eng. Chem. Res.,* no. 45, pp. 8846-8851, 2006.

[50] A. Charitos, N. Rodríguez, C. Hawthorne, M. Alonso, M. Zieba, B. Arias, G. Kopanakis, G. Scheffknecht and J. C. Abanades, "Experimental Validation of the Calcium Looping CO2 Capture Process with Two Circulating Fluidized Bed Carbonator Reactors," *Industrial & Engineering Chemistry Research,* pp. 9685-9695, 2011.

[51] R. Barker, "The reversibility of the reaction ⟦CaCO⟧_3↔CaO+⟦CO⟧_2.," *J. appl. Chem. Biotechnology 23,* pp. 733-742, 1973.

[52] L.-S. F. Shwetha Ramkumar, "Thermodynamic and Experimental Analyses of the Three-Stage Calcium Looping.," *Process Ind. Eng. Chem. Res. 49,* p. 7563–7573, 2010.

[53] M. C.Romano, "Modeling the carbonator of a Ca-looping process for CO2 capture from power plant flue gas," *Chemical Engineering Science 69,* pp. 257-269, 2012.

[54] D. Glykeria, P. Ioannis, B. A.R., S.-L. Vladimir, D. Heiko and S. Günter, "Calcium looping process for CO2 capture: experimental characterization of the regenerator operation under oxy-fuel conditions in a 10 kWth dual fluidized bed facility.," in *Proc. 6th Int. Conf. Clean Coal Technol.*, Thessaloniki, Greece, 2013.

[55] A. Charitos, C. Hawthorne, A. Bidwe, L. Korovesis, A. Schuster and G. Scheffknecht, "Hydrodynamic Analysis of a 10 kWth Calcium Looping Dual Fluidized Bed for post-combustion CO2 capture," *Powder Technology 200,* pp. 117-127, 2010.

[56] G. Kopanakis, "Characterization of the Carbonator and Regenerator for the Calcium Looping CO2 capture Process," 2010.